A European endeavor for optimizing Zonal Isolation, Drilling and Exploitation of EGS projects

STRUCTURAL CHARACTERIZATION OF THE BEDRETTO UNDERGROUND LABORATORY FOR GEOENERGIES (BULGG)

Author: Dr. Raymi Castilla, Geo-Energie Suisse.

Date: December 2021

The GEOTHERMICA is supported by the European Union's HORIZON 2020 programme for research, technological development and demonstration under grant agreement No 731117

1. Introduction

The Bedretto Underground Laboratory for Geoenergies (BULG) is used in the frame of DESTRESS as a demonstration site to prove the feasibility of multi-stage stimulation in granitic rocks. A detailed knowledge of the reservoir initial characteristics is very important to understand the behaviour of the rock mass in the face of the series of tests and treatments carried out during the project. A detailed reservoir characterization is used as an input in different phases of the project:

- To choose the zones to be stimulated.
- To choose the packers sits for hydraulic tests, minifrac tests and stimulation treatments.
- As an input for the Advanced Traffic Light System.
- As a base to formulate hypotheses on the reservoir extent, size and geometry.
- To build numerical models and simulations.
- As an input for the generation of DFN models.

Since it is expected that matrix porosity and permeability are negligible, fluid pathways in a granitic rock mass are expected to be concentrated along and around faults zones and fractures. For this reason, the present analysis focuses on the structural features observed in the sampled volume. Proven techniques in the geological characterization of fractured reservoirs are coupled with classical structural geology analyses in order to build a conceptual model of the BULGG.

The main goal when building a conceptual model is to make a coherent description of a rock volume and its properties. It allows to find coherency in apparent chaotic data, find correlations between different properties, make informed interpolations in sparse datasets, and propose hypotheses for extrapolations outside the sampled volume.

An executive summary has been included as a condensed version of the report where the main results are described. Subsequent chapters are organized by data sources. Chapter first describing a reassessment of fracture data collected in the tunnel walls and presented originally in Jordan (2018).

1.1 Conventions used in this report.

The official name of the Bedretto lab is the Bedretto Underground Lab for Geosciences and Geoenergies (BULGG). Bedretto lab and BULGG are used in this report interchangeably.

All depths in boreholes correspond to measured depth in meters unless stated otherwise.

Image logs are loaded and interpreted in a "high side" reference system. This was necessary as all boreholes are inclined and the reference to the North makes no sense. A High-side reference means that the horizontal axis in the logs represents the angle from the highest line in the borehole. This angle increases clockwise when looking towards the bottom of the borehole (Figure 1). The left, vertical axis of the log represents angle zero (aka. the high side).

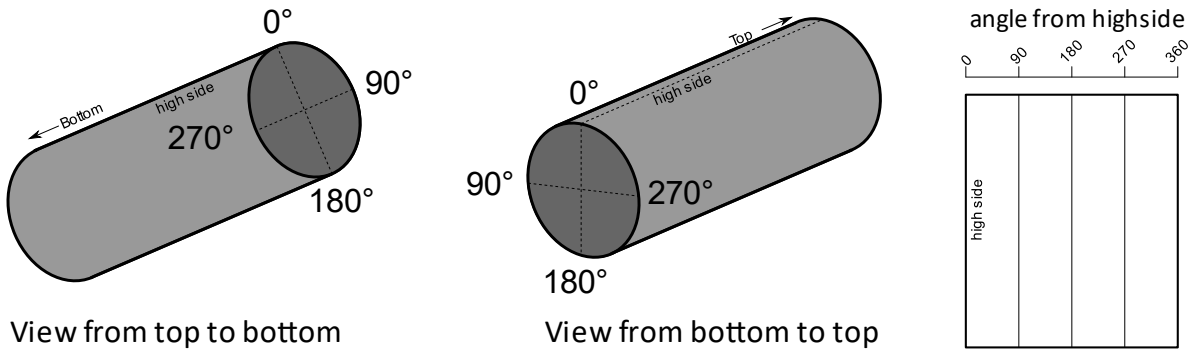

Figure 1. The "High side" of the borehole is the reference used in image logs from deviated wells. When unravelling the image log to display it in 2D, the high side (0°) coincides with the left border of the log. The angle increases clockwise when looking down the borehole.

Borehole orientations are given as azimuth (clockwise angle from north, 0°-360°) and inclination (angle from a vertical axis that is pointing down, 0°-90°). An inclination of 0° corresponds to a vertical borehole while 90° describes a horizontal borehole.

The orientation of planar elements (i.e faults & fractures) is given in strike (clockwise azimuth from north of a horizontal line in the plane) and dip (angle from the horizontal of a line perpendicular to the strike). The right-hand rule is applied, meaning that when standing above the plane and looking in the direction of strike, the dip direction is to the right. This convention uses azimuthal values between 0° and 360° for the strike. Following this convention, the orientation of a plane looks like this: N45°/50° (i.e. a plane which strike is oriented NE-SW and dipping 50° to the SE).

Three different coordinate systems are used in this report (Figure 2). Tunnel metrics (TM) refers to the linear distance along the tunnel measured from a point near the southwestern entrance. These coordinates are in meters and increase linearly towards the Northwest. The BULGG is located between TM 2000-2100. A local cartesian grid has been defined with its origin (0,0,0) at the point of TM 2000. X, Y and Z coordinates in the local grid correspond to Easting, Northing and Up. The entire BULGG lies in positive Northing and negative Easting local coordinates. The third system is the national LV95 coordinate system (EPSG:2056). The local origin and TM 2000 correspond to the following LV95 coordinates:

- *Easting: 2679720.696*
- *Northing: 1151600.128*
- *Elevation: 1485*

CB1, CB2 and CB3 are the original names of the first 3 long boreholes drilled in the BULGG. The cores and most image logging were described and analyzed when this nomenclature was still in place. Later on these wells were enlarged and renamed to MB1, MB2 and MB3 respectively. These names are used here interchangeably.

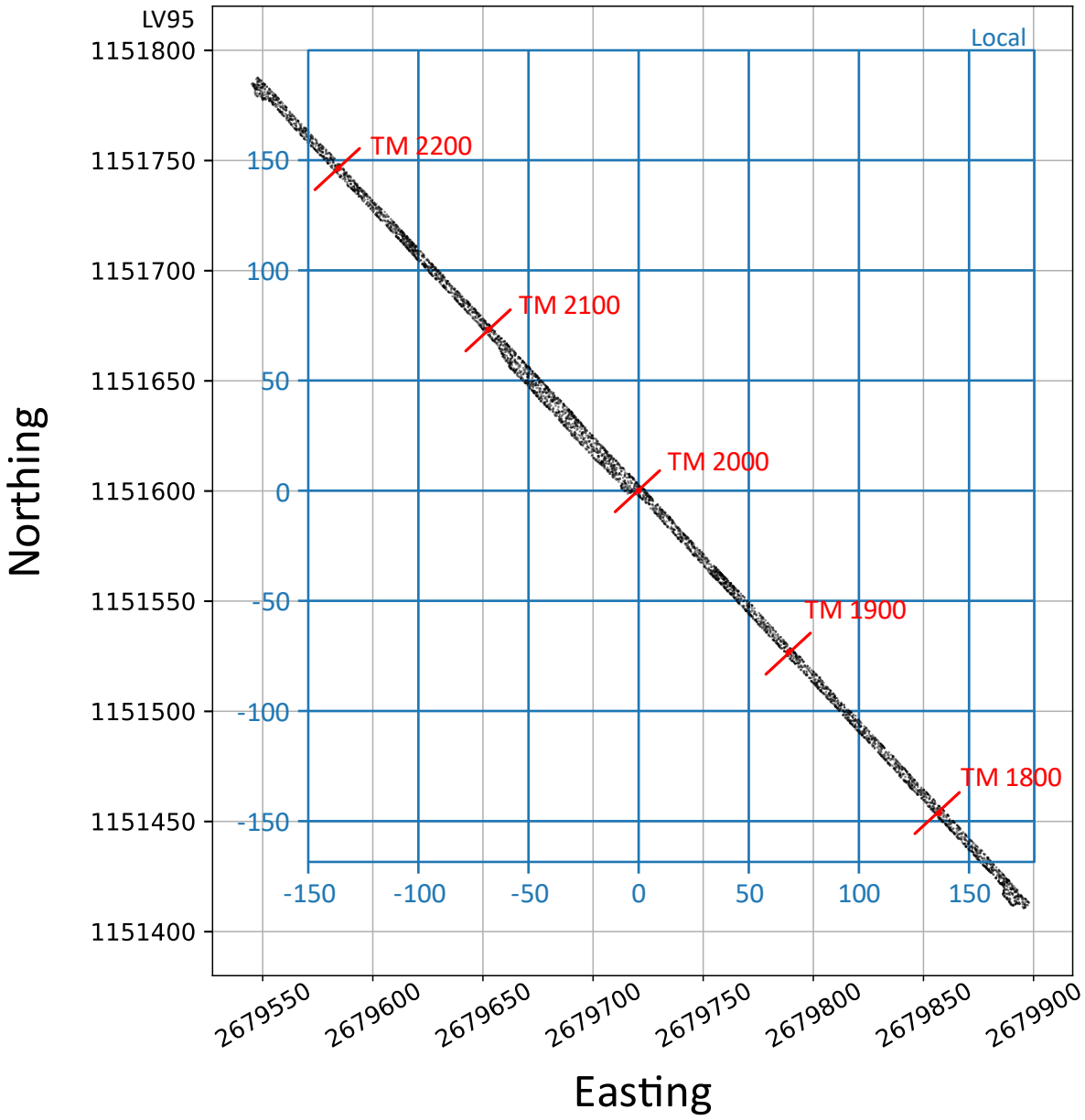

Figure 2. Different reference systems used in this report. The TM coordinates which is measured along the tunnel axis, the Swiss grid (LV95) and a local grid with origin at TM 2000 and aligned with North and East directions. All coordinates are in meters.

Contents

2. Executive summary

Structural data from the Bedretto Underground Laboratory for Geoenergies (BULGG) has been analyzed. This dataset is composed of structures measured in the tunnel wall, core descriptions and the interpretation of image logs along boreholes drilled in the laboratory between 2019 and 2021.

The main objectives of the analysis presented here are:

- To characterize the distribution of structures and propose a consistent scenario where this distribution is understood in the light of structural geology concepts.
- To define units in which main structural parameters are homogenous and characterize the limits of these units.
- Propose a structural conceptual model that will be used as a base line for other analyses concerning for instance the interaction between structure, stress, hydraulics and induced seismicity.

To perform the analysis, different documents were built where parameters such as strike, dip, structure types and fracture frequency were visualized and integrated. Much of the analysis performed here used a classification of structures where a distinction was made between fault zones and generic fractures (Figure 3). This classification has the advantage of being applicable to different sources of information (i.e., tunnel wall, drilling cores, image logs) allowing the integration of all data into a single set.

The main conclusions reached though the analysis presented here are:

- The frequency of structures is, in general, low near the tunnel and it increases after below fault zones FZ-01 and FZ-02. Maximum frequencies are usually found in the mid-section of the boreholes while they decrease gradually towards the bottom (Figure 4).
- The main structure sets in terms of orientations are (from higher to lower occurrence) (Figure 5):
    - NE-SW to E-W dipping to the North.
    - North-South dipping to the West.
    - NW-SE dipping both to the NE and SW.
- 90% of identified fault zones (i.e 69 out of 74) belong to the NE-SW oriented set (Figure 6).
- Fault zones were correlated across boreholes. A total of 15 connected fault zones were identified (Figure 7).

In contrast with the constant orientation of fault zones, the dominant orientation of fractures changes across the BULGG. Based on these changes, the BULGG can be divided into 4 units according to the dominant orientation of fractures. These units are bounded by some

of the fault zones correlated across the boreholes (

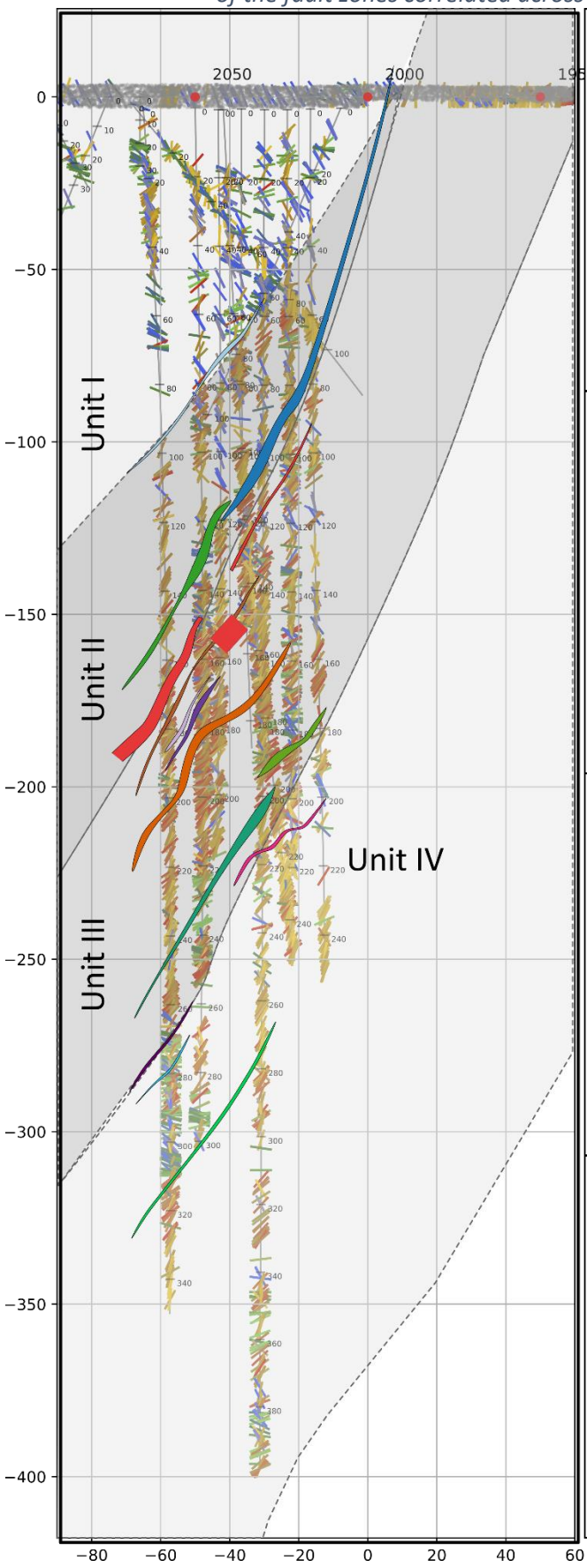

Unit I:
- Above Fz-01.
- N-S fractures are dominant.
- Consistency btw tunnel and BHs.

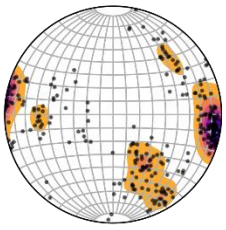

Unit II:
- Between Fz-01 and "Bad Boy".
- Transitional between N-S and NE-SW fractures.

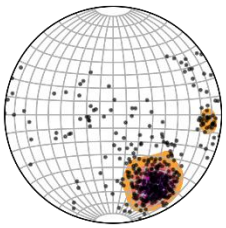

Unit III:
- Between "Bad Boy" and Fz-11 & 12.
- Fractures oriented NE-SW are clearly dominant.

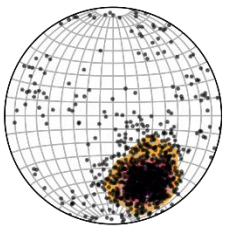

Unit IV:
- Bellow Fz-11 & 12.
- NE-SW fractures still dominant but NW-SE direction is more frequent than above.

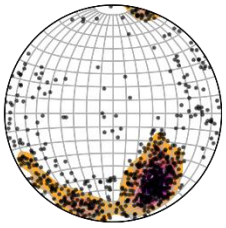

- Figure 8):
    - Unit I: This unit includes the BULGG section of the tunnel and the shallowest section of the boreholes. The dominant fracture orientation is N-S. The lower limit of this unit is a fault zone (FZ_1).
    - Unit II: Includes the volume between FZ_1 and the fault known as the "Bad Boy" (FZ_2 and FZ_3). It is a transitional unit where the orientation N-S becomes less frequent while fractures oriented NE-SW become more frequent.
    - Unit III: Unit below the "Bad Boy". Most fractures are oriented NE-SW.
    - Unit IV: Located towards the bottom of the boreholes. The NE-SW orientation is still dominant, but the NW-SE orientation becomes relatively more important.
- A conceptual structural model of the BULGG is proposed in which fault surfaces of around 30-200m length constitute the boundaries of structural units. Each one of these structural units presents a dominant fracture orientation. The structural units are around 100-200m thick. The orientation of fractures in units II and III are greatly influenced by the orientation of the main fault surfaces while the orientations in units I and IV are somewhat different.
- Some implications of this conceptual model are:
    - The orientation of main fault zones is unimodal. This is important to consider if fault zones constitute boundaries or pathways to fluid flow.
    - If the background fractures are in some way influencing fluid flow then it is expected that the interactions fluid flow-structure are different in distinct structural units.
    - Fault zones and generic fractures are expected to behave differently because they have inherently different properties. In addition, the differing distribution of orientations is expected to accentuate these differences and influence of the interactions between structure and other reservoir parameters.

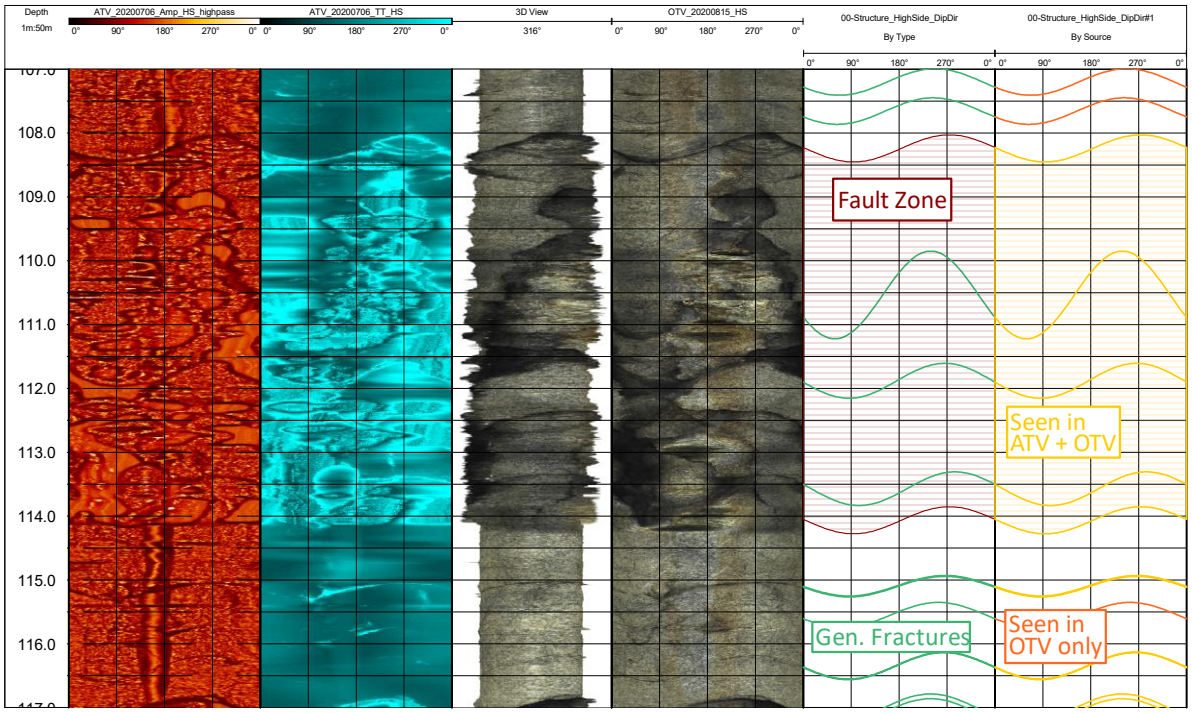

Figure 3. Example of image logging data. From left to right: Amplitude from the ATV (red), travel time from the ATV (blue), 3D representation from the borehole built with a computed caliper (from the travel time) and the OTV image wrapped around, OTV RGB image. The interpretationof structures is shown twice. Structures were clasified by their nature (Fault zones vs. Generic fractures) and by the data source (Seen on ATV+OTV vs. OTV only).

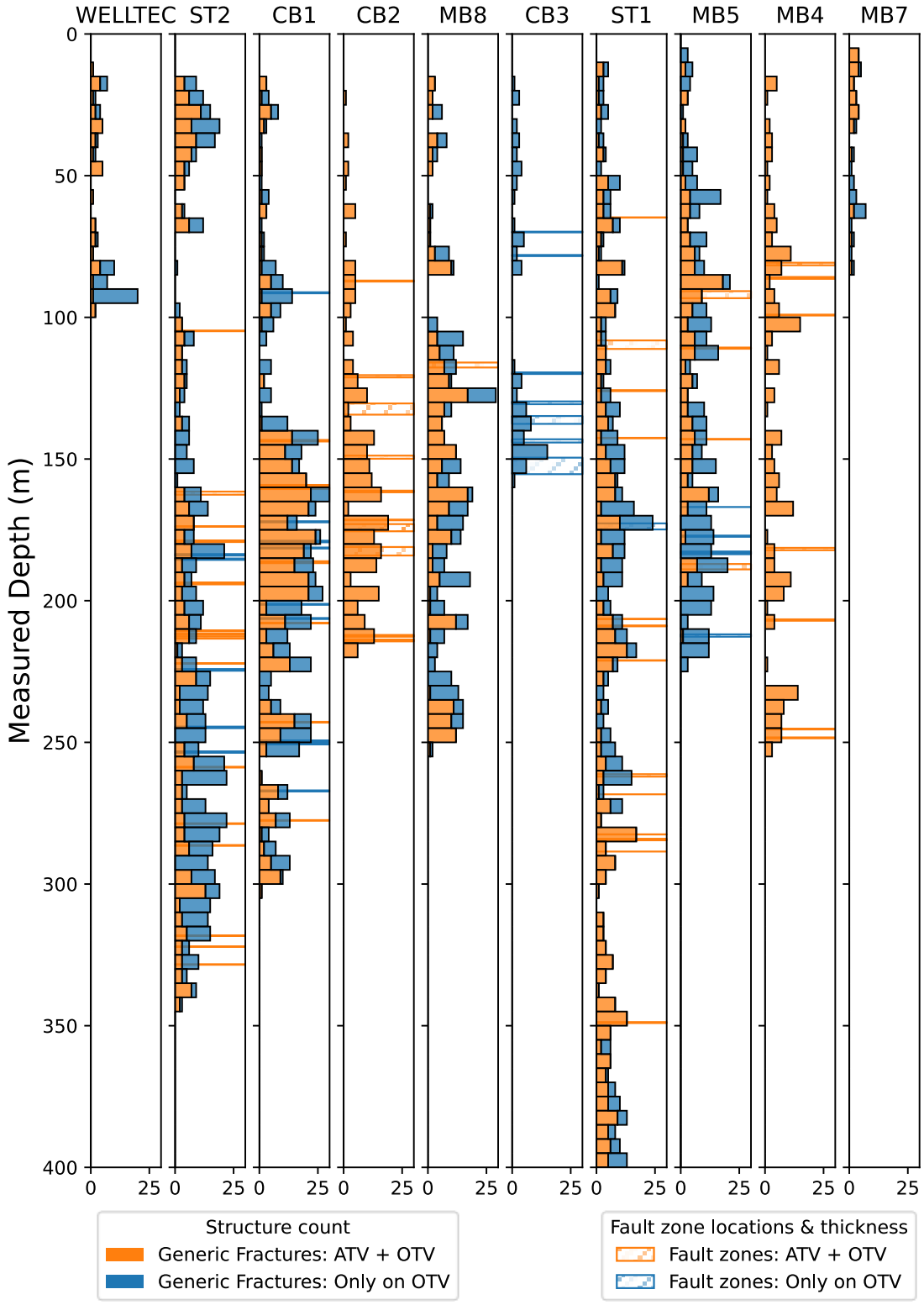

Figure 4. Structures count in bins of 3m along the boreholes. Hatched polygons show the location and thickness of fault zones.

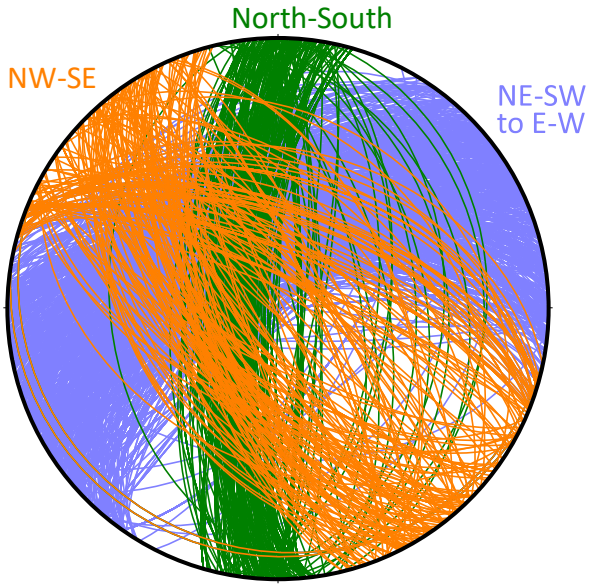

Figure 5. Stereonet projection of all structures in the structural dataset. The three main orientations are shown.

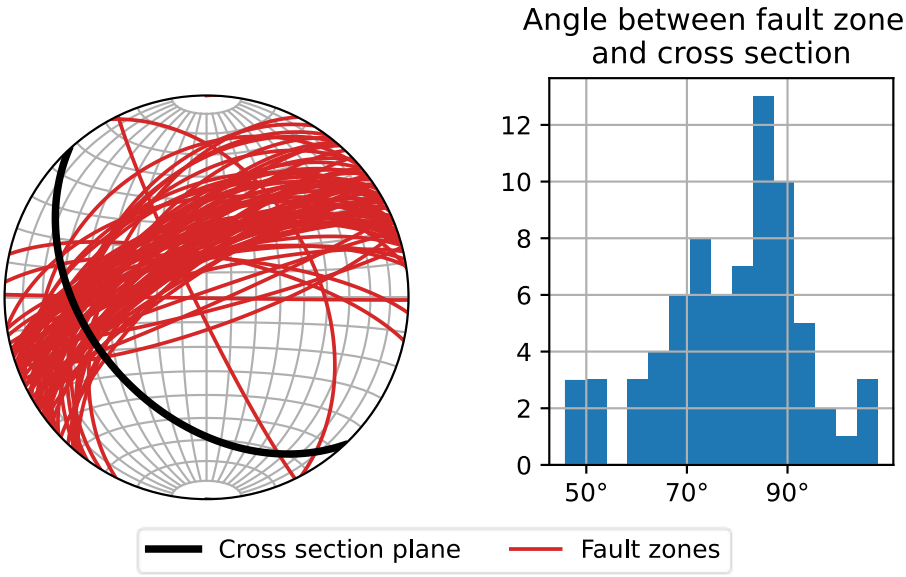

Figure 6. 90% of fault zones (69 out of 74) are oriented NE-SW and are perpendicular to a plane oriented N137°/42°.

Figure 7. Next page. Correlation of fault zones across boreholes in the BULGG. The fault zones are built using markers from the interpretation of borehole image logs and GPR images for each borehole. This view is inclined 48° downwards and is perpendicular to the cross-section plane shown in Figure 6.

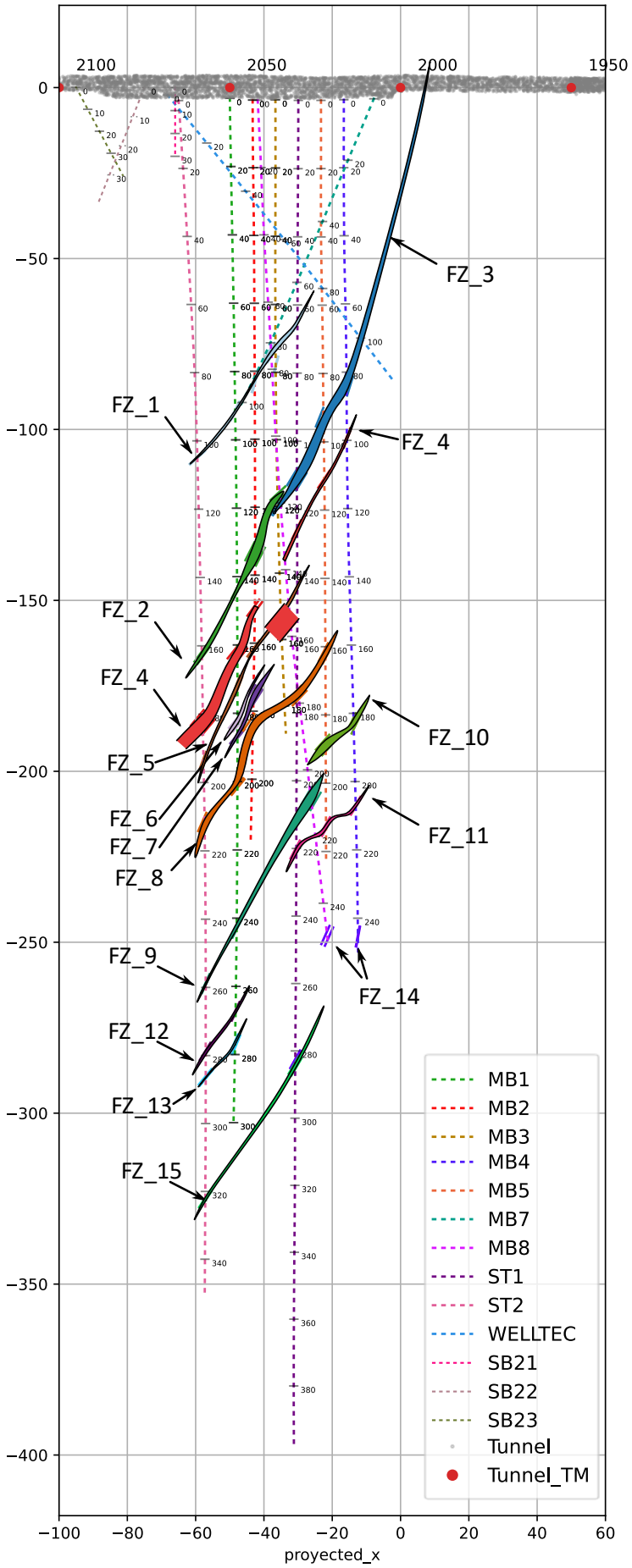

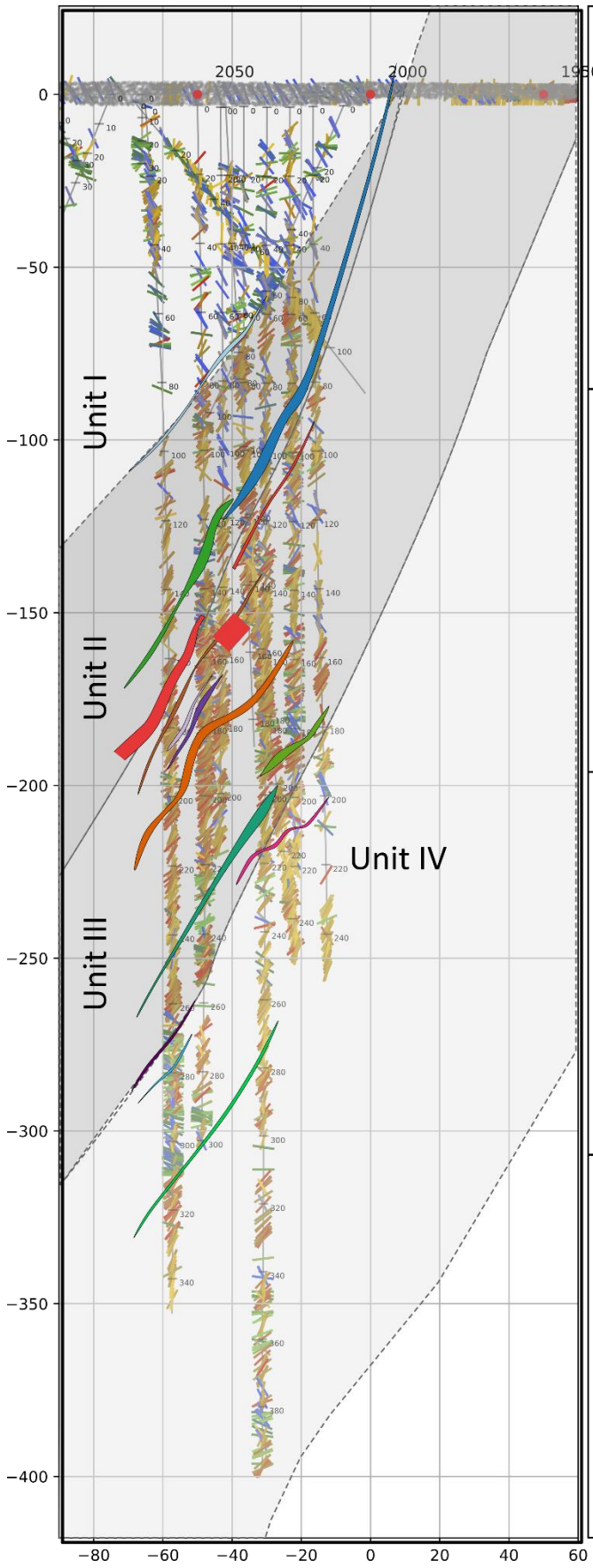

Unit I:
- Above Fz-01.
- N-S fractures are dominant.
- Consistency btw tunnel and BHs.

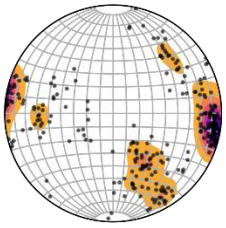

Unit II:
- Between Fz-01 and "Bad Boy".
- Transitional between N-S and NE-SW fractures.

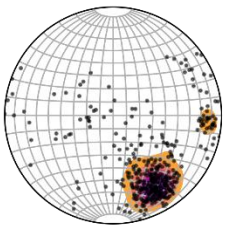

Unit III:
- Between "Bad Boy" and Fz-11 & 12.
- Fractures oriented NE-SW are clearly dominant.

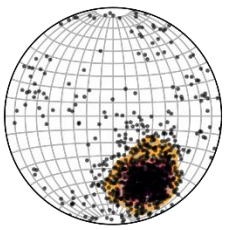

Unit IV:
- Bellow Fz-11 & 12.
- NE-SW fractures still dominant but NW-SE direction is more frequent than above.

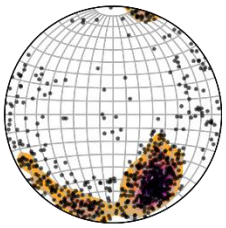

Figure 8. Previous page. Structural units defined in the BULGG based on dominant fracture orientations and bounded by fault zones.

Figure 9. Next page. Map showing fractures measured along tunnel and long boreholes in the BULGG. Structures are colored by their strike. It can be clearly seen that N-S fractures (blue) are dominant close to the tunnel while NE-SW to E-W (yellowish and red) are dominant in the mid sections of the boreholes. SE-NW fractures (green) are mostly seen towards the bottom of the boreholes.

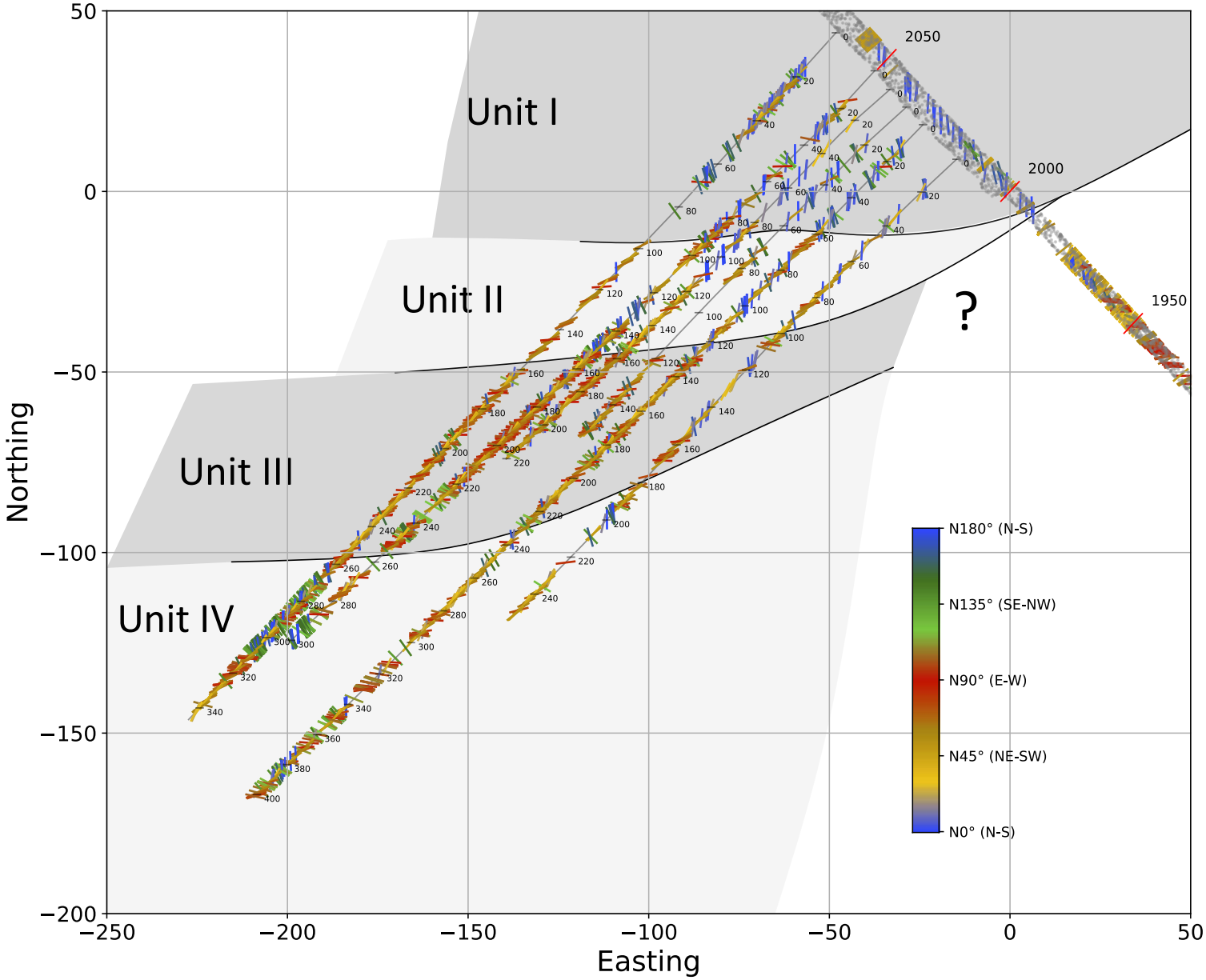

3. The Bedretto Lab for Geosciences and Geoenergies (BULGG)

The Bedretto Lab for Geosciences and Geoenergies is located inside the Bedretto tunnel in the Canton of Ticino, Switzerland. Originally built as a service gallery during the construction of the Furka tunnel, the Bedretto tunnel has been repurposed by the ETH Zurich to build an underground laboratory. The main goal of the BULGG is to:

"Study, in close collaboration with national and international partners, techniques and procedures for a safe, efficient, and sustainable use of geothermal heat"

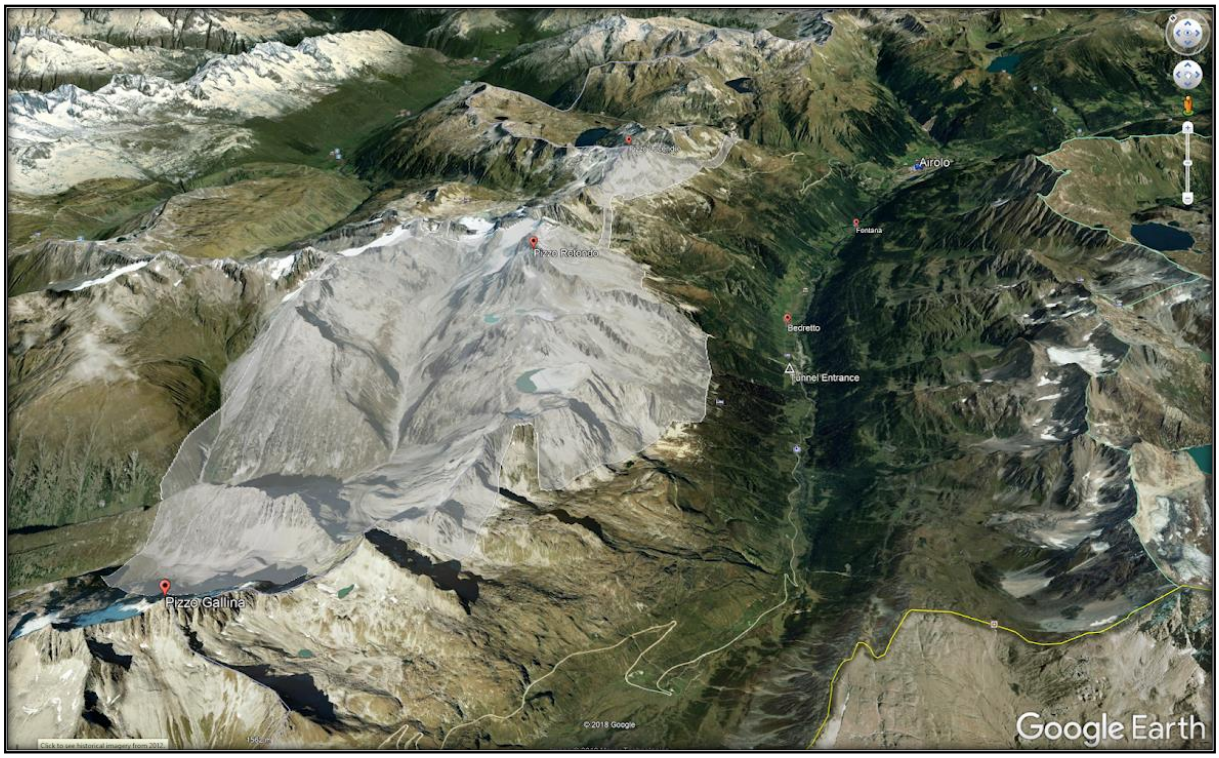

Figure 10. Oblique view satelite images and DEM depicting part of the Gotthard massif. The image shows the Bedretto Valley, the Bedretto tunnel entrance and the outcrop of the Ronco Granite (white patch). The BULGG is located inside the Bedretto tunnel entirely inside the Ronco Granite. View towards the NE.

The Bedretto tunnel runs from its southeastern entrance in the Val Bedretto, to its intersection with the Furka Base tunnel, approximately 5km to the Northwest. The BULGG is located at around 2 km from the south entrance of the tunnel (Figure 11). The BULGG sits entirely inside the Rotondo Granite, a magmatic body that intruded Archean gneissic terrains during the Permian.

3.1 Geological Setting

The BULGG is located in the Gotthard Massif which is part of the External Crystalline Massifs of the Central Alps (ECM). The ECM represent the pre-Mesozoic European basement and consist of Precambrian metamorphic units and Precambrian to Paleozoic sedimentary, volcanic, and plutonic rocks (Debon & Lemmet, 1999).

A major collisional, mountain-forming event (the Variscan Orogeny) took place towards the end of the Paleozoic. This process was associated with intense deformation, thickening of the continental crust and the formation of important topographic relief. Towards the end of this orogeny, the collapse of the thickened crust (i.e., post-orogenic collapse) induced a state of extensional tectonics, a relative thinning of the crust and the emplacement of alkaline plutons (Pfiffner, 2010). The BULGG is located inside one of these alkaline plutons (i.e., the Rotondo Granite), which was emplaced towards the end of the Variscan Orogeny. The intrusion of the Rotondo Granite has been dated at 294.3±1.1 (Sergeev and Steiger 1995).

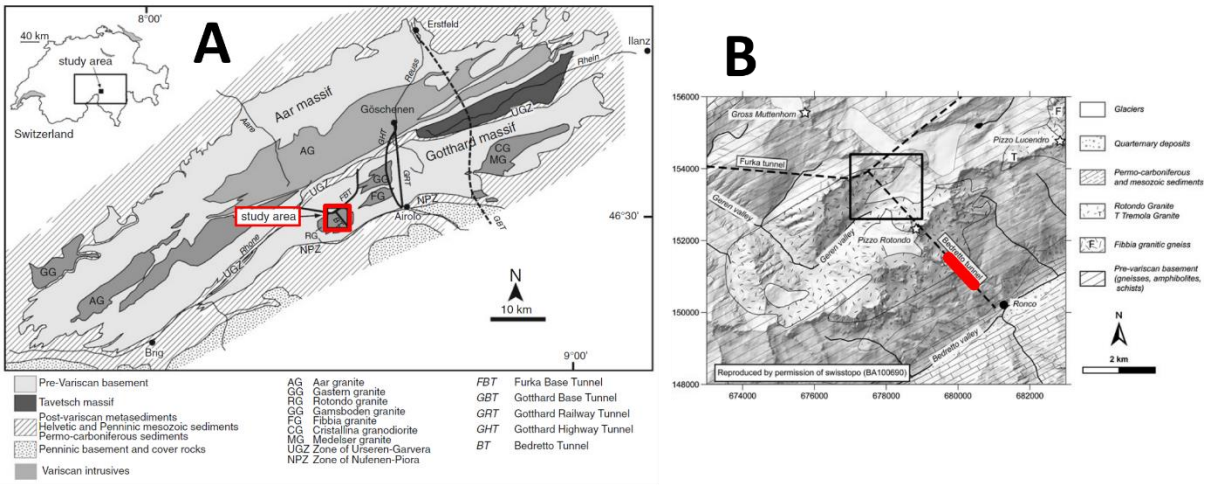

Figure 11. A) Location map and simplified geological map of the Aar and Gotthard massifs, B) Zoom on the Bedretto tunnel trajectory and approximate location of the section studied in this report, C) Schematic cross section along the Bedretto tunnel. A and B from Lützenkirchen & Loew (2011) and C from from Jordan (2018).

The Rotondo granite is composed of 29.9% quartz, 5.2% of mafic minerals and 64.9% of feldspars (Debon & Lemmet, 1999). This composition places it in the broad group of granites. When a QAP diagram is considered, the Rotondo Granite falls into the group of Syenogranites. This means that its Feldspars are mainly in the alkali series and it has relatively lower amounts of Plagioclase.

The deformation patterns of the Rotondo Granite are significantly different from other granitoids of the Gotthard Massif. The Fibbia and Gambsboden granites present a homogeneous deformation characterized by the presence of foliation (schistocity) planes. Due to this distributed deformation,

the Fibbia and Gambsboden granites are often qualified as orthogneisses (i.e., igneous rocks that have undergone some degree of metamorphism). The Rotondo granite presents a generally massive aspect (i.e., less foliated) and the rare, foliated zones are usually concentrated around individual shear zones. Based on the measurement of structural features in the field, Marquer (1990) reported that the deformation that affected the Fibbia orthogneiss might have been more shearing dominant with respect to those processes that affected the Rotondo granite. A generally accepted explanation for these differences is that the slightly older Fibia and Gamsboden intrusions were affected by a late Variscan deformation phase that predated the emplacement of the Rotondo granite.

3.2 General configuration of the BULGG

The BULGG is in an enlarged section of the tunnel between coordinates TM 2000 and 2100 (Figure 2). At the time this report is written a total of 16 boreholes had been drilled in the BULGG. Six short boreholes which lengths range between 30 and 40m were drilled in 2018. 10 long boreholes ranging between 102 and 400m long were drilled between 2019 and 2021 (Table 1). The 10 long boreholes have been drilled towards the south-west side of the lab with initial inclination angles (from vertical) around 39°-81° (Figure 13).

Table 1.

Borehole	*Easting (m; LV95)*	*Northing (m; LV95)*	*Elevation (m)*	*Total Depth (MD m)*	*Local X (m)*	*Local Y (m)*
Short boreholes						
SB1-1	2679891	1151417	1483.4	30	170.5	-182.838
SB2-1	2679676	1151648	1484.95	30	-45.012	48.269
SB2-2	2679670	1151655	1485	40	-51.15	54.852
SB2-3	2679656	1151670	1485.1	40	-64.79	69.479
SB3-1	2679550	1151783	1486.1	30	-170.5	182.838
SB4-1	2679625	1151703	1485.47	30	-95.48	102.39
Long boreholes						
CB1 (MB1)	2679683	1151634	1485.41	301	-37.436	33.432
CB2 (MB2)	2679687	1151628	1485.12	220	-33.216	28.252
CB3 (MB3)	2679692	1151624	1485.28	191	-28.666	23.372
MB4	2679706	1151609	1484.96	251	-14.796	8.902
MB5	2679701	1151614	1485.03	222	-19.583	13.593
MB7	2679712	1151603	1485.37	102	-8.795	2.5
MB8	2679689	1151627	1485.49	252	-32.172,	27.193
ST1	2679697	1151619	1484.91	402	-24.066	18.492
ST2	2679673	1151644	1485.41	350	-48.186	43.932
WELLTEC	2679671	1151647	1486.42	118	-49.61	46.994

Figure 12. View inside the tunnel. Source: https://www.wernersiemens-stiftung.ch/en/projects/bedretto-underground-lab/. Accessed on 05/02/2021

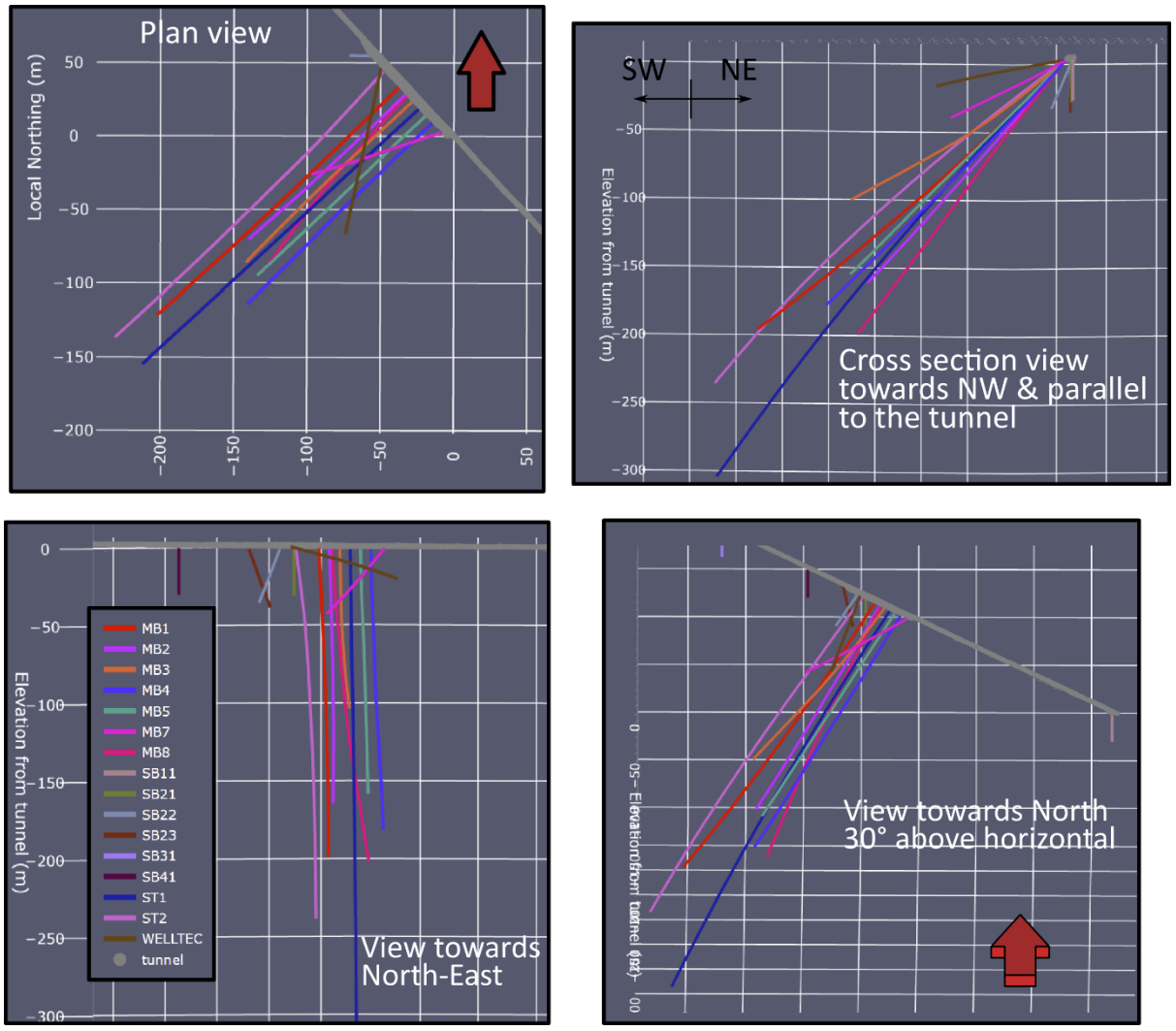

Figure 13. 3D views of the Bedretto lab. Most experiments in the Bedretto lab are concentrated in an enlarged section of the Bedretto tunnel located between TM 2000 and TM 2100. All ten long boreholes drilled so far were drilled from this section of the tunnel and towards the southwest. The plunge (angle from horizontal) of the log boreholes is variable between 9° and 51°.

4. Tunnel Wall Structure Analysis

4.1 Summary

- The best available database of structures from the tunnel walls is a set of measurements made with a laser survey. This measurement method determines the position of several points that lie on well exposed fracture surfaces in the tunnel. A plane for each structure is reconstructed using the least square method.
- This database is strongly biased towards big structures as small and medium sized structures with poor exposure cannot be measured.

- The analysis of this biased database shows that structures are distributed in clusters segregated by their orientation and position and, to a lesser extent, their spacing.
- Each cluster forms a rather homogenous unit with one or two dominant structural orientation.
- The dominant main structural orientations found in this database are 1) East-West, 2) NE-SW and, 2) North-South.
- The limits of these clusters coincide approximately with limits in fracture frequency.
- Based on this analysis it seems that the highest fracture frequencies are found in domains where the dominant fracture orientation is North-South.
- The fracture frequencies obtained using this database concern only the "big" structures measured by the surveyor and cannot be easily linked to the databases built on borehole data which are much more systematic and include small-scale structures.
- The tunnel section corresponding to the BULGG sits in one of these segments dominated by North-South structures with a relatively high fracture frequency.

4.2 Existing structural databases from the tunnel wall

Four different structural datasets exist in the Bedretto tunnel between the southern entrance and TM 3000. The methodologies used to gather these 4 databases differ considerably and they cannot be easily integrated. The description of each dataset and a discussion on their differences is important to establish the advantages and limitations of each one. The choice regarding which dataset was used to develop the structural analysis of the tunnel walls is derived from this discussion.

4.2.1 Laser scan

The first database was reconstructed using points measured by a laser survey in the tunnel wall. The survey was carried out by Flotron AG in April 2019 and measured a total of 1071 points on 243 surfaces. For each structure, the 3D position of several points was determined. The number of points measured at each station is variable with 4 points per station being most frequent (Figure 14). Stations with less than 3 points were skipped in the plane fitting process. A least squares algorithm was used to reconstruct the structure planes and obtain their position and orientation. Plane fits are generally good with residuals being very small in most cases (Figure 15). Only big persistent structures can be measured using this system, so this database is strongly biased and the medium to small size fractures are underrepresented.

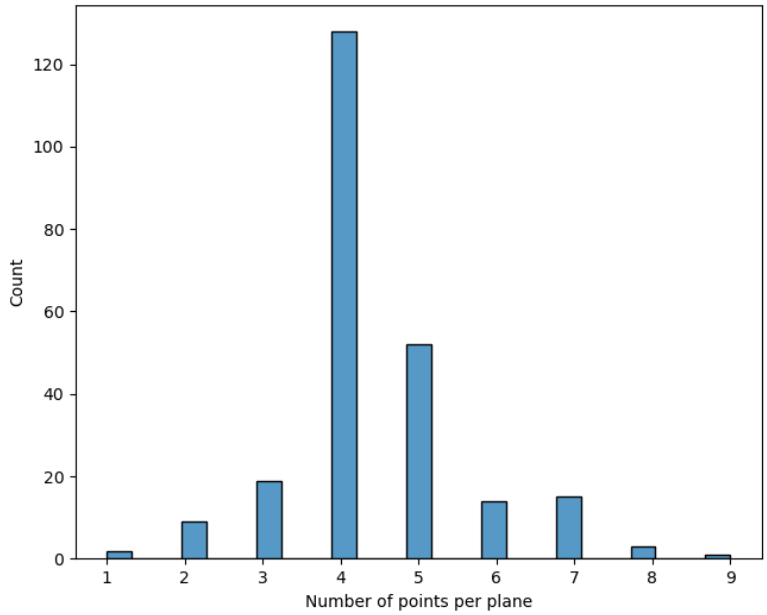

Figure 14. Histogram of number of points available to fit a plane in the laser survey database.

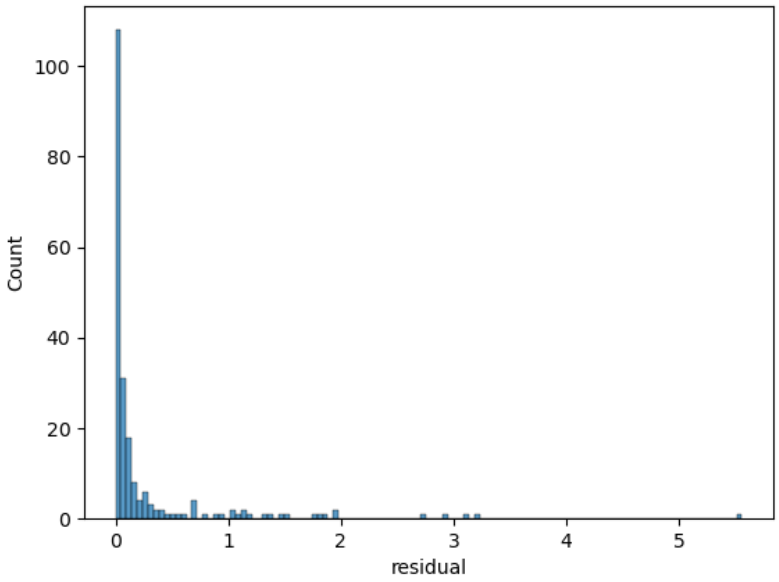

Figure 15. Histogram of residual values for planes fitted to points measured in the laser survey.

4.2.2 Jordan (2019)

The second database was made in the framework of an ETH Master thesis during a first attempt of structural characterization of the BULGG. The method used to build this database is not clear. Data collection was not systematic. A plot of fracture occurrence and orientations (**Error! Reference s ource not found.**B) shows clearly that clusters with high fracture density and constant fracture spacing have been "forced" into the database. A general overview of fracture occurrences along the

tunnel (Figure 16) shows that this and the surveyor database can be correlated but a 10m shift must be applied. Despite its forced clustered look at a small scale, a similar behaviour with the surveyed database is observed when comparing normalized fracture frequencies (Figure 19).

4.2.3 Rast (2020)

This database is an updated version of the database from Lützenkirchen (2002) and includes measurements of foliation, mineral lineations, incohesive shear zones and ductile shear zones. Only the incohesive and ductile shear zones are included in the present comparison.

4.2.4 GES

This structural database was built by measuring systematically all fractures observed in the tunnel wall. This method is more accurate that the other two presented above but it is very time-consuming (approx. 30m of tunnel covered per day) and not suitable to survey long segments of the tunnel.

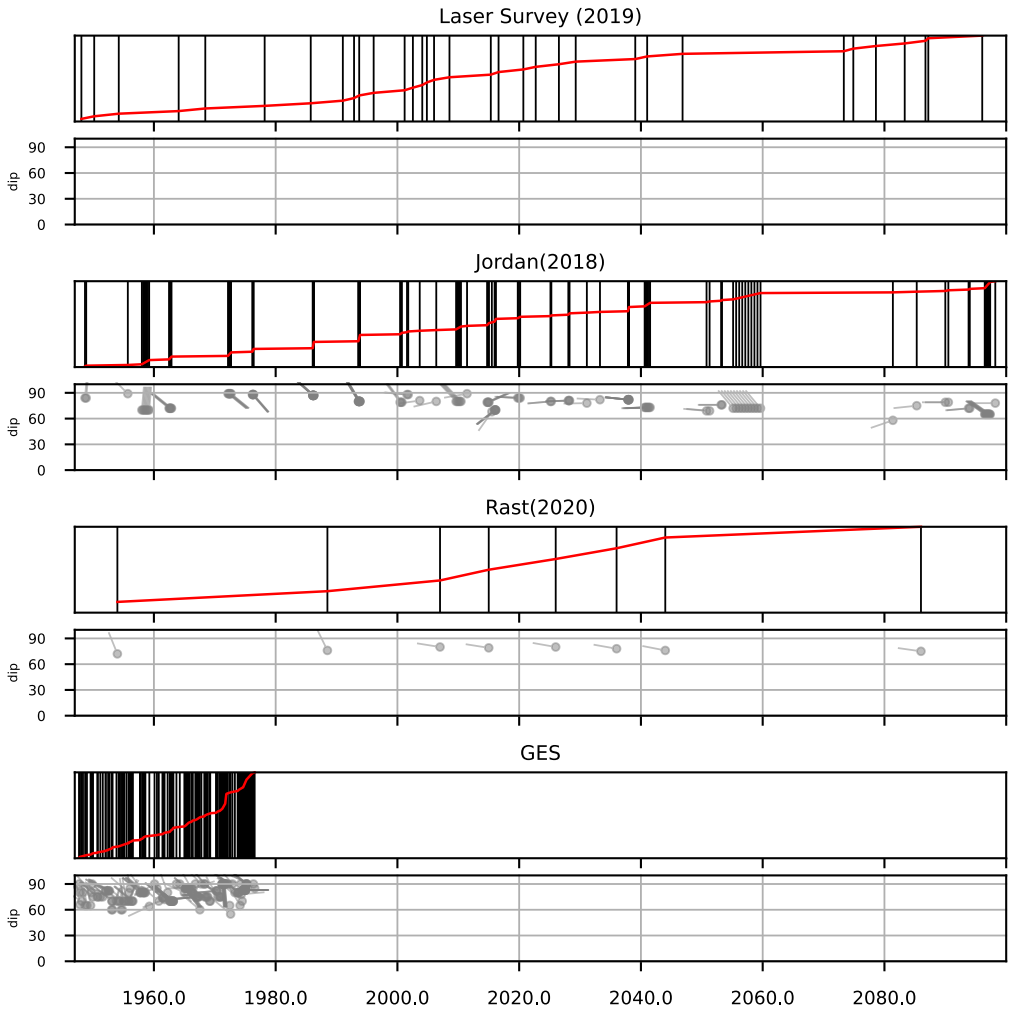

Figure 16. Four different tunnel wall structural datasets available in the BULGG.

4.2.5 Choosing a dataset

Based on the observations outlined above, the database of planes fitted to laser-surveyed points was chosen to carry out a structural analysis of the tunnel walls. Despite its strongly biased character, this database is the most complete of all 4 sets considered here. Unfortunately, this dataset lacks any kind of feature description, so it is impossible to establish a classification based on structural characteristics. The analysis presented here is therefore based only on geometrical considerations.

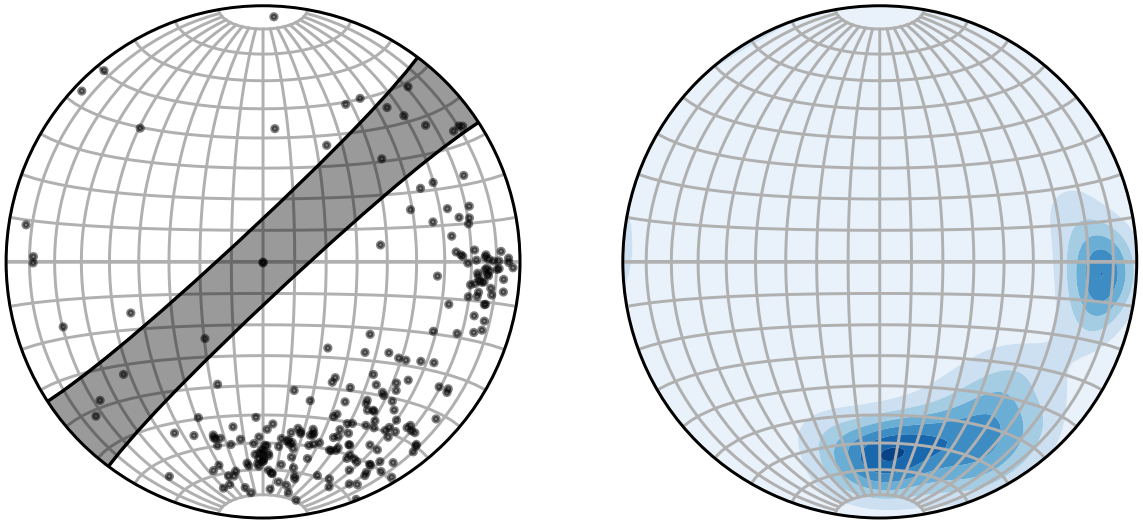

Figure 17. Poles of the fracture planes measured on the tunnel walls by a laser survey. Two main orientation sets can be seen: A fisrt set oriented NE-SW to E-W and a second set less important (in terms of number of fractures) oriented N-S.

4.3 Structure orientations

Stereonet plots show the dominant strike orientations of structures in the tunnel wall: 1) East-West, 2) NE-SW and, 2) North-South. Structures are usually steep, and most dip values are above 70°. The grayed area corresponds to structures that are subparallel to the tunnel within a 20° range. The density of poles inside the grayed area is expected to be low because these orientations are subparallel to the tunnel (orientation bias).

4.4 Cross-cutting relationships

Measurements performed in the field did not include any cross-cutting relationship. This aspect was examined using image log data and will be discussed in the chapter 6 Structural Analysis of Image Logs.

4.5 Distribution of structures

A strike walkout diagram shows the distribution and potential clustering of orientation sets in the measured structures (Figure 18). Eight segments can be identified where the dominant orientation shifts repeatedly from East-West/NE-SW to North-South. The BULGG sits entirely in a section dominated by North-South structures.

The segments with a dominant structural orientation shown in Figure 18 are compared to the fracture frequency along the tunnel in Figure 19. All three segments where the North-South orientation is dominant sit in places where fracture frequency is high. Four out of five segments where the structural orientation is East-West/NE-SW sit in places of reduced fracture frequency, the exception being the segment between 2800 and 3000m TM. The BULGG (grayed area) is characterized by a clearly dominant N-S orientation and the transition from medium to low fracture frequency.

Figure 18. (Next page) Walkout strike plot for fractures in the surveyor database. Values given in meters correspond to TM coordinates along the tunnel.

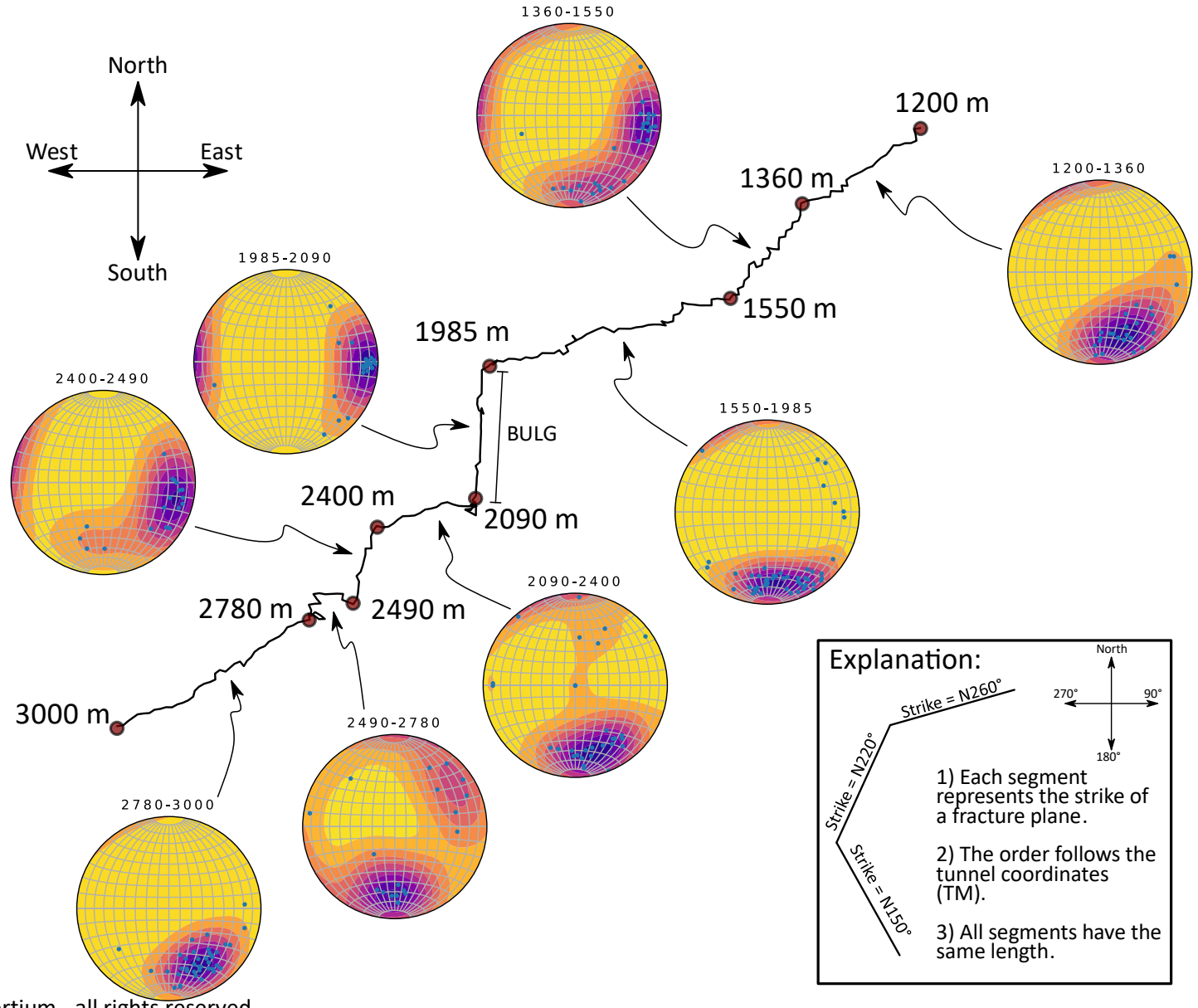

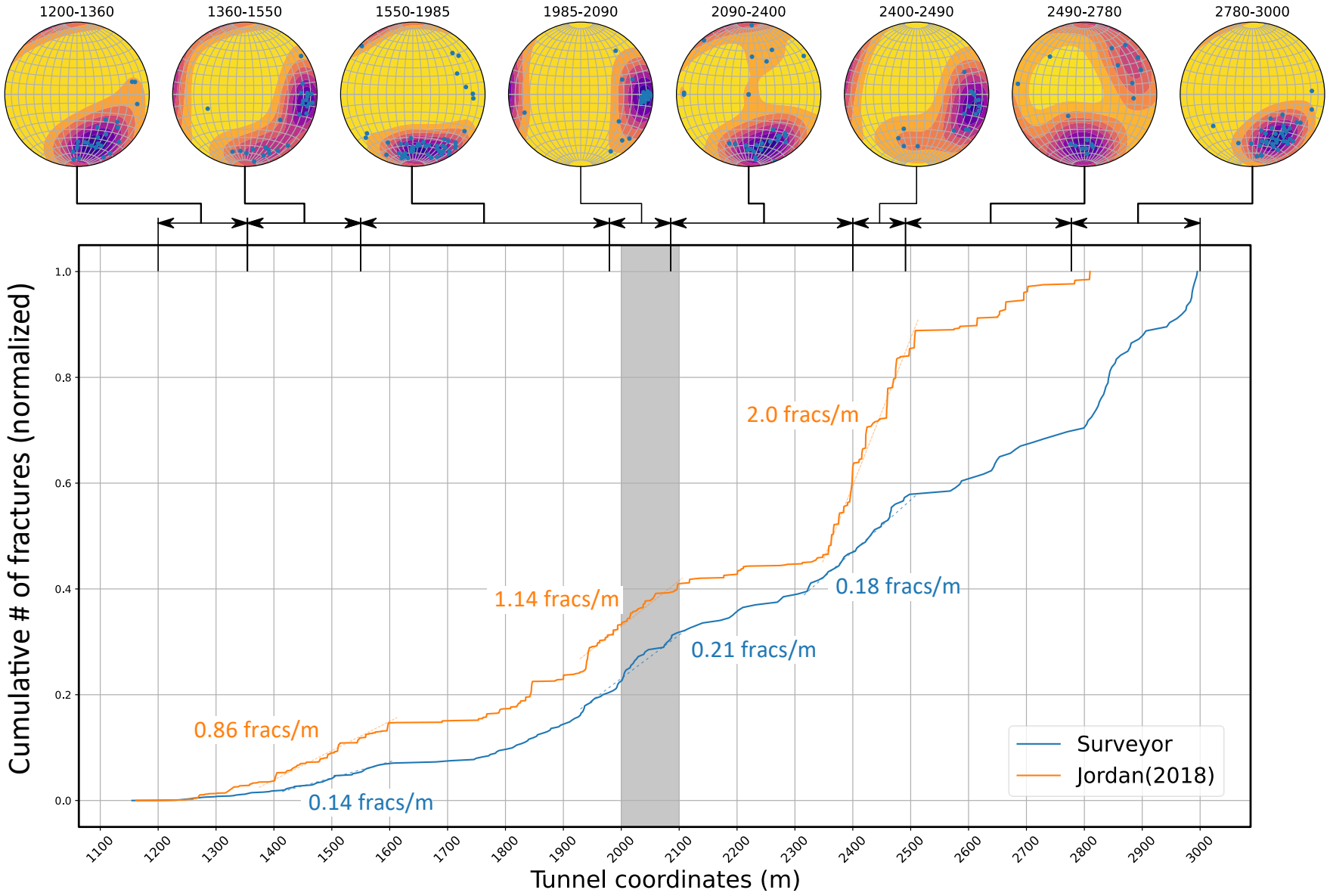

Figure 19. Previous page. Structure orientation vs. frequency.

It might seem paradoxical that overall, North-South fractures which are present in lesser numbers (Figure 17) coincide with segments of higher fracture frequency (Figure 19). But these segments of higher frequency tend to be shorter, so despite the higher frequency of structures they contain less total structures than other segments where East-West and NE-SW structures are dominant.

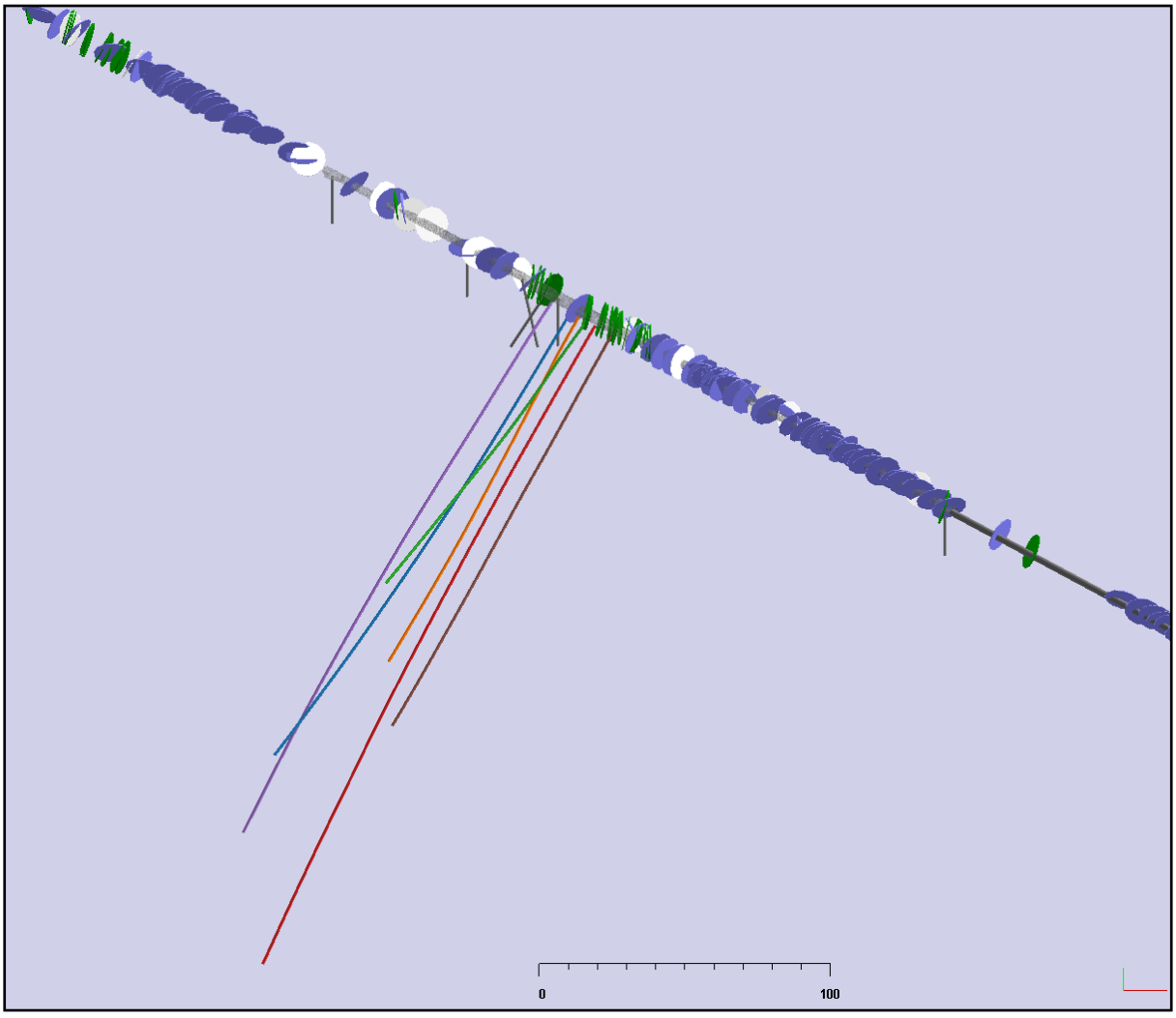

Figure 20. Zoomed 3D view of the BULGG with the surveyor fracture dataset (disks) colored by strike. Purple disks (E-W or NE-SW planes). Green disks (N-S planes). White disks (other orientations). Fractures with a N-S strike (green disks) are dominant in the BULGG.

5. Core description and analysis

5.1 Summary of main observations on drillcore structures

More than 700m of core were recovered during drilling of CB1, CB2 and CB3 boreholes. These cores were described to establish a classification of structures (Figure 21) and their distribution along the boreholes (Figure 23). The description also allowed the identification of individual fault zones (Figure 22) and their upscaling. A composite log (Figure 23 and Appendix 26) was built with the core description and the orientation of structures extracted from the interpretation of image logs (cf. Structural interpretation of image logs report).

The resulting model proposed for the BULGG is composed of a shallow section between MD 0m and 80m dominated by dykes (mostly aplitic dykes) and isolated shear fractures. In general, this shallow section of the cores has the aspect of a rather intact and tight rock with very few deformation features. Deformation is more intense between 120m and 200m MD where most individual fault zones have been identified. These faults zones are composed of multiple branches of anastomosing individual fault cores. The grouping of anastomosing fault cores and damage zones allows the upscaling of deformation and the proposition of complex fault zones with thicknesses ranging between 5-40 meters. Below MD 200m deformation seems to diminish as fault zones are fewer and thinner than in the section above.

The distribution of orientations show that fault zones are dominantly oriented NE-SW while the structures outside these zones show other orientations like N-S and NW-SE.

5.2 Methodology

Around 700 m of unoriented drillcore were recovered from CB1, CB2 and CB3 boreholes. The cores were cut in sections measuring 1 meter and disposed in wooden boxes containing 4 sections, totaling 4m of core per box. The cores were described to define a typology of structures present in the Bedretto lab. The description focused on structural features while very few observations were done on the petrological and mineralogical characteristics of the rock.

Structures were reported into a field notebook on a scale equivalent to 1:200m meaning that each 1-meter section of drillcore was represented in a 5mm section of the notebook. In practical terms this means that structures were not reported in a systematic way, especially in sections of high structure density. The criteria to describe sections with high structural density were:

- In sections with more than 5-6 structures per meter the choice was made to report only the most important features.
- If the density was higher than 15-20 structures per meter the whole section was described as characterized by fracture cleavage if structures were parallel, or crackle breccia if the orientations seemed more chaotic.

Despite these simplifications, the generated core log reflects the overall distribution of structures in the drilled volume and allows us to establish a hierarchy of the observed features.

5.3 Structure's typology

The main structures found during the core's description were (Figure 21):

- **Shear fractures:** The most common structures found in the core. Small structures with thickness between 1 mm and 5 mm, internal filling by a dark mineral (biotite?) and evidence of shear displacement. These structures are most often closed but the core is sometimes split along their surface. Slickenlines are often observed when the surface of these structures is exposed. Other shear indicators are often seen like the displacement of markers or relay zones with restraining or releasing structures.
- **Aplytic dykes:** Most observed in the shallowest depths of the boreholes. Thickness is usually of several centimeters.
- **Mylonites:** Zones intensively deformed and foliated. The original granitic fabric has completely disappeared. Foliation is formed mainly by bands of dark minerals (biotite) intercalated with porphyroblasts of clear color (K-Feldspar?).
- **Rugose fractures:** Fractures that contrast with the ones described as "Shear Fractures" by the rugose appearance of their surface. This rugosity is often associated to vuggy porosity and the precipitation of secondary minerals. The core is very often split along these rugose surfaces exposing the nature of these secondary minerals (Quartz, Stilbite, etc) which develop crystals of up to several centimeters.
- **Crackle breccia:** crackle breccias are defined in the literature as tectonic breccias composed almost exclusively by clasts and lacking a matrix component (Woodcock and Mort, 2008). In the present work, we have assigned the name crackle breccia to intensively fractured sections of the core where the fractures do not seem to present a coherent orientation. The sections where the core integrity has remained where called "Closed crackle breccia" while the sections where the core was disassembled were called "Open crackle breccia".
- **Fault zones:** Zones of concentrated deformation from several centimeters to several meters thick. The basic characteristics of fault zones are variable as they can be constituted by several other structures in different numbers and combinations. No cataclasite or fault gauge zones were recognized in the cores although they were suspected to be present in zones where only disaggregated rock was recovered during the coring process. Observations in image logs made after the core description seem to confirm the presence of these fault rocks in zones where the core is missing.

  Fault zones often show the coexistence of ductile deformation features (c-s fabric, foliation, deformed porphyroblasts, pressure shadows, etc) and brittle structures (shear fractures with slickensided surfaces, crackle breccia).

Figure 21. Main structural cathegories found in the description of the cores extracted during the drilling of CB1, CB2 and CB3. The most common structures found are shear fractures.

5.4 Fault zones

Fault zones were identified as the combination of several features that indicate a considerable increase and concentration of deformation. For instance, an increase in shear fracture density and

the presence of a mylonitic section were factors observed often in the core description and used to identify individual fault zones.

The presence of fault rocks was another factor used to infer the presence of fault zones. We have chosen to use the fault rock classification proposed by Woodcock and Mort (2008) (Appendix 1). The 700m of recovered drillcore lack completely of fine-grained brittle fault rocks (i.e., cataclasite and fault gouge). This observation is contrasting with the fault zone descriptions made in the tunnel wall, were these kind or rocks are commonly observed. The only fault rocks identified in the 700m of described drillcore were Crackle Breccias and Mylonites. The lack of fault gouges and cataclasites is most probably due to the core not being preserved in these poorly consolidated sections.

The classical model of Fault Core-Damage zone proposed by Chester et al. (1993) (Appendix 2) is difficult to identify directly on the core probably because the scale in which the description is made is finer than the size of individual components of most fault zones present in the BULGG. The Fault Core-Damage zone model proposed by Chester et al. (1993) is a simplified model that works best to describe faults as an ensemble. In detail, fault zones tend to be much more complex and are composed of multiple branches that anastomose, link with each other and surround blocks of less deformed material (Appendix 3). It is therefore necessary to integrate all the observations made in the core description and upscale them to identify and propose an interpretation of the distribution of fault zones.

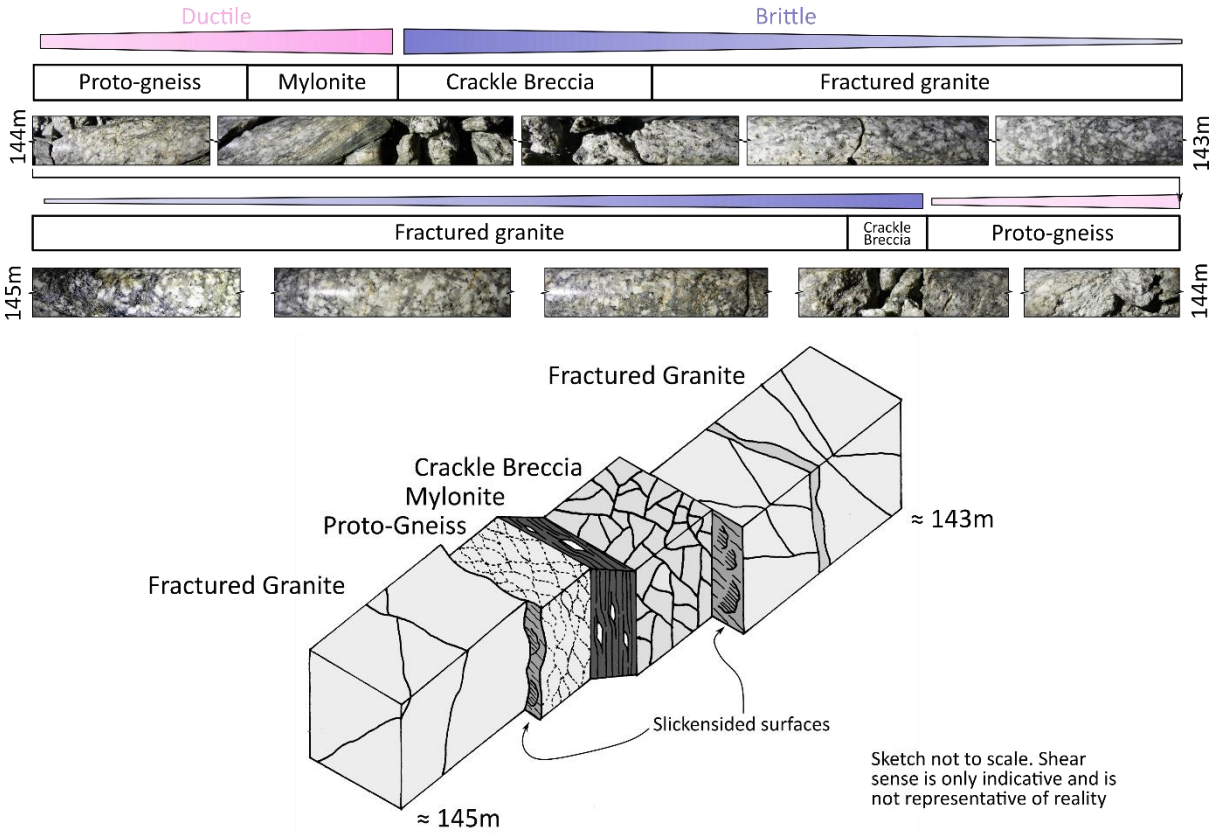

Figure 22. Drillcore images composition and sketch of the "Bad Boy" fault as seen in the CB1 borehole. Ductile and brittle structures can be seen near each other. Brittle structures seem to locate in the boundaries of ductile features. A) Increased presence of shear fractures and veins, B) Crackle breccia, C) Mylonite, D) Proto-gneiss.

The proximity of ductile and brittle features adds an additional complexity to the exercise. Indeed, it is very common to observe typically ductile features (i.e., foliation, c-s fabric, etc) intercalated with brittle structures like shear fractures and breccias (Figure 22).

All the factors mentioned above make it difficult to define a single list of criteria that can be systematically used to define fault zones. However, all faults defined in this work have some of the following elements:

- An increased frequency of structures with respect to surrounding values.
- A relative increase in the intensity of deformation (e.g. from weak foliation to proto-gneiss to mylonite).
- The presence of crackle breccias.
- The presence of open rugose fractures with vuggy porosity.
- The absence of core recovering. ≈

5.5 Composite core log

The compilation of core description, structure typology, fault zone identification and stereonets with fracture orientations has been compiled in a composite log (Figure 23). The color code was chosen so darker colors represent structures that convey more deformation and are, potentially, more prone to fluid flow.

The structural orientations in the stereonets were measured on image logs (acoustic and/or optical) and incorporated in this analysis. No direct measurement of structural orientations was made in the drillcore simply because it was not oriented.

Figure 23. Next Page. Composite core log at a 1:2000 scale showing the core description and structural orientations measured in the acoustic and optical televiewers. A more detailed version of the log is available in

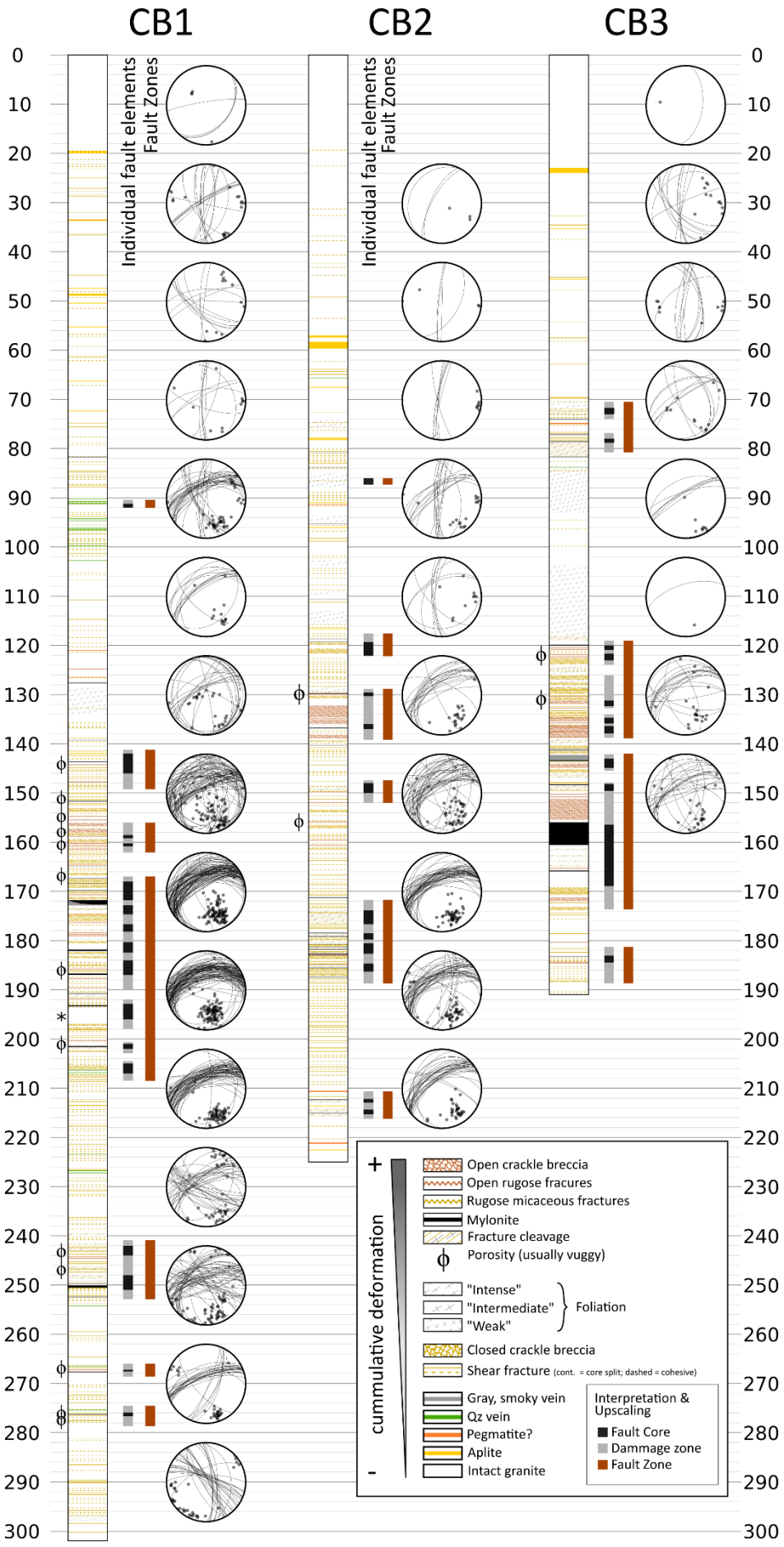

5.6 Core log analysis

5.6.1 Fault zones and upscaling

Individual fault elements identified in the drillcore description were marked in the core log (black stripes in Figure 23). Damage zones around these individual fault core elements were identified using the density of structures as a guide (grey sections in Figure 23). The resulting pattern shows fault zones composed of multiple branches of core zones with overlapping damage zones and internal lenses of rock with little deformation. This configuration is close to the conceptual model of fault zones proposed by Faulkner et al. (2003) (Appendix 3) and differs from the single fault core model of Chester et al. (1993) (Appendix 2).

5.6.2 Structure types vs. Orientations

The analysis of structural orientations vs. structure types (Figure 24) shows that the most important structures in terms of cumulated deformation (lower row) have strikes oriented almost exclusively NE-SW. The same pattern is shown when plotting structure orientations around fault zones vs. structures in between fault zones (Figure 25). Near fault zones, the distribution of orientations tend to be unimodal around the NE-SW direction while the zones in between include also structures oriented N-S and NW-SE.

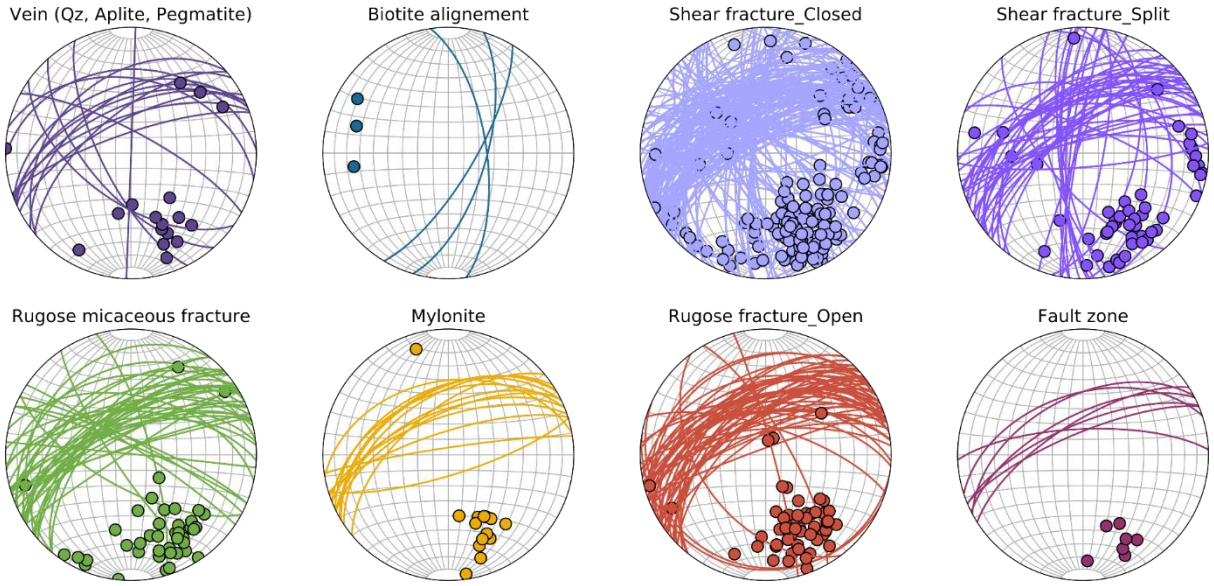

Figure 24. The typology established in the core description (Figure 21) was integrated with the corresponding structural orientations picked in the image logs (next chapter). The main orientation of structure strikes is NE-SW. The most common structures are shear fractures. The upper row shows the orientation of structures that are mainly closed (from a visual perception when describing the cores). The lower row shows the orientations of structures with higher strain and can be perceived as "open". The lower row shows that important structures are almost exclusively oriented NE-SW.

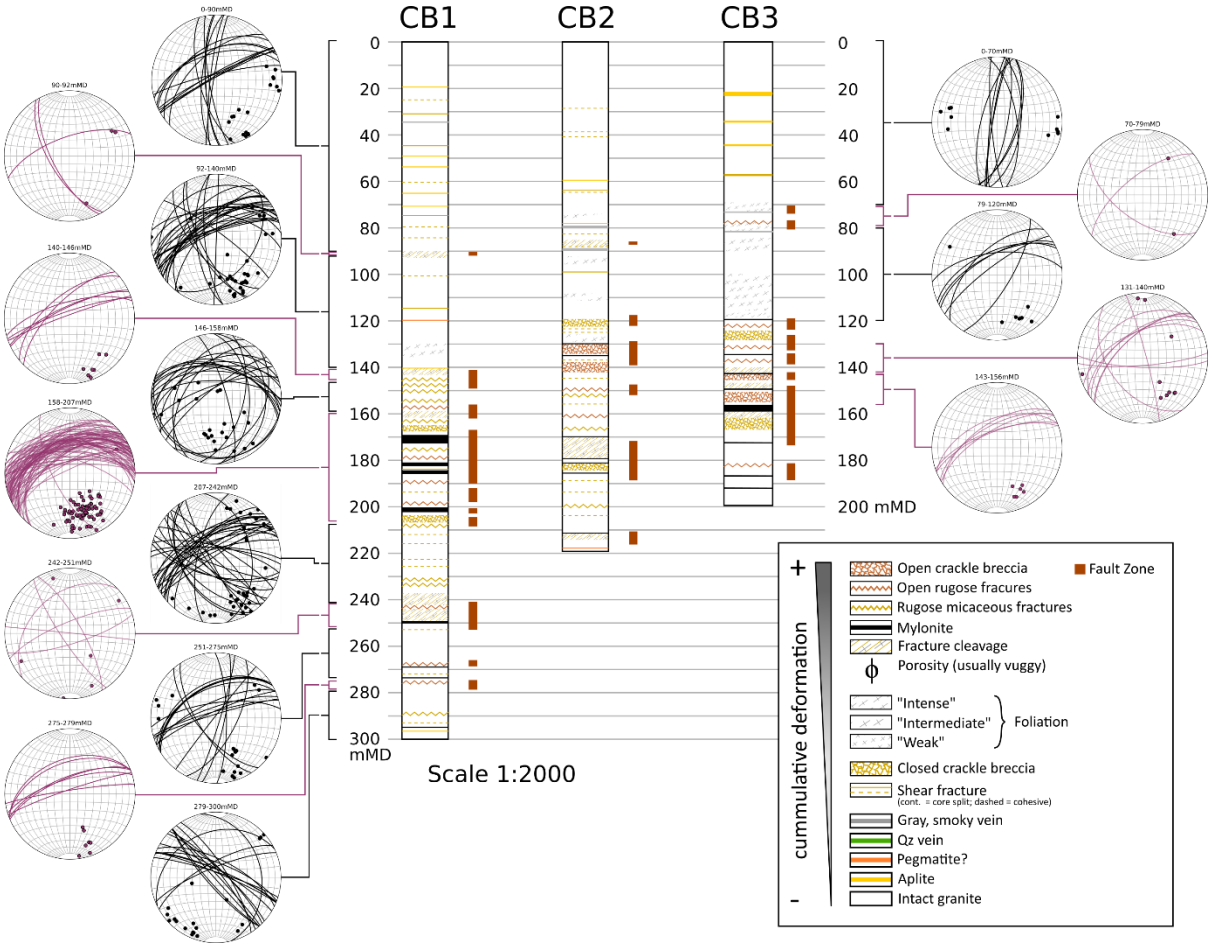

Figure 25. Simplified core logs for CB1, CB2 and CB3 boreholes. Interpreted fault zones are indicated by black squares next to the logs. Structures have been plotted in stereonets and separated in two groups, 1) Structures around fault zones (purple), 2) Structures in segments between fault zones (black). The strikes of structures in and around fault zones are in general dominated by the NE-SW direction

6. Structural Analysis of Image Logs

6.1 Summary of main observations on image logs

An extensive analysis has been carried out on image logs acquired in the ten long boreholes drilled so far in the BULGG. The analysis includes:

1. The picking of structures on image logs and the application of a double classification system (*Figure 26*).
2. Building basic statistic plots of picked structures (Figure 27, Figure 28 and Figure 29).
3. The analysis of crosscutting relationships.
4. A calibration of fault zone characteristics using drillcores (Figure 33 to Figure 36)
5. A correlation of fault zone cores across boreholes (Figure 43 and Figure 44).
6. The analysis of background fracturing in terms of fracture spacing and orientation (Figure 50 to Figure 52 and Table 4 to *Table 8*).
7. The proposition of a conceptual structural model for the BULGG (*Figure 33*).

The main conclusions of this work are:

- As it was shown with the analysis of structures in the drillcore, all the important structures in terms of deformation are oriented NE-SW and dip towards the NW.
- Crosscutting relationships are not conclusive. No orientation is dominantly cutting or offset by other fractures. More detailed analysis might be necessary to uncover meaningful relationships.
- Most fault zones have a brittle overprint over ductile deformation. The quantity of ductile and brittle deformation has not been quantified and there is not an easy way to do this. But a qualitative assessment has been done to document faults zones that are mainly ductile, fault zones that are mainly brittle and the whole spectrum in the middle.
- The fault zones defined in the image logs are actually fault core branches that constitute higher-order fault zones. These individual branches of fault core can be correlated between different boreholes and a model doing exactly that has been proposed in an inclined cross section.
- These fault core branches constitute limits to structural units. Each structural unit is characterized by a specific distribution of the background fractures.
- Four structural units were defined for the BULGG. In Units II and III the NE-SW fractures are dominant while N-S and SE-SW orientations are dominant in Units I and IV respectively.
- Fracture frequency and spacing also varies considerably but including this parameter into the model has proven challenging due to the heterogeneity of data sources among boreholes (ATV vs. OTV logs).

The observations, analyses and conceptual model contained in this report will be used as the basis to analyze hydraulic data and induced seismicity in further reports. Geomechanical aspects linked to the structural model will also be considered.

6.2 Methodology

Image logs for 10 long boreholes were interpreted using the commercial software WellCad®. The logs include acoustic (ATV) and optical (OTV) images. *Table 2* shows which log is available for each borehole.

Table 2. Image logs available for each long borehole. ATV=Acoustic Televiewer; OTV=Optical Televiewer.

Borehole	ATV	OTV
CB1(MB1)	✓	✓
CB2(MB2)	✓	✗
CB3(MB3)	✗	✓
MB4	✓	✗
MB5	✓	✓
MB7	✓	✓
MB8	✓	✓
ST1	✓	✓
ST2	✓	✓
WELLTEC	✓	✓

Structures were interpreted in a classical way by fitting sinusoidal curves to observed features. A classification of structures was established using 2 attributes (*Figure 26*):

- **Types of structures:** A simple classification was adopted to differentiate 1st order structures (fault zones) from smaller features (generic fractures):
    - *Fault zones:* Several criteria were used to define fault zones,
        - Sections with increased deformation and with a thickness of at least several tens of centimeters.
        - Recognizable internal structures, i.e., foliation, fractures and/or veins can be identified inside the deformed section.
        - Caliper shows borehole deformation.
        - In boreholes with core descriptions (MB1, MB2 and MB3), fault zones were defined first during the core description and then in the televiewer logs following the same criteria described above.
    - *Generic fractures:* Usually thin, linear structures recognized in the amplitude/travel time/optical image and without any considerable borehole deformation seen on the

caliper log. Generic fractures defined in televiewer logs correspond to shear and rugose fractures defined in the core description. Generic fractures are, generally speaking, the structures that don't fit into the categories vein/dyke, fault zone, mylonite, mineral alignment or foliation.

- **Where the structure can be seen or "source"**:
    - *OTV only*: Structures seen only in the optical images with no or very little response observed in the amplitude/travel time from ATV.
    - *ATV + OTV*: Structures seen in both acoustic and optical logs.
    - *ATV only:* Only valid in boreholes where only ATV logs were available (CB2 and MB4). If both types of logs were available, then any structure seen in ATV was also observed in the OTV.

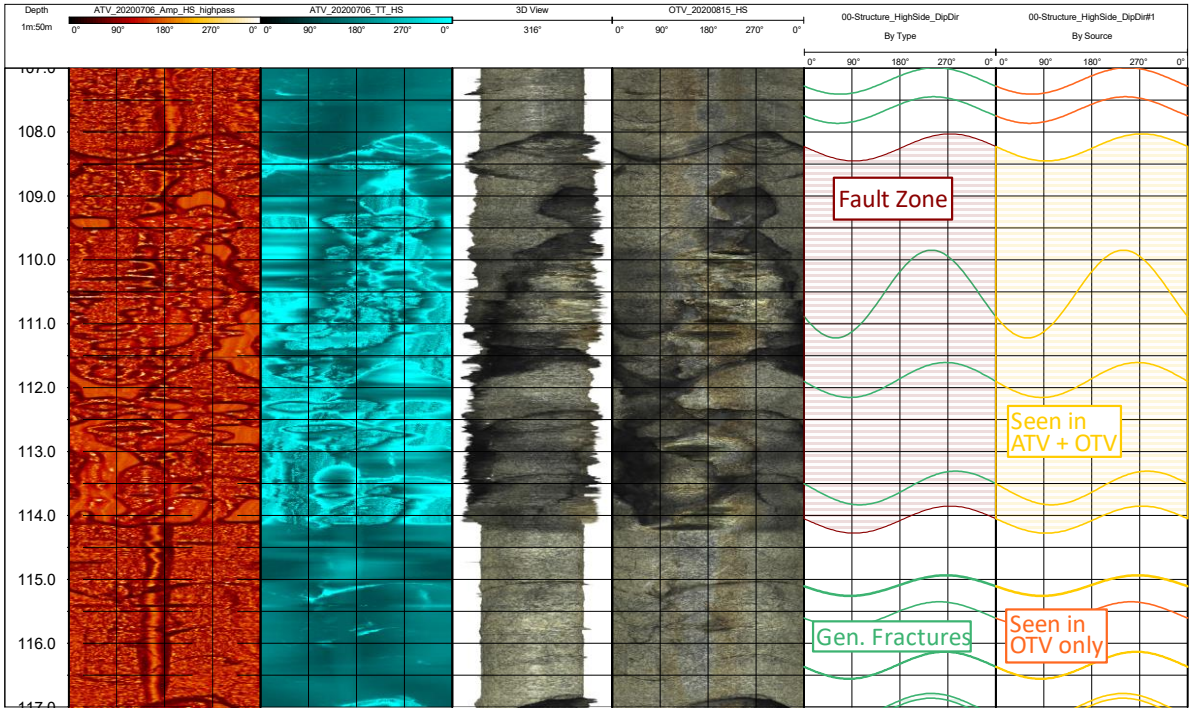

Figure 26. Example of image logging data and interpretation. From left to right: Amplitude from the ATV (red), travel time from the ATV (blue), 3D representation from the borehole built with a computed caliper (from the travel time) and the OTV image wrapped around, OTV RGB image. The interpretation of structures is shown twice. Structures were clasified by their nature (Fault zones vs. Generic fractures) and by the data source (Seen on ATV+OTV vs. OTV only).

6.3 Structures – Basic Statistics

Figure 27 shows the count of all structures for 3-meter intervals along all boreholes. Fault zones are indicated by rectangles with oblique hatch fillings. The thickness of the rectangles corresponds to the fault zone thickness (thin fault zones look like simple horizontal lines). Boreholes are arranged in the same spatial configuration as the wellheads in the BULGG from northwest (left) to southeast (right). The increase in structure frequency is evident at around 150m for the boreholes to the left

and around 100m for the boreholes to the right. The migration of this increased fracture frequency highlights the presence of a boundary with a strike oriented NE-SW and dipping towards NW.

A histogram of strike values for all structures is shown in Figure 28. Most strikes are between N220° and N260° and correspond to structures dipping NW. For the most part, structures have a steep dip between 50° and 80°

Stereonets with all structures plotted by type (Generic fractures vs. Fault zones) per source (OTV vs. ATV) and per boreholes are shown in Figure 29. Several features are worth noting from this representation:

- Apart from the dominant NE-SW orientation shown already in Figure 28, North-South and NW-SE orientations are also present.
- Structures parallel to the boreholes (i.e., poles that would sit inside the zone limited by 2 black great circles) are lacking in this database.
- Fault zones (red poles) are almost exclusively oriented NE-SW.

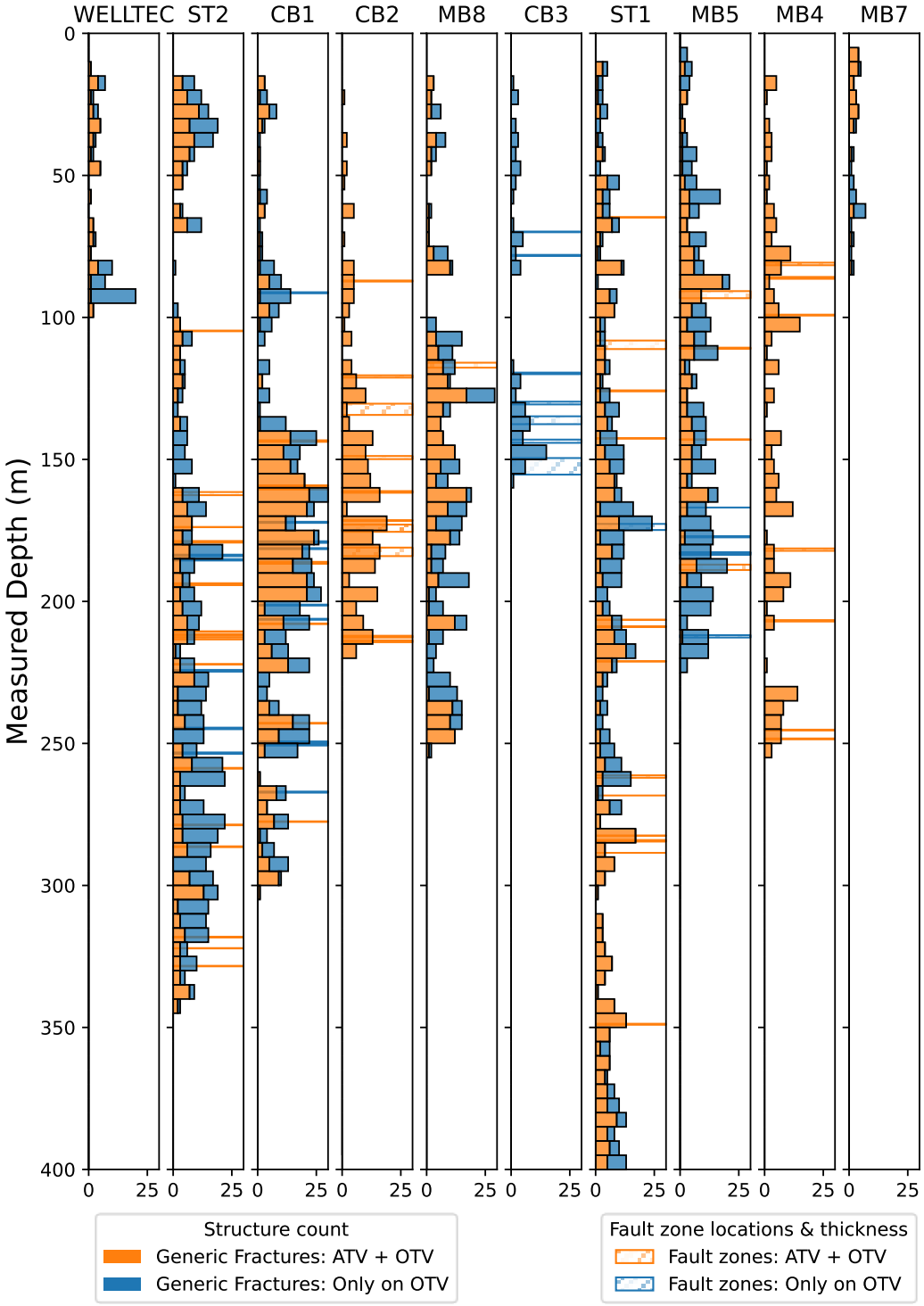

Figure 27. Structures count in bins of 3m along the boreholes. Hatched polygons show the location and thickness of fault zones.

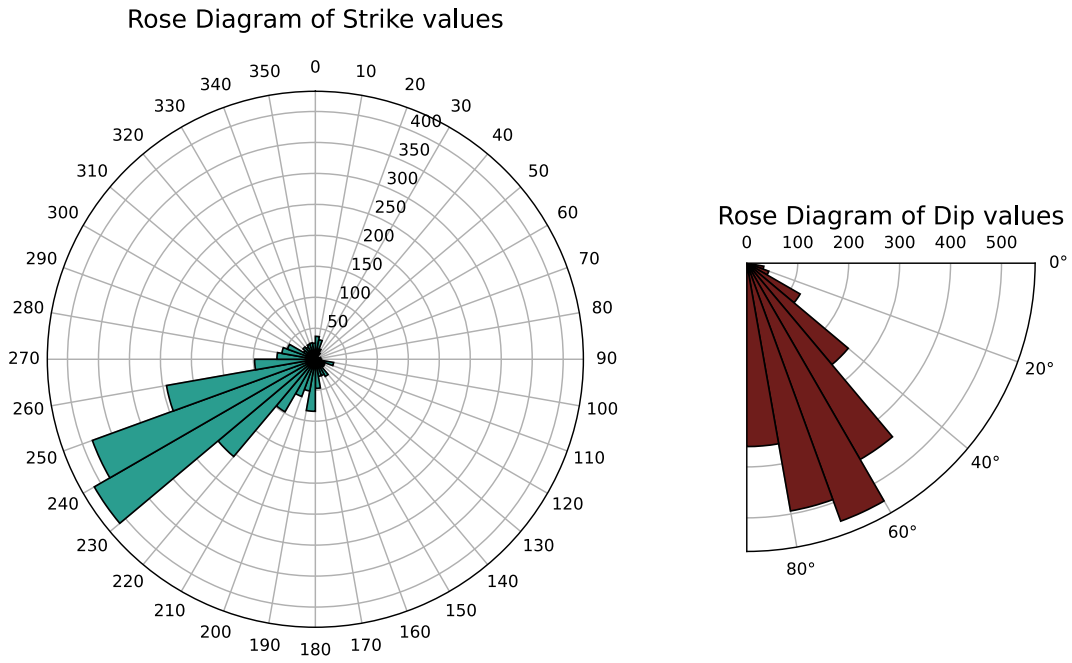

Figure 28. The most frequent strike values are in the range N230° and N250° while most dips are between 50° and 80°.

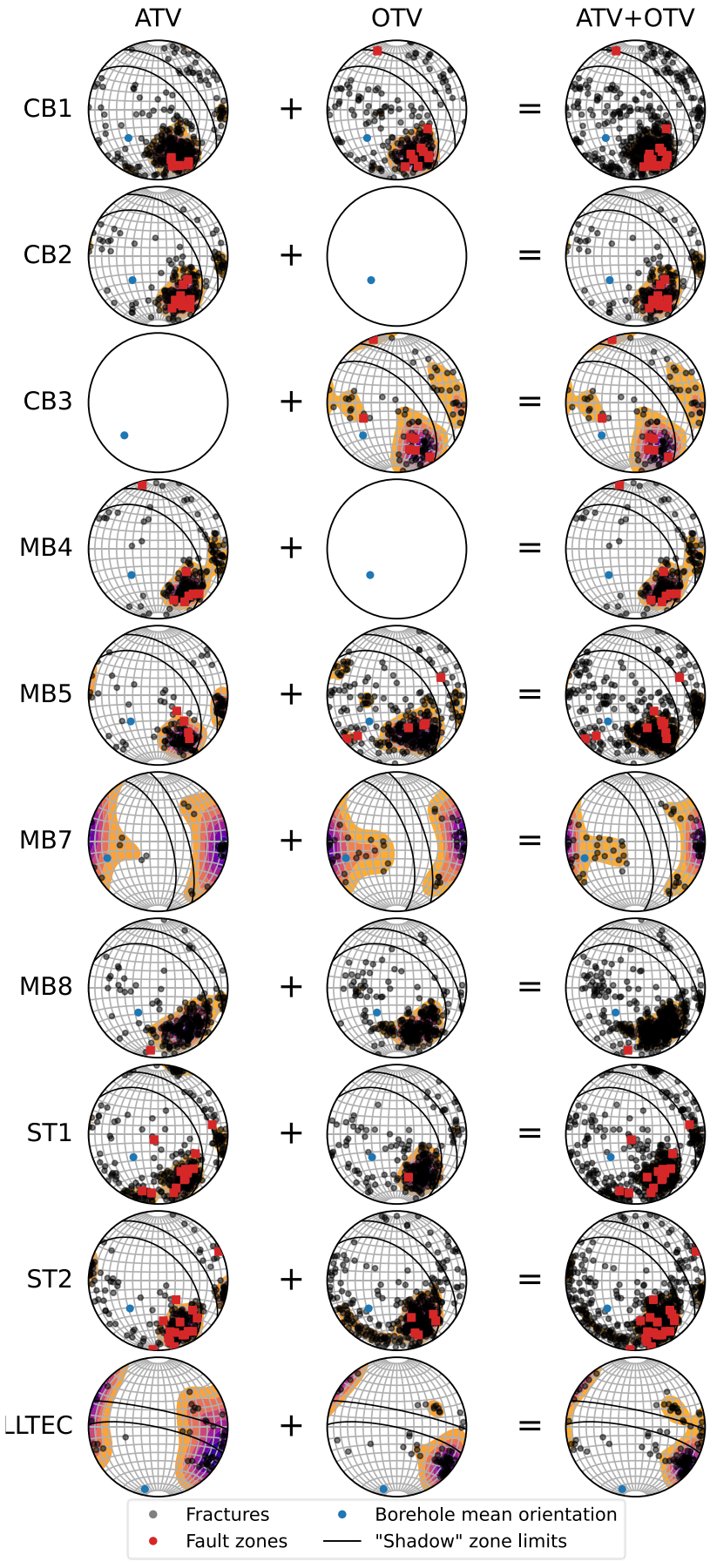

Figure 29. Stereonet projection of structural data by borehole, type and data source. Two main orientations for the strike of structures appear clearly and are the same as the ones defined in the tunnel 1) E-W to NE-SW and, 2) N-S. The overwhelming majority of fault zones have strikes oriented NE-SW. The black polygons are the limits of the "shadow zone", an area representing the orientations of planes that are subparallel to the borehole. The fact that fracture frequency in this area is low is linked to the sampling bias. Planes parallel to the boreholes will be sampled less frequently than those that form a high angle with the boreholes.

6.4 Crosscutting relationships

The crosscutting relationships between different structures can be used to infer which structural sets were active in later stages of the deformation. This can be an important piece of information when trying to understand which structures are most likely to form a hydraulically connected network.

Crosscutting relationships were picked in the image logs of all 10 long boreholes. An attribute was used to record when a fracture was A) Cutting other structure or B) Offset by other structure (Figure 30). Crosscutting relationships are often complex and cases where a fracture both cuts and is offset by another fracture are common. The example shown in Figure 30 is one of such cases where fracture A clearly cuts and offsets fracture B but it is also sheared in point "C" by a fracture with the same apparent orientation as B.

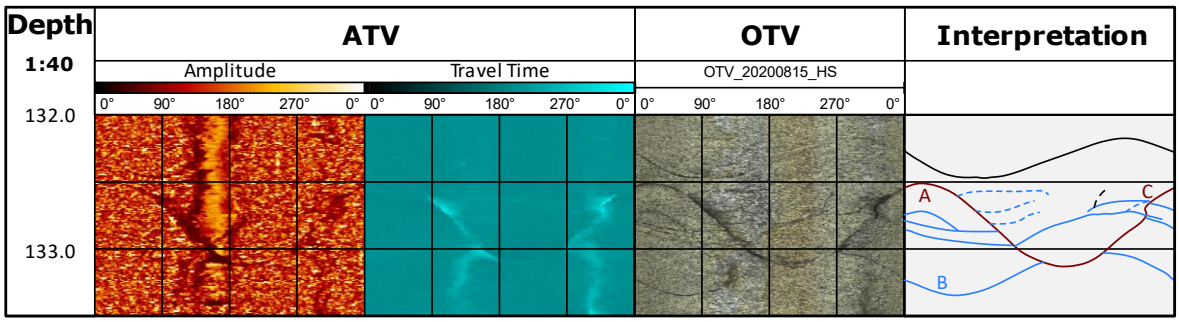

Figure 30. Example of crosscutting relationship in borehole ST1. Fracture A cuts several structures. B is cut by A.

Out of 3535 structures picked on image logs, only 328 show crosscutting relationships. The distribution of these 328 fractures is shown in Figure 31.

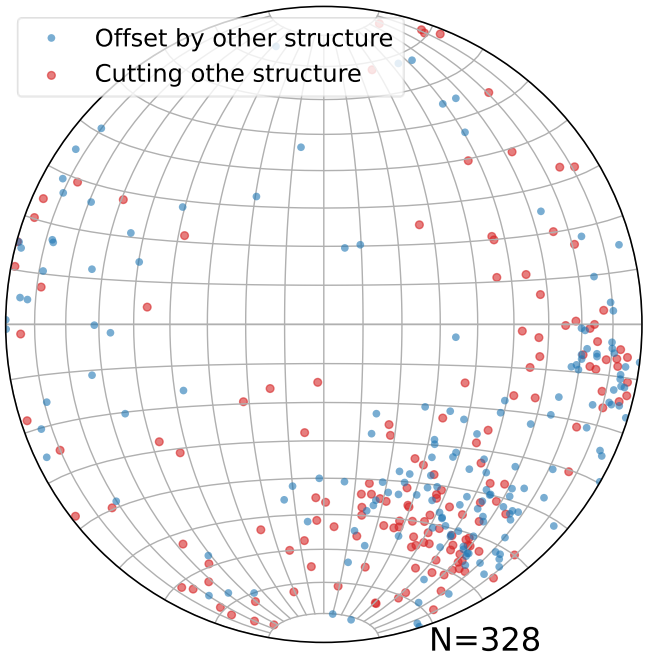

Figure 31. Crosscutting relationships in all 10 long boreholes. Structures that cut other structures (red) and structures offset by others (blue).

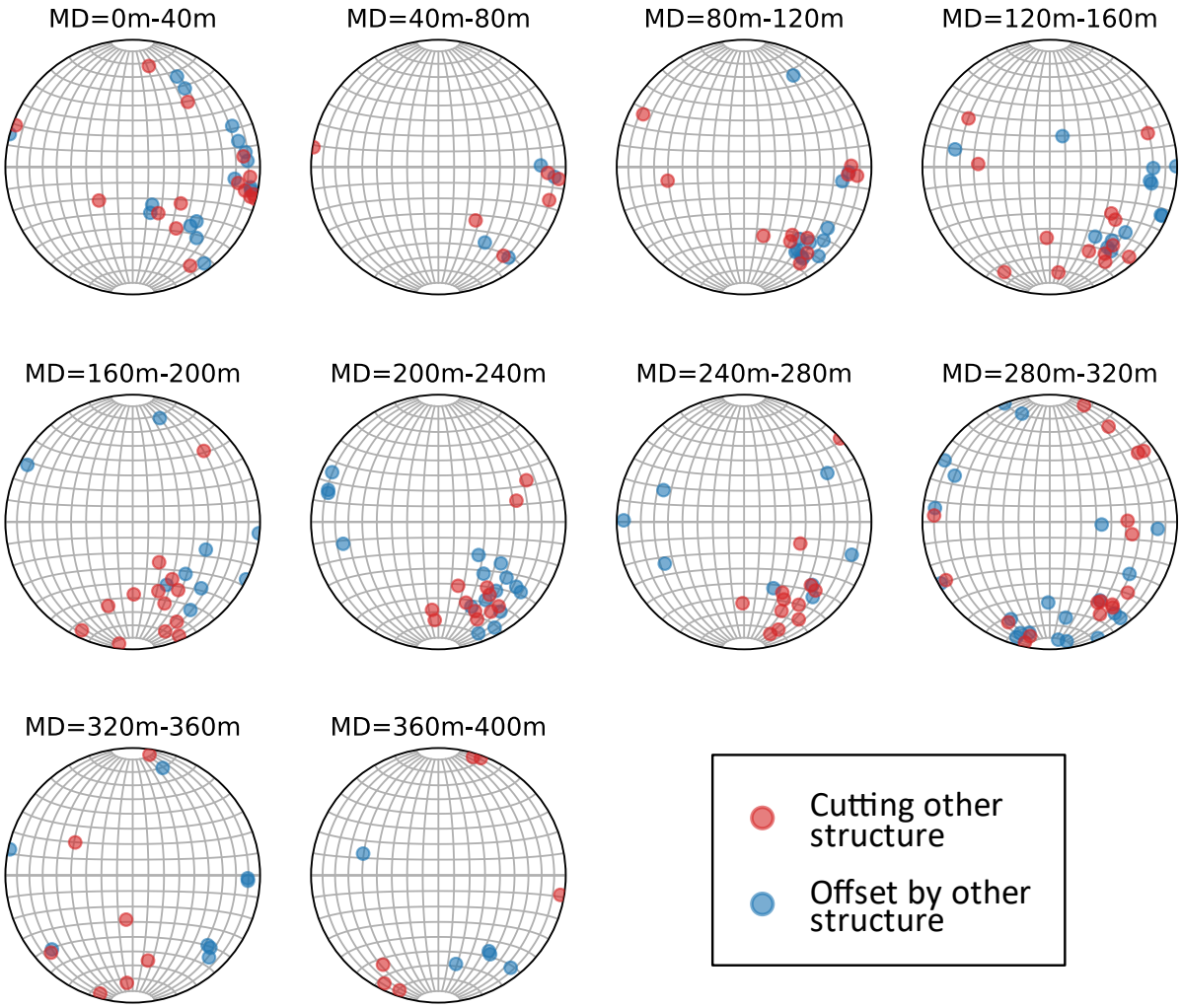

Figure 32. Crosscutting relationships by depth in all 10 long boreholes.

There is not a clear pattern of one fracture set cutting of being cut systematically by another set. The lack of definitive cross-cutting relationships could mean that all the measured structures were active synchronously in the most recent deformation phase. A more detailed analysis could help detecting clearer fracture interactions, but such analysis is out of the scope of this report.

6.5 Fault zones

6.5.1 Fault zones description

Fault zones in the BULGG are characterized by the overlap of components of ductile and brittle deformation. It is common to observe brittle features like slickensided fracture surfaces next to or inside strongly foliated rock with signs of ductile shear.

A clear distinction between ductile and brittle cannot be done because different structures have different degrees of both components. A ductility-brittleness scale could be conceived to assign

values to each fault zone and better characterize them and classify them. This was not done for the purposes of the analysis presented here but can be envisaged for future works.

Table 3. Four fault zones in CB1 that represent the spectrum of ductile-to-brittle deformation in the BULGG.

Brittle vs. Ductile	Depth	Description
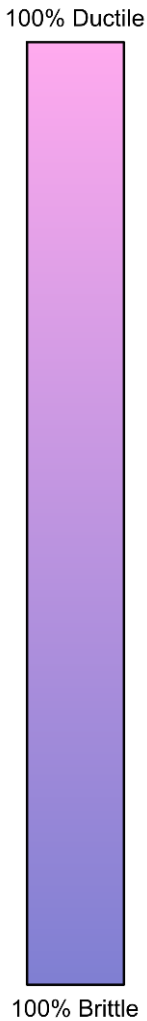	201 m	*Figure 33*: Fault zone with strong mylonitic foliation grading downward to a less foliated rock (proto-gneiss). A single brittle feature (fracture) was identified in the ATV with good amplitude contrast but no response in travel time. Direct inspection on the drillcore shows vuggy porosity associated to the fracture.
	143 m	*Figure 34*: One-meter-thick section representing the core zone of a wider fault zone (approx. 6 meters). This fault zone can be laterally correlated to a structure observed in the tunnel and referred to as the "Bad boy". A 30 cm strongly foliated section (mylonite + proto-gneiss) is surrounded by rock with strong brittle overprint showing a graded deformation from crackle breccia to fractured granite. The rest of the fault zone (not shown in figure) is composed mainly by fractured granite.
	242 m	*Figure 35*: Fault zone with a mylonite-to-proto-gneiss gradation and numerous brittle fractures. Two brittle features (fractures) have localized in the top and bottom boundaries of foliated sections. The ATV shows a strong response in both, amplitude and travel time.
	267 m	*Figure 36*: One-meter-thick fault zone defined by a significant increase of fracture frequency and a strong response in the ATV amplitude. No foliation is observed in OTV or drillcore although beyond the proximity of fractures. It is possible that the main fracture surface observed in OTV represents a thin mylonitic structure.

Four fault zones have been chosen to illustrate the full spectrum of ductile-to-brittle relationships observed in fault zones in the BULGG. All examples were drawn from CB1 since it is the only borehole with ATV and OTV logs and a drillcore. The fault zones are shown in *Figure 33* to *Figure 36*. The figures are arranged in decreasing order of ductile deformation compared to the brittle component. a description of the 4 fault zones is presented in *Table 3*.

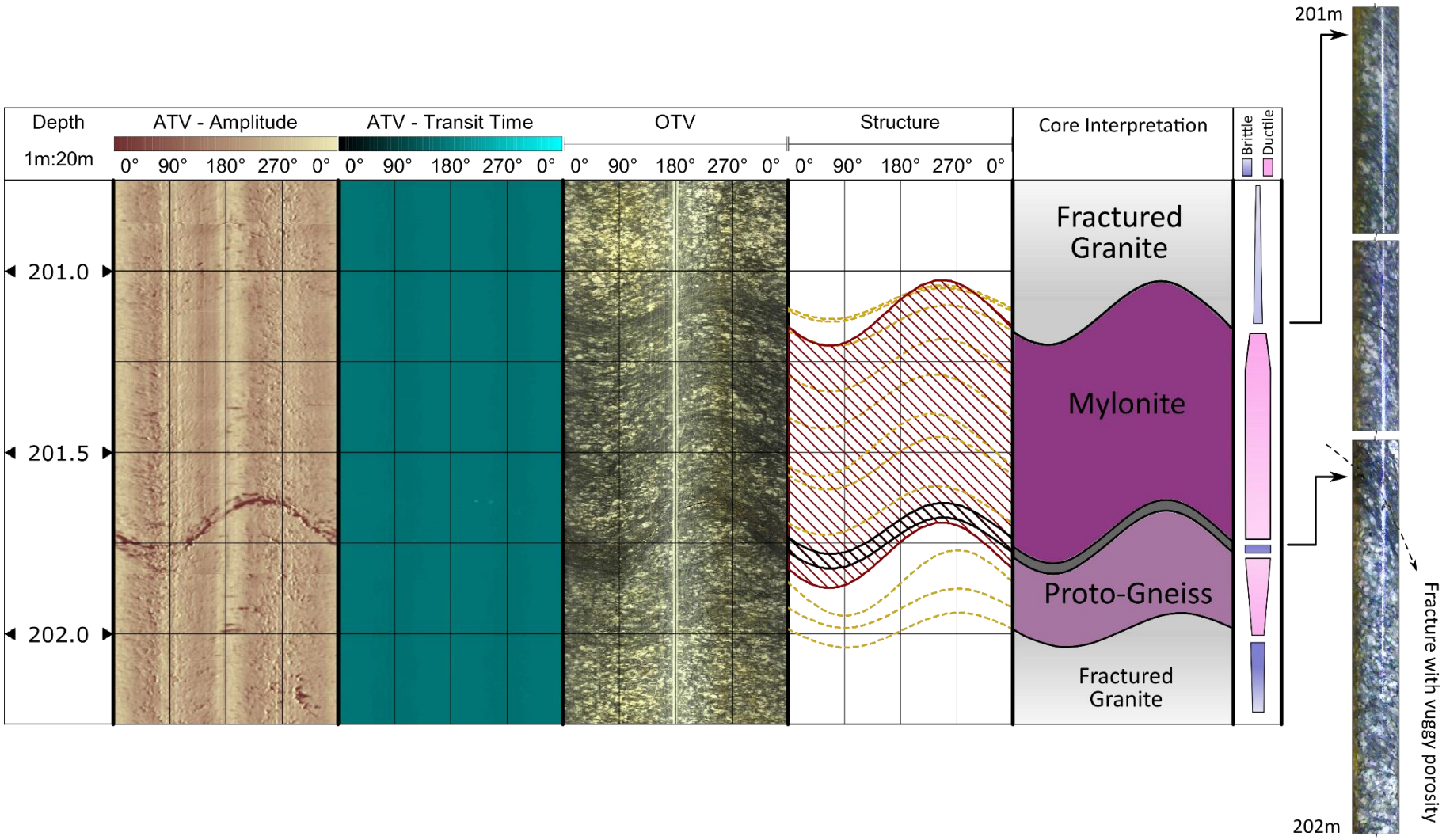

Figure 33. Fault zone at 202m. Ductile processes are dominant and only a brittle feature can be observed. Drillcore photos by F. Serbeto.

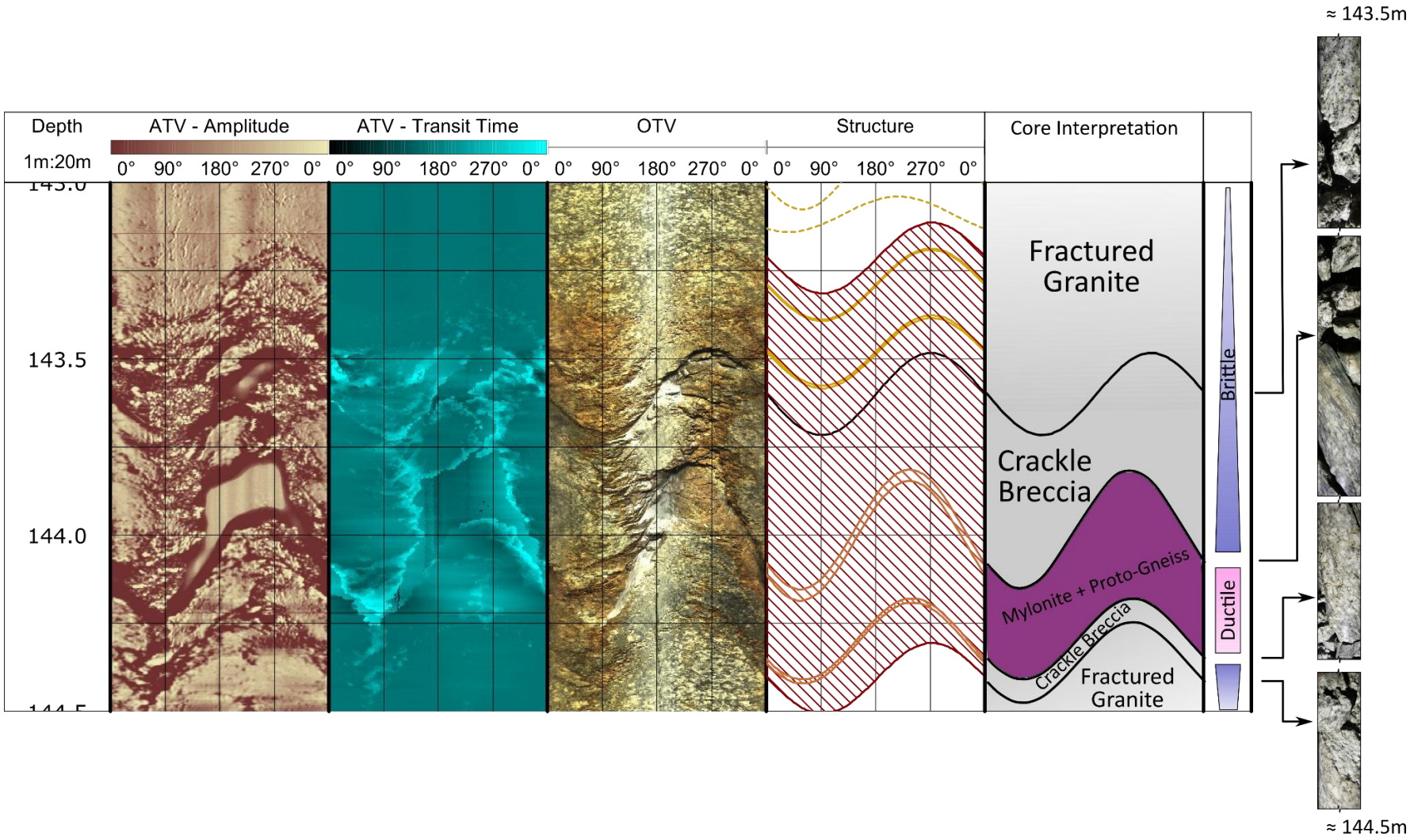

Figure 34. Fault zone at 143m correlable with the Bad boy in the tunnel wall. Strongly foliated rock is flanked above and below by brittle deformation (crackle breccia and isolated fractures)

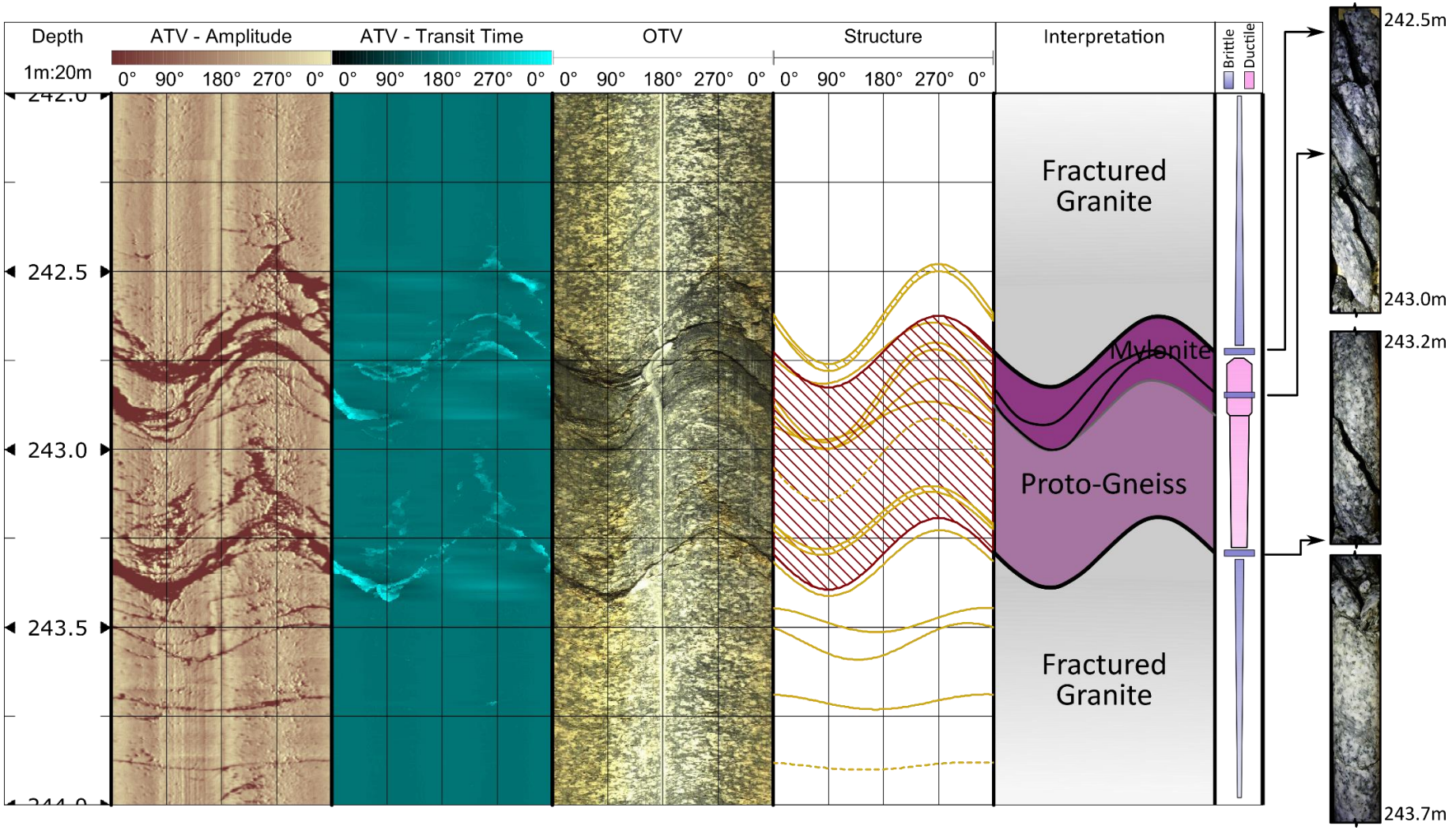

Figure 35. Fault zone at 242m. Ductile deformation in the form of tighly foliated proto-granite and mylonite. The boundaries of foliated rock were reactivated as brittle fractures.

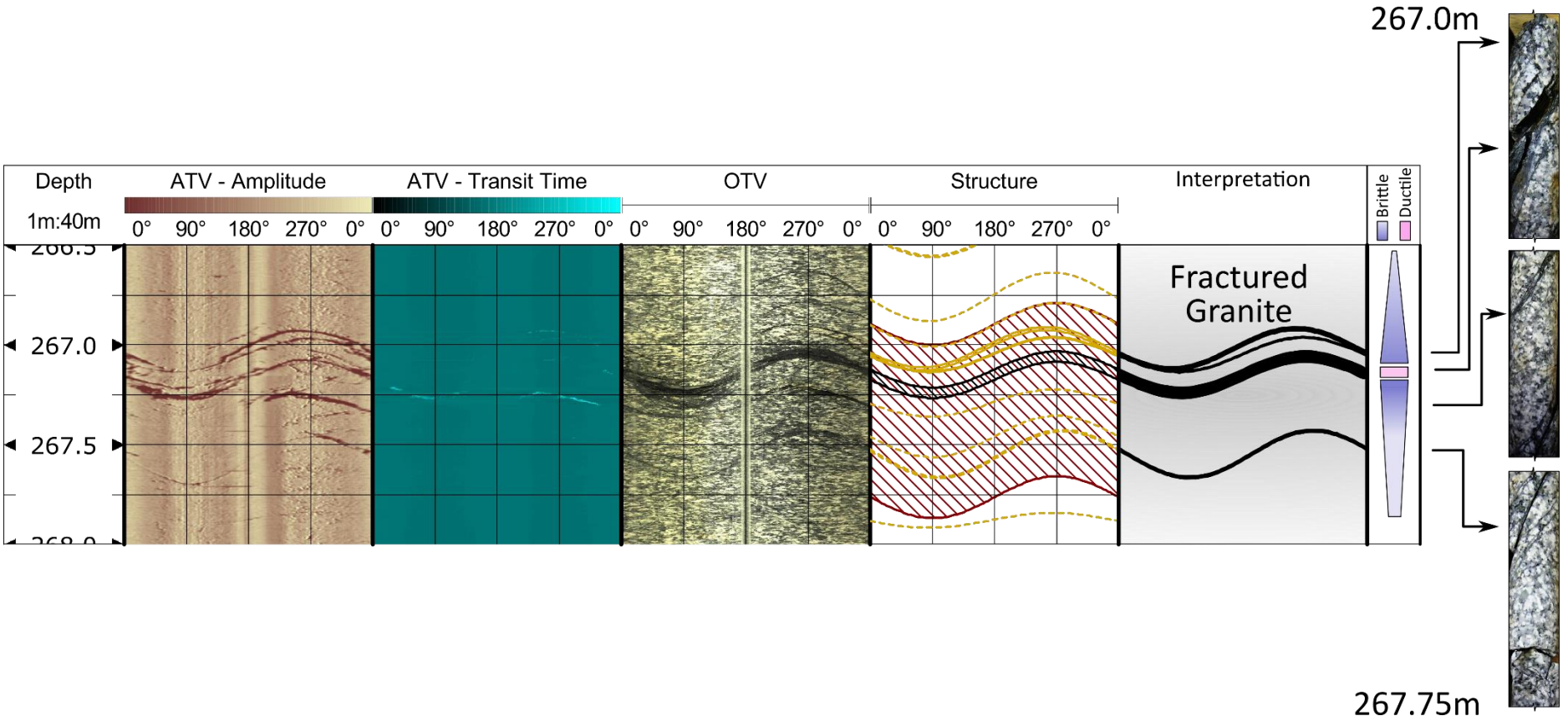

Figure 36. Fault zone at 267m. Increase in fracture frequency and localized foliation around individual fractures. Ductile deformation is limited to isolated zones and the brittle overprint is stronger than other cases.

6.5.2 Fault zones correlation

To build a coherent model, individual fault zones identified in the image logs were correlated across boreholes. Only the distribution in space and alignment of individual fault zones was used in the correlation. The intrinsic characteristics of each fault zone was not used as a criterion due to the well-known lateral heterogeneity of fault zones. A total of 15 correlated fault zones were built in the model, using 53 out of the 78 individual zones identified in the boreholes. Figure 37 shows 3 examples of correlated fault zones built by grouping individual zones which position, and orientations are likely to form a single surface.

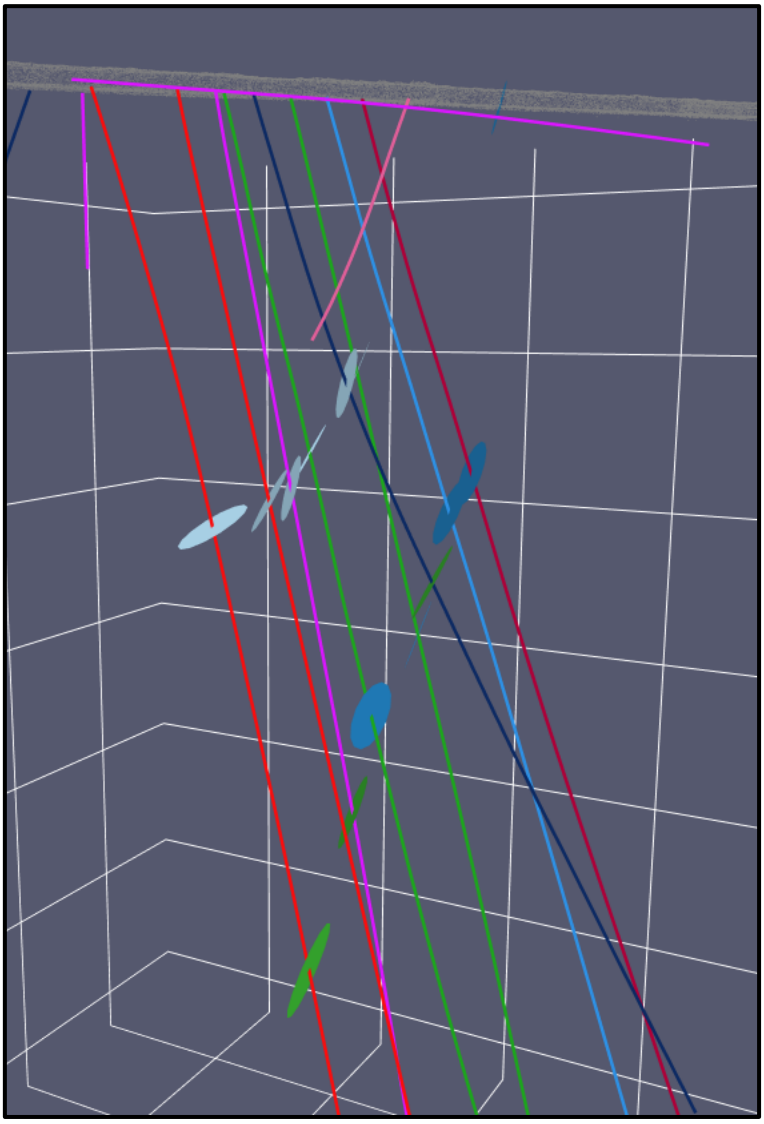

Figure 37. Examples of fault zone elements represented as disks and correlated across boreholes. FZ_1 (light blue), FZ_2 (green) and FZ_3 (dark blue). FZ_2 and FZ_3 are two segments of the fault named "Bad boy"

GPR plots (provided by A. Shakas, ETH) were incorporated in the analysis and used to interpolate and extrapolate fault traces. When markers and GPR data are projected on a plane that is both

perpendicular to most fault zones and a good fit to all borehole trajectories (Figure 38 and Figure 39) there is good fit between fault markers and the geometry of GPR reflectors (Figure 40).

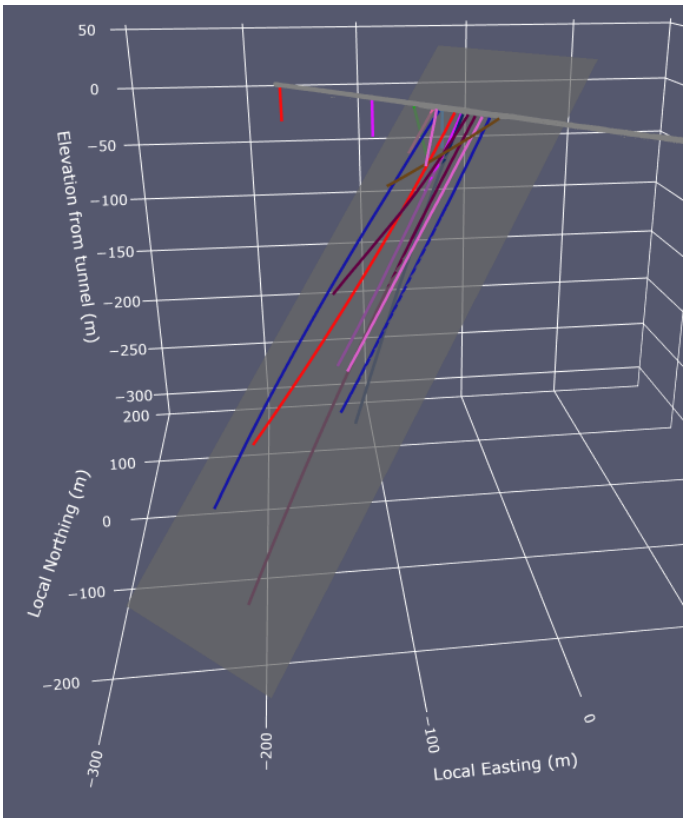

Figure 38. Oblique view of the BULGG. A plane parallel to the tunnel and inclined 42° to the SW (N137°/42°) is the best compromise to project data from the long boreholes with minimum distortion. This plane was used to project the fault zone markers and GPR data to propose correlated surfaces.

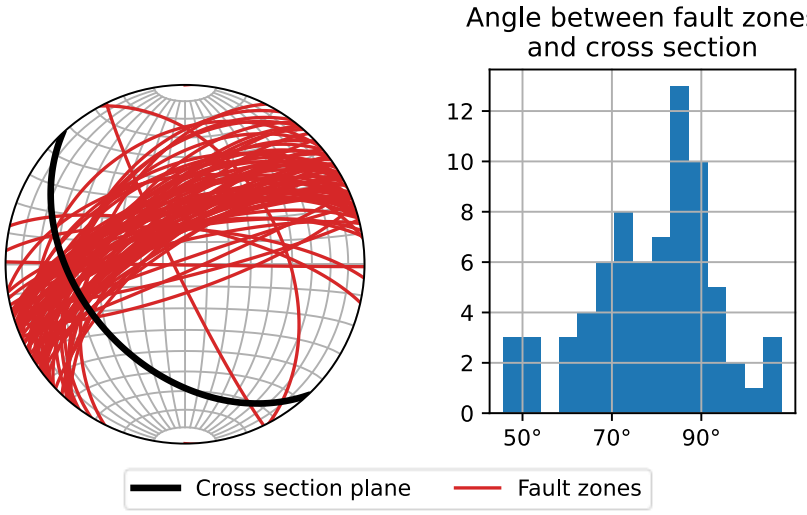

Figure 39. Most individual fault zone elements interpreted from image logs are oriented NE-SW and are perpendicular to a plane oriented N137°/42°.

The detail provided by GPR data was used to identify segmented fault zones and geometrical changes in zones not sampled by the borehole image logs (Figure 41).

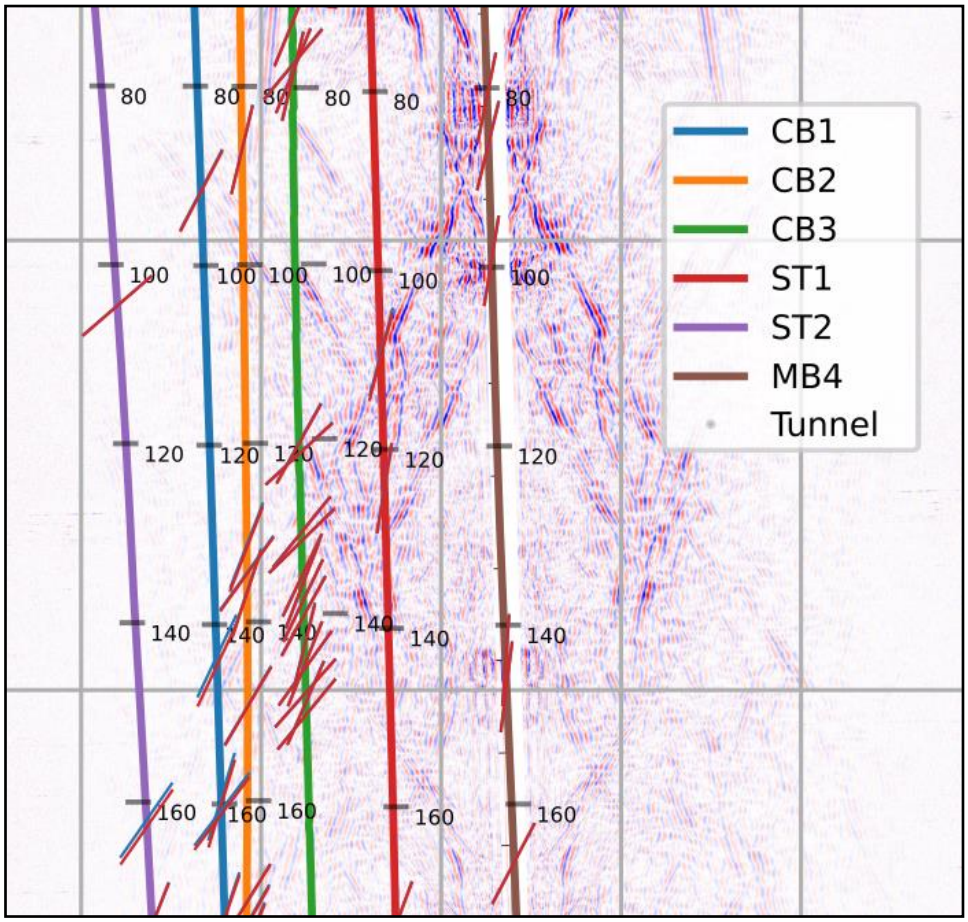

Figure 40. Fault zones markers from boreholes (blue=top; red=bottom) fit well with high amplitude markers from GPR data. This view is perpendicular to the cross-section plane shown in Figure 38 and Figure 39. The background image corresponds to the GPR acquired in the MB4 borehole and seen here mirrored in both sides of the borehole (left and right). The strong amplitude that crosses CB2 at 140m and MB4 at 80m corresponds to the fault zone known as "Bad Boy". The duality of orientation in strong amplitudes is resolved using the orientations of markers picked in the boreholes. Views including GPR data for each borehole are shown in the appendix.

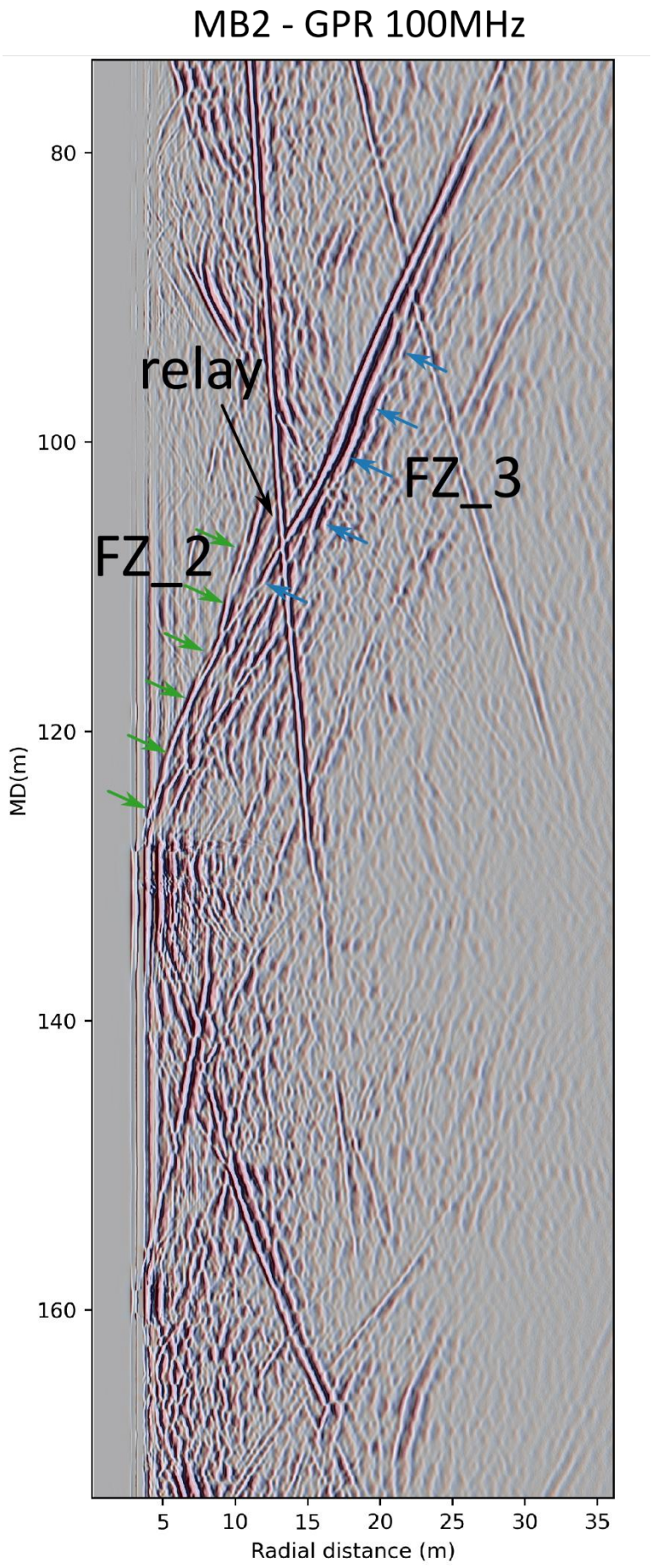

Figure 41. GPR data from MB2 showing a segmented fault zone.

A map view of the BULGG (Figure 42), a vertical correlation chart (Figure 43) and views perpendicular to the inclined plane presented in Figure 38 (Figure 44 and Figure 45) show the correlated fault zones. Fault zones dip towards the NW and are concentrated below MD 120m. A zone between FZ_2, FZ_3 and FZ_8 shows the highest concentration of correlated surfaces. Below FZ_8 fault zones seem less important, but this might be an effect of the diminishing amount of data with depth in the BULGG. Most faults are less than 200m length in any direction and those that are longer (e.g. Bad boy) are likely to be segmented.

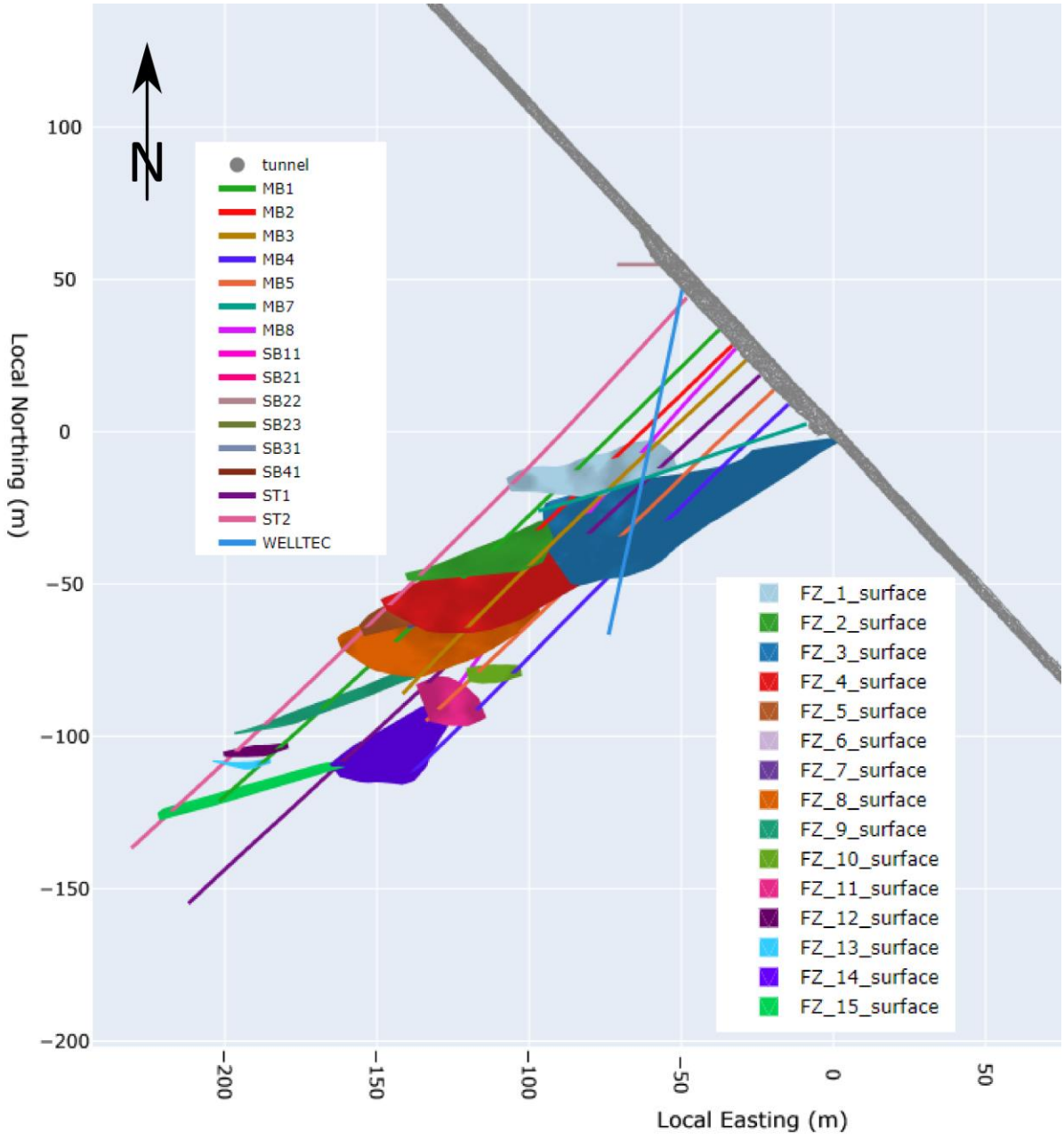

Figure 42. Map view of the BULGG with correlated fault surfaces.

The fault system that connects the tunnel and the boreholes ("bad boy") constitutes a multibranch fault zone with a total thickness of about 30-40m. The total length is impossible to determine due to the lack of data to the NW but it is expected to extend further deep in this direction. If this system were symmetrical then it would probably be at least twice as long of what depicted in Figure 44.

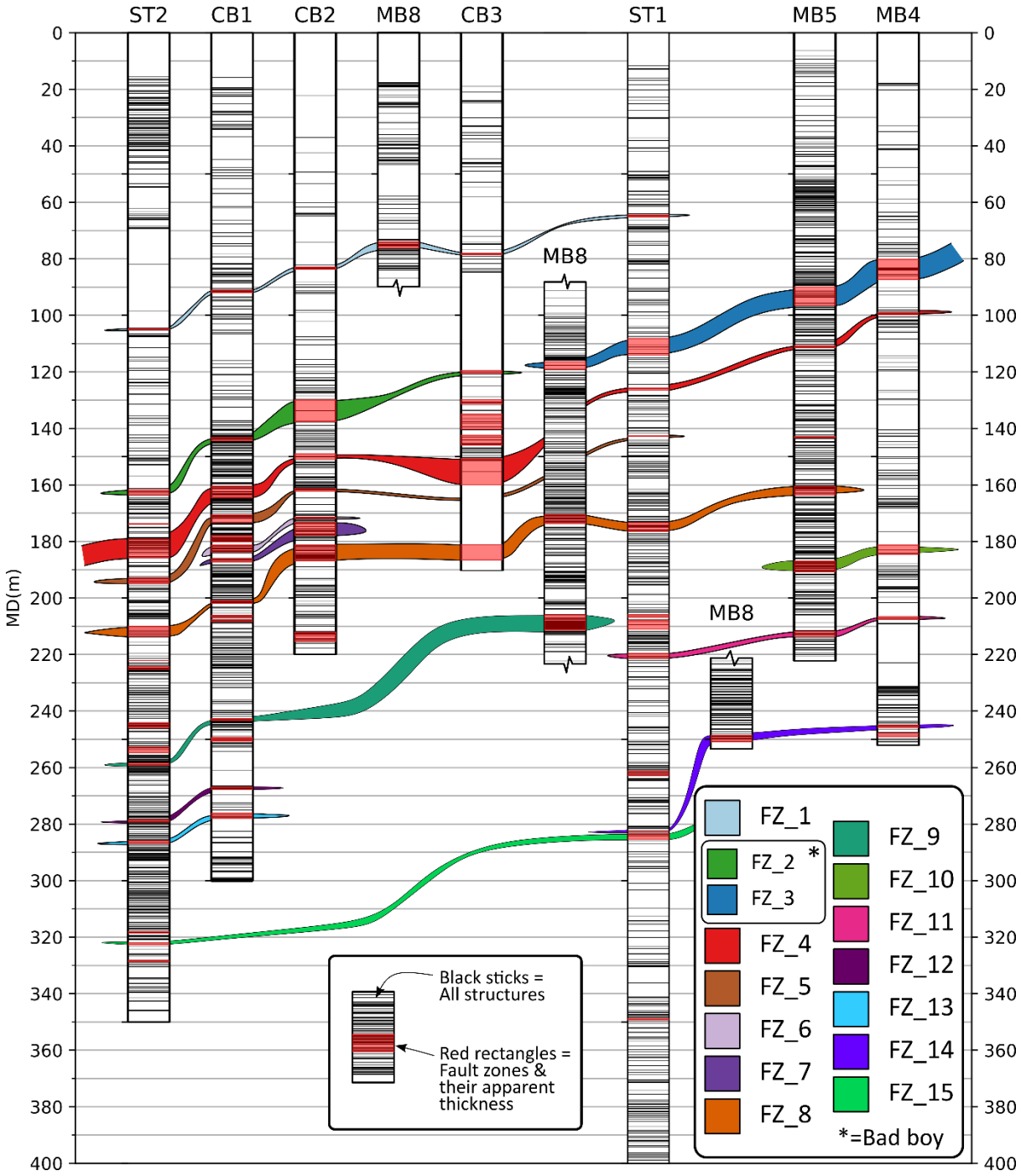

Figure 43. Borehole chart view of the correlated fault zones.

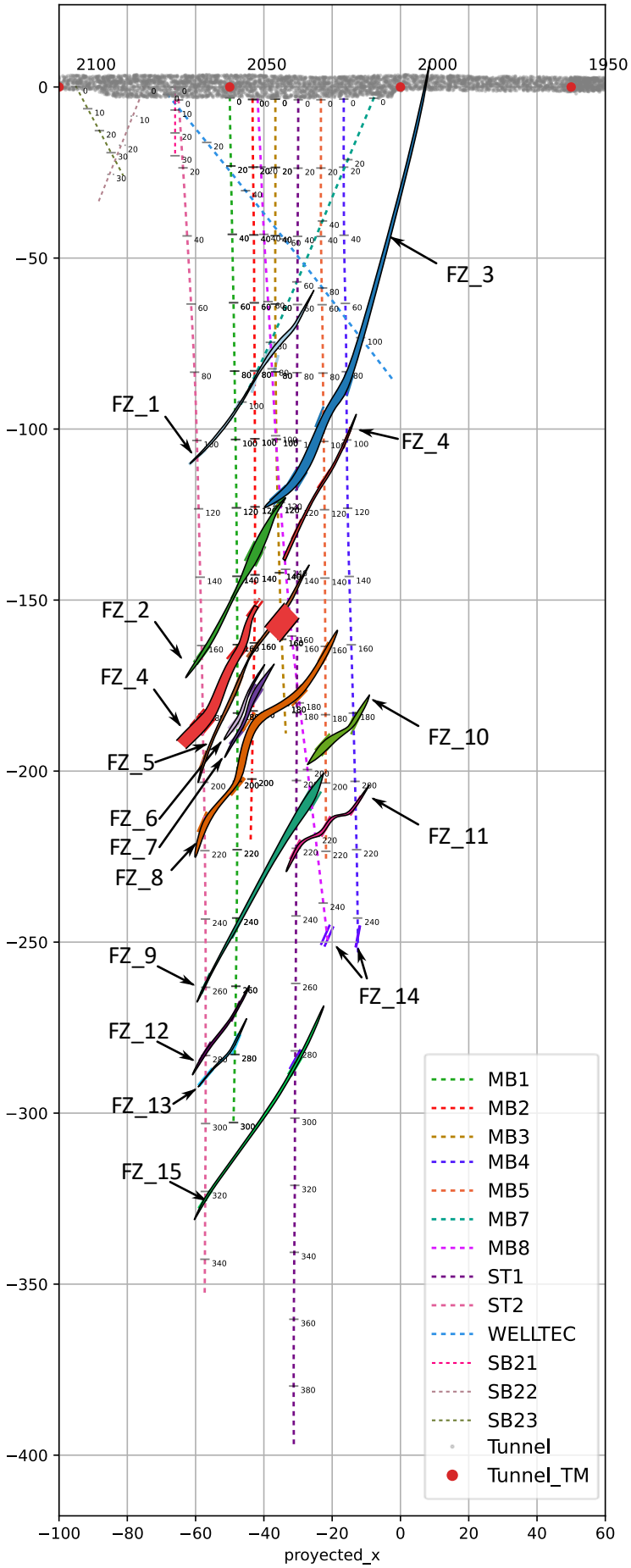

Figure 44. Correlation of fault zones across boreholes in the BULGG. The fault zones are built using markers from the interpretation of borehole image logs and GPR images for each borehole. This view is perpendicular to the plane shown in Figure 38 and Figure 39.

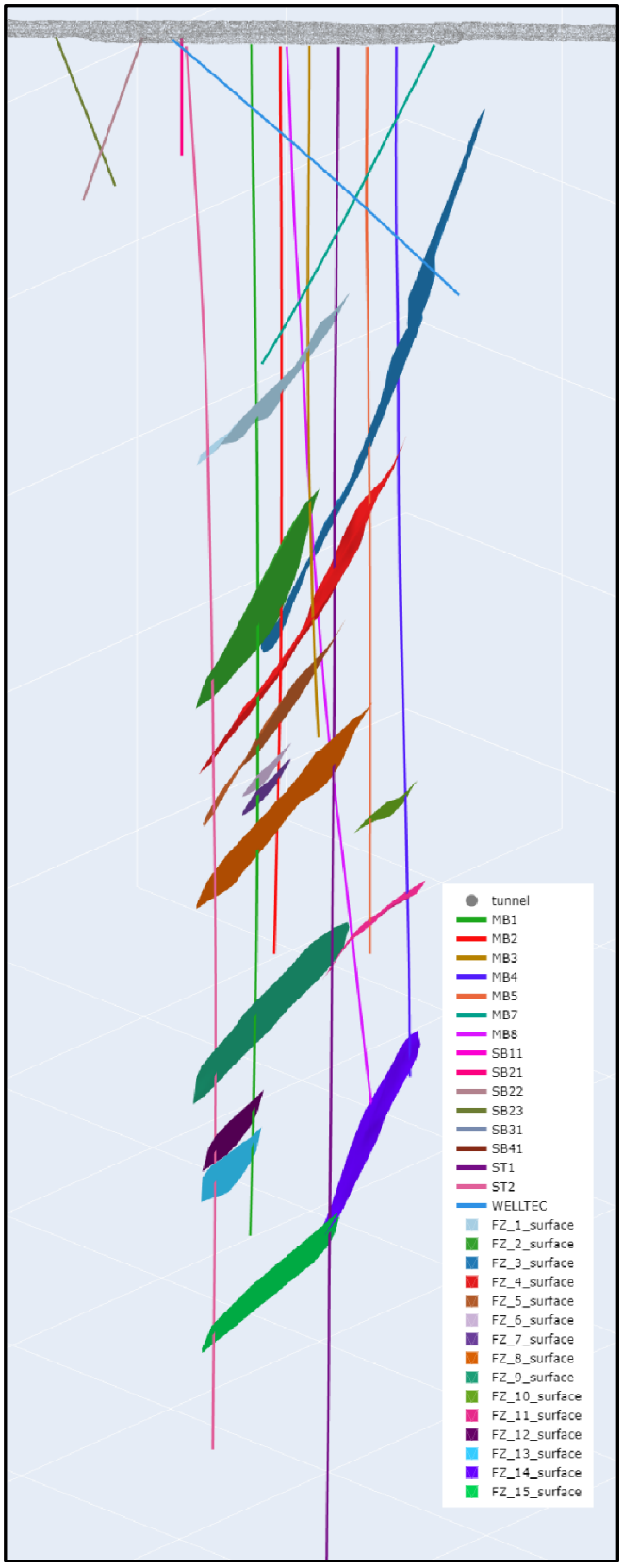

Figure 45. Correlated fault surfaces in 3D model. View equivalent to that on Figure 44.

A detailed description of the different fault zones and their internal structure is out of the scope of the present report. However, some examples are shown in Figure 46 to Figure 48 while the remaining logs are available in the appendices.

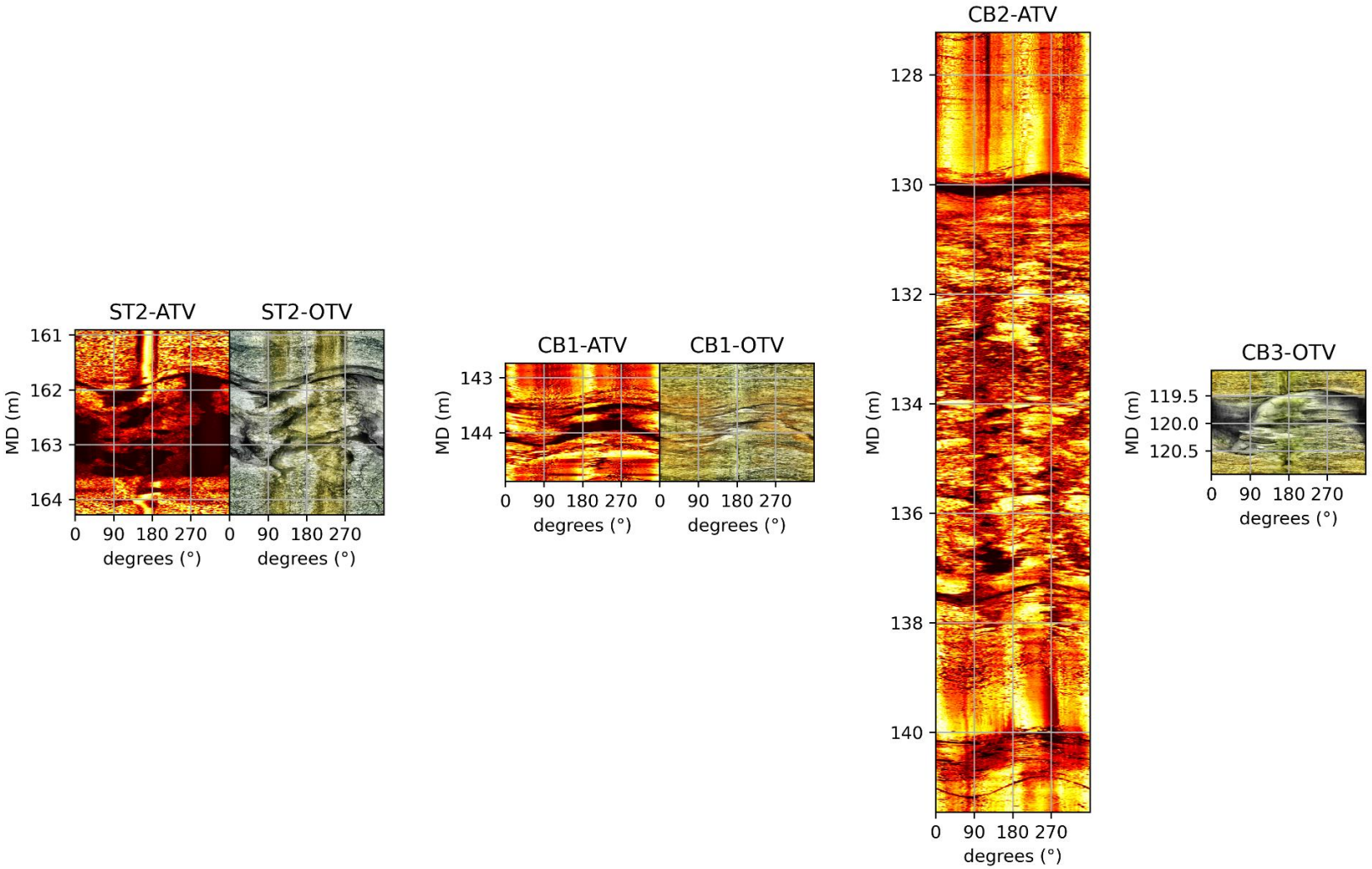

Figure 46. Individual fault zone elements correlated to form FZ_2. This is the-western segment of the "Bad boy" fault zone.

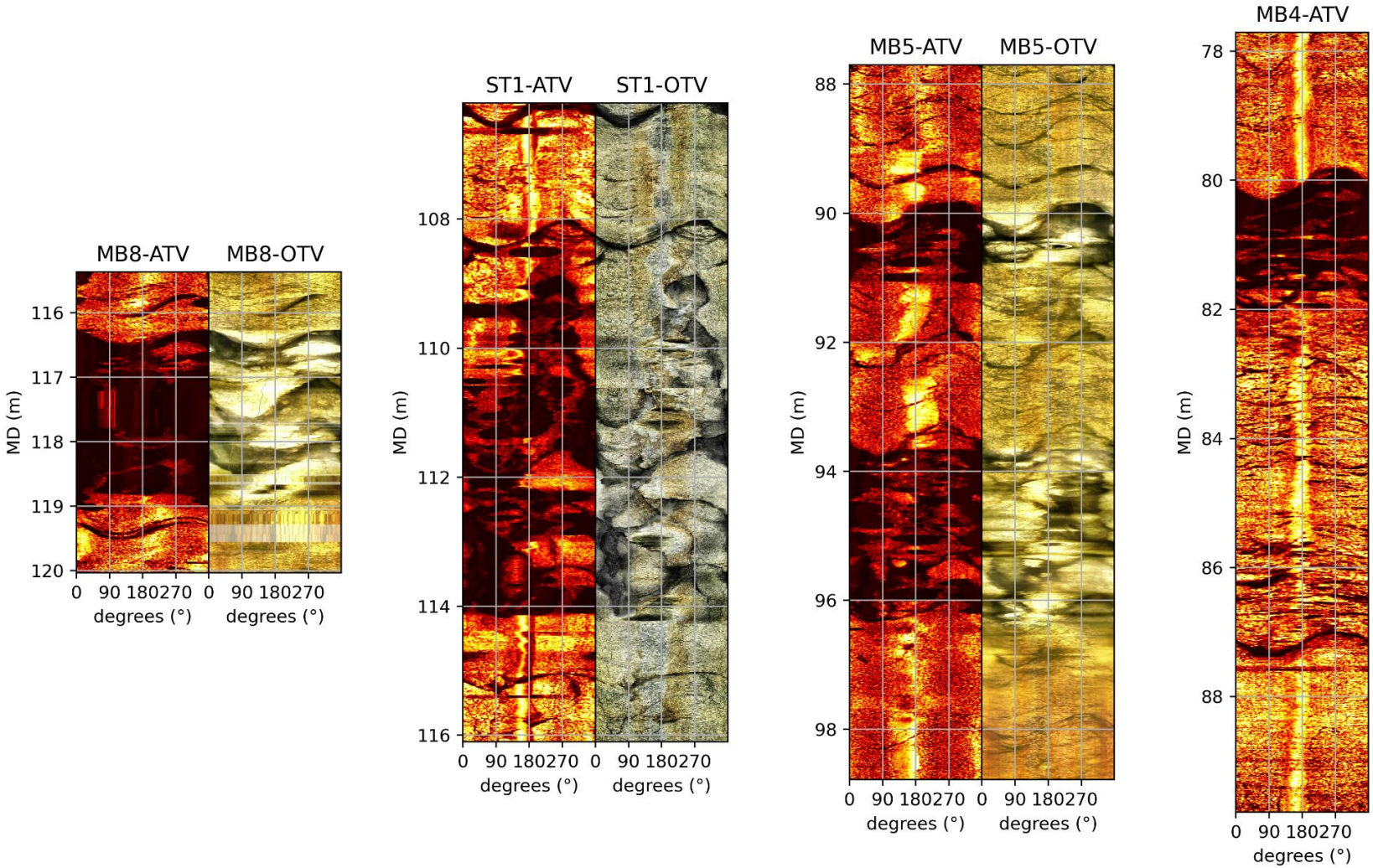

Figure 47. Individual fault zone elements correlated to form FZ_3. This is the-eastern segment of the "Bad boy" fault zone.

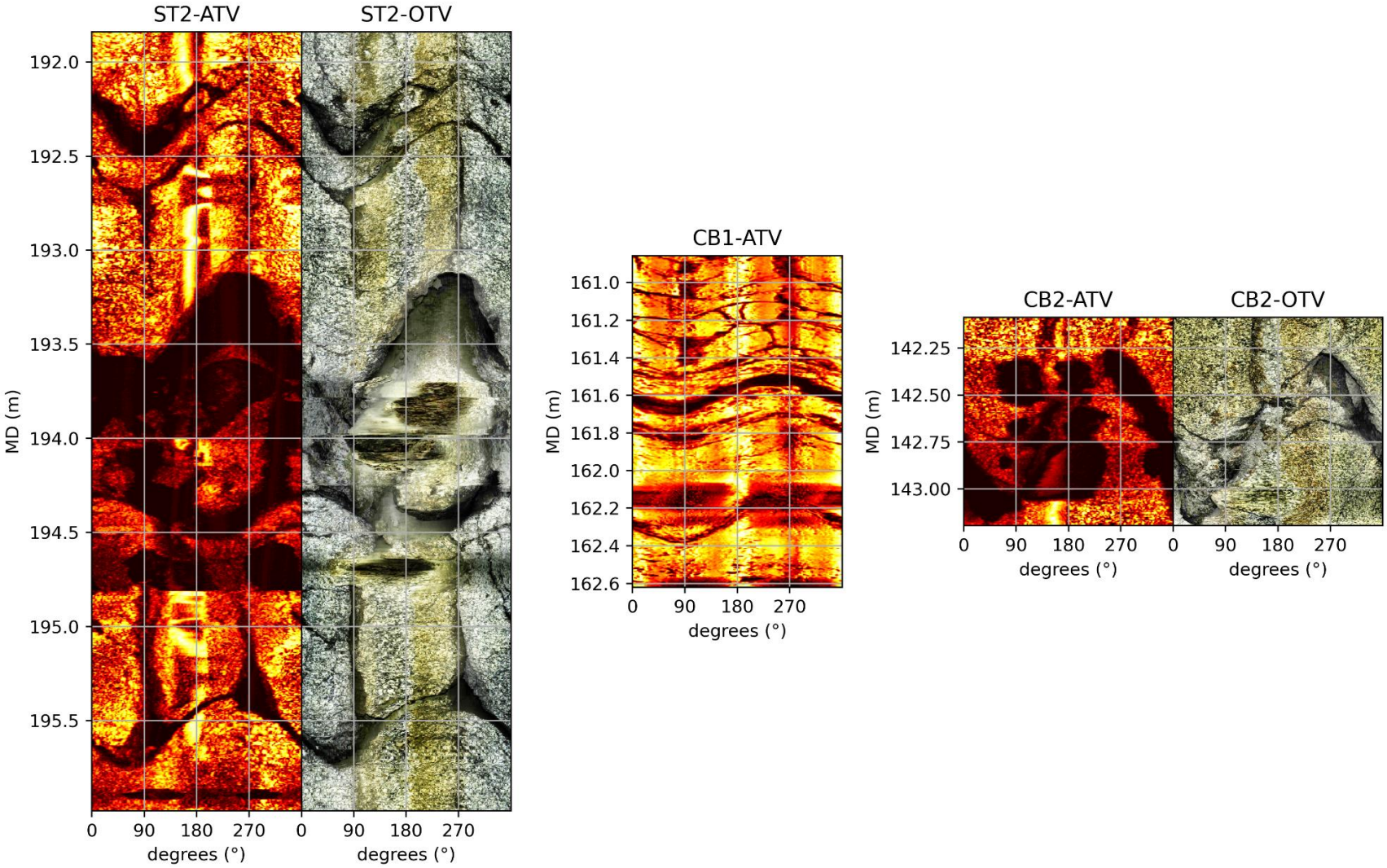

Figure 48. Individual fault zone elements correlated to form FZ_5.

6.6 Fractures

Fractures interpreted in the boreholes were analyzed to determine the dominant orientation and frequency distributions in different areas and the BULGG. Rose plots (Figure 28) and stereoplots (Figure 29) show how the variability is greater for the strike of the structures than for their dips. For this reason, the analysis that follows focus on the different strike sets. Cross plots of strike vs measured depth for different boreholes show how the dominant set (NE-SW) is omnipresent in the whole length of the boreholes while N-S fractures (blue) are more abundant near the tunnel (i.e. low md). Significant clusters of SE-NW (green) fractures are present towards the bottom of the boreholes (Figure 49).

When the fracture frequency (i.e. number of fractures per meter) is corrected for the orientation bias and interpolated between boreholes to form a grid (Figure 51), the same patterns appear. N-S fractures are more abundant in shallow depths while SE-NW form well defined clusters towards the bottom of the BULGG.

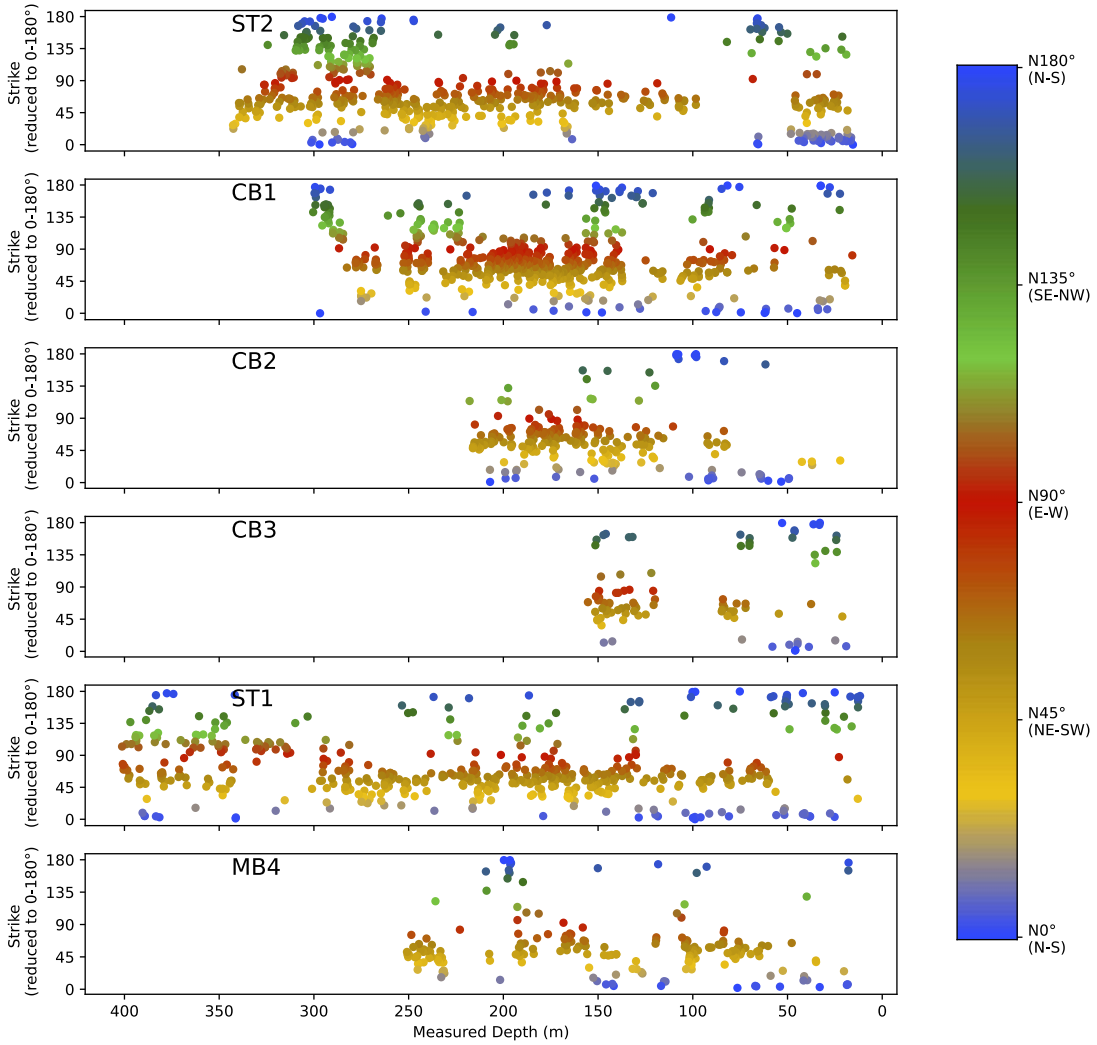

Figure 49. Crossplots of reduced fracture strikes (i.e. range 0° to 180°, if strike >180° then it is represented here as strike-180). The y-axis and the color code present the strike of structures picked in the image logs.

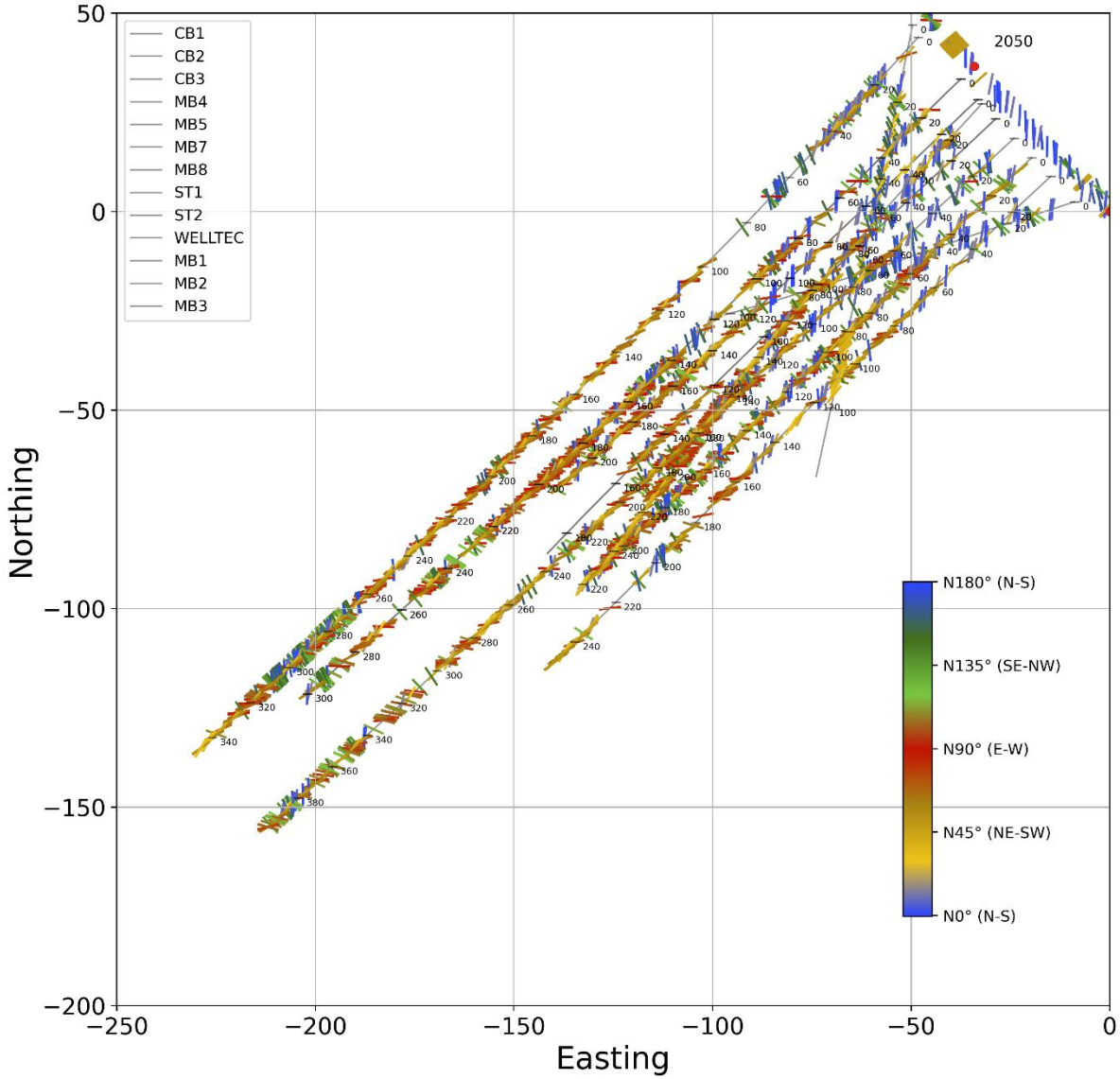

Figure 50. Map showing fractures measured along the tunnel and long boreholes in the BULGG. Structures are colored by their strike. It can be clearly seen that N-S fractures (blue) are dominant close to the tunnel while NE-SW to E-W (yellowish and red) are dominant in the mid sections of the boreholes. SE-NW fractures (green) are mostly seen towards the bottom of the boreholes.

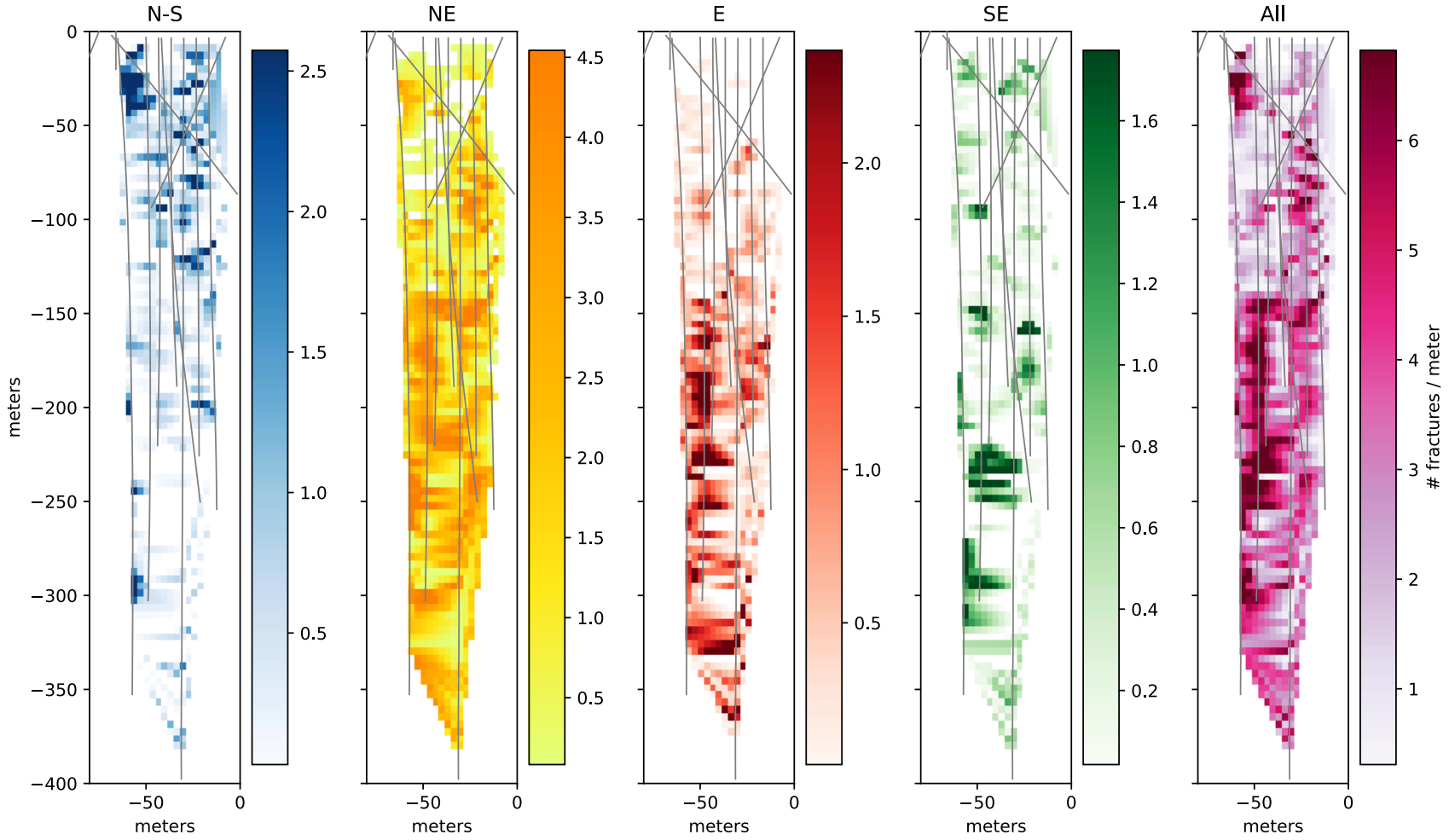

Figure 51. Gridded fracture frequencies by strike sets and for all sets. N-S fractures are more frequent near the tunnel (up in this figure) while SE-NW directions are more frequent towards the bottom.

Figure 50 shows a map view of the BULGG with all fractures picked in the different boreholes and surveyed in the tunnel. The color code represents the azimuth of the fractures.

Another tool used to analyze the variability in fracture orientations is the walkout diagram. Figure 52 shows an example of a walkout diagram used in the analysis of strike and dip of structures and their evolution with depth. The walkout diagrams are used to define segments with a dominant orientation. Once those segments are defined, the structures included in each segment are plotted in stereograms. The segments defined by a dominant structural orientation are integrated with fracture frequencies. The result is a detailed definition of segments with homogenous orientation and structure spacing.

The frequencies presented in this diagram have not been corrected for the orientation bias effect because only the relative changes are important in this analysis rather than the absolute frequencies.

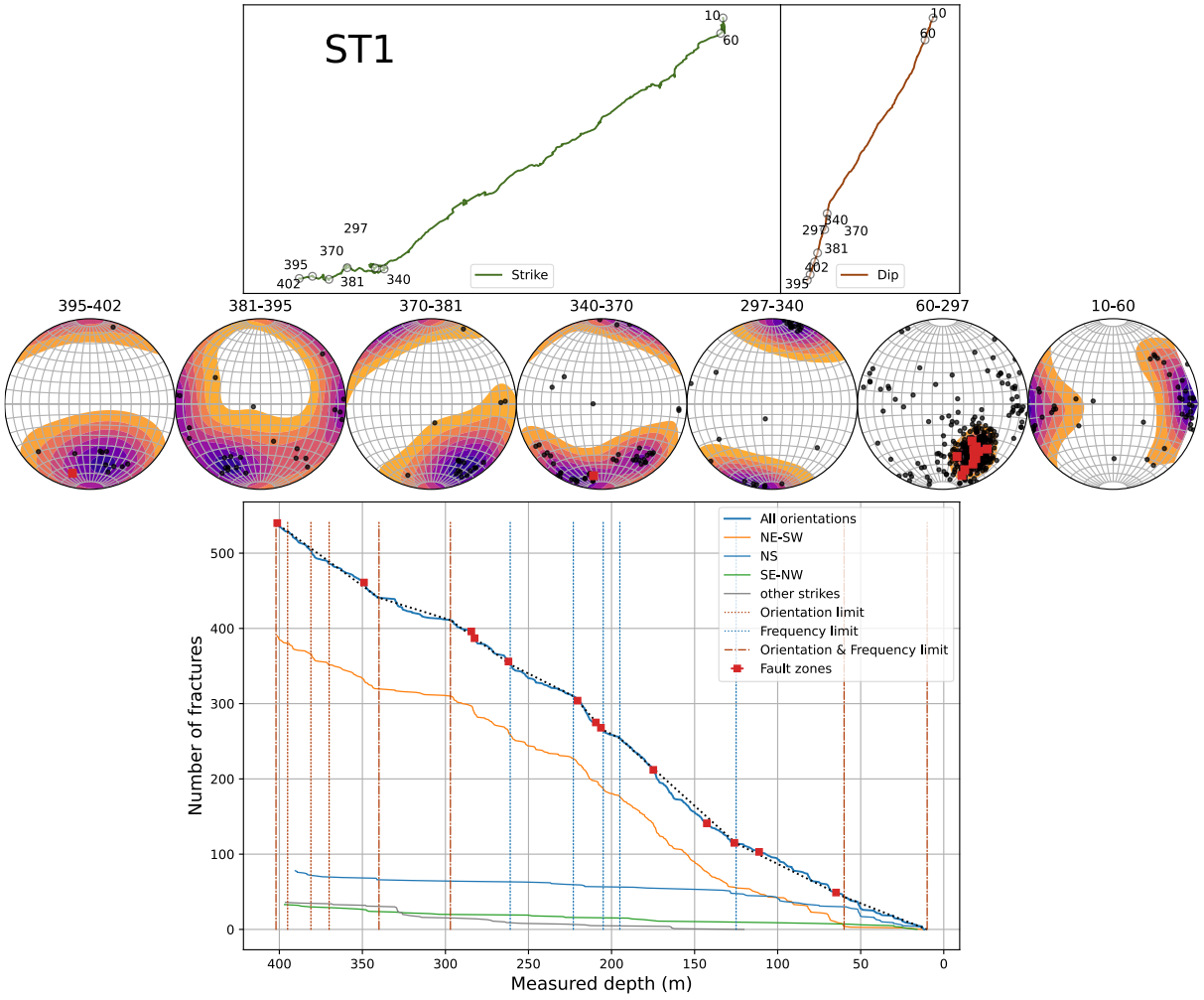

Figure 52. Walkout diagram, stereonets and frequency plot for ST1. Changes in dominant strike and/or dip are marked in the walkout diagrams and used to group fracture populations in stereonets. The corresponding diagrams for the rest of the boreholes can be seen in the appendix.

The measured depth at which those changes take place is marked with a red circle and its corresponding depth (MD). Strike (green polyline) is much more variable than the dip (red polyline). There are 4 main features that are consistently observed in all boreholes:

1) The N-S direction is dominant in the first meters of the borehole,
2) The mid-section is characterized by strikes oriented NE-SW,
3) The deepest section of the boreholes shows a significant change in the dominant strike and the SE-NW orientation is more frequent,
4) Dips increase in the deepest section of the boreholes.

Only one walkout diagram is shown here in the main text of the report. The corresponding diagrams for the rest of the boreholes are available in Appendix 4 to Appendix 12.

6.7 Fault zones and fractures: integrated model

The following hypothesis was tested to integrate the interpretation of fault zones and the analysis of background fractures and propose a conceptual model of the BULGG:

"Fault zones constitute boundaries separating units were background fracturing is different"

Based on observations on walkout diagrams (Figure 52) and plan views of the lab with fractures coloured by strike (Figure 50) a scenario of units distribution is proposed in *Figure 53*. The BULGG can be divided in 4 structural units:

1) Unit I: Includes the tunnel section of the BULGG and the shallowest depth of the boreholes. The dominant fracture orientation is N-S although NE-SW structures are also present. The lower limit of this unit is a fracture corridor identified in drillcores and image logs between 100m (ST2 and CB1) and 40m (MB4).
2) Unit II: Transitional unit between Unit I dominated by N-S structures and faults Fz-2 y Fz-3 ("Bad boy").
3) Unit III: The fracture density increases considerably, and the distribution of strikes is basically unimodal with most fractures oriented NE-SW. This unit is limited by the "Bad boy" and faults Fz-11 and Fz-12.
4) Unit IV: The deepest unit is characterized by the appearance of steep fractures with strike SE-NW.

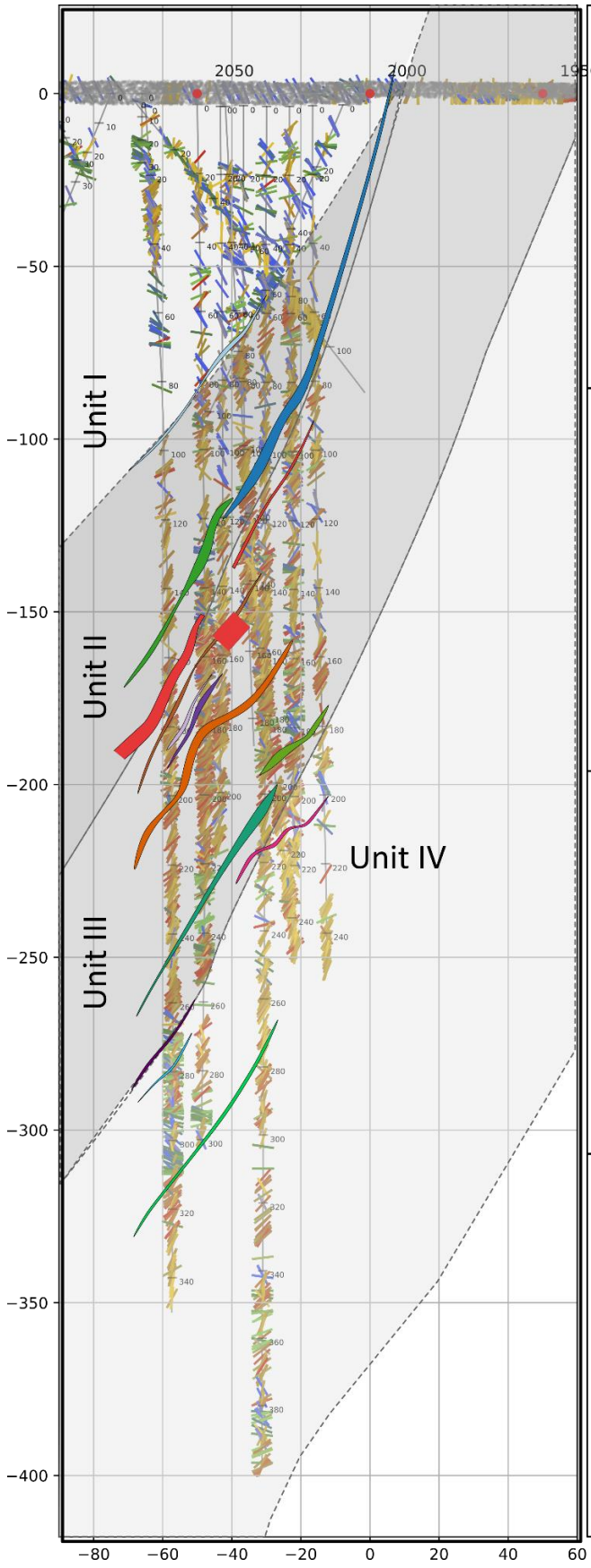

Unit I:
- Above Fz-01.
- N-S fractures are dominant.
- Consistency btw tunnel and BHs.

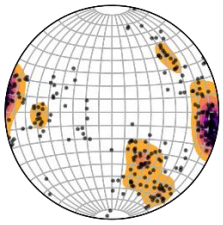

Unit II:
- Between Fz-01 and "Bad Boy".
- Transitional between N-S and NE-SW fractures.

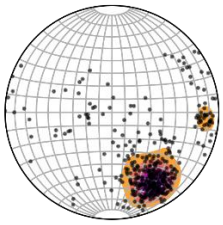

Unit III:
- Between "Bad Boy" and Fz-11 & 12.
- Fractures oriented NE-SW are clearly dominant.

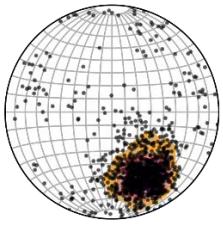

Unit IV:
- Bellow Fz-11 & 12.
- NE-SW fractures still dominant but NW-SE direction is more frequent than above.

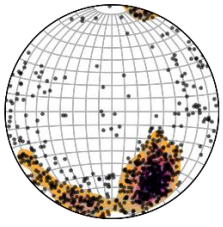

Figure 53. Integrated model where specific fault zones constitute the limits of units with different configurations in the background fractures.

Table 4. Fracture spacing per unit, orientation and boreholes. Spacing has been corrected using the borehole trajectories (Terzaghi's correction).

		Fracture Spacing - Corrected (m)					
Unit	**Orientation**	**st2**	**cb1**	**cb2**	**cb3**	**st1**	**mb4**
unit_1	**N**	2.6	28.6		9.1	2.7	
	S	1.5	4.1	3.6	3.8	2.9	2.6
	NE						
	SW	2.2	5.1	7.5		15.6	6.4
	E						
	W		7.0				
	SE	8.7				6.4	
	NW						
unit_2	**N**		1.8	3.3			
	S		13.2	4.4		3.2	7.3
	NE						
	SW	1.7	1.3	1.6	2.1	1.4	1.2
	E						
	W	5.0	3.2	16.3		9.9	
	SE		6.9	12.6			
	NW		4.6				
unit_3	**N**		9.8	9.4		8.4	
	S	7.6	3.1	9.1		12.7	4.8
	NE	42.7	18.9	23.8		21.8	9.8
	SW	0.7	0.5	0.8	1.4	0.8	1.8
	E	20.9	11.4		8.7		22.7
	W	1.9	0.8	1.8	3.8	2.2	6.8
	SE	22.9	5.4			20.1	
	NW		14.1	13.0			
unit_4	**N**	2.8	3.1			19.2	
	S	3.0				18.5	4.1
	NE	13.6	4.9			43.1	
	SW	1.1	1.4			1.3	1.5
	E		2.4			6.1	
	W	1.8	1.4			4.2	10.4
	SE	4.6	6.9			26.0	15.4
	NW	0.9	2.4			8.0	

Table 5. Fracture count per unit, orientation and borehole

		Fracture Count					
Unit	**Orientation**	**st2**	**cb1**	**cb2**	**cb3**	**st1**	**mb4**
unit_1	N	21	3	1	4	10	
	S	32	17	8	10	17	10
	NE	1	2				1
	SW	37	14	3	2	4	3
	E	1	1				
	W	2	11			1	
	SE	8	2		1	8	1
	NW	2			2	2	
unit_2	N	1	12	3		1	
	S		5	13		15	7
	NE		2				2
	SW	29	45	42	7	42	30
	E						
	W	8	18	5		6	2
	SE		9	3	1	1	
	NW		6	1	1	1	
unit_3	N		8	6	2	4	1
	S	12	8	5	2	5	9
	NE	3	3	3		3	4
	SW	132	158	89	23	71	39
	E	4	7		3		4
	W	52	118	38	9	23	10
	SE	4	16	2	2	3	1
	NW	2	7	6	2	2	
unit_4	N	17	9			10	
	S	10	1			12	10
	NE	3	6			5	
	SW	79	31			169	47
	E	2	4			20	1
	W	44	35			51	5
	SE	12	9			9	4
	NW	52	23			27	1

Table 6. Fracture counts per unit, simplified orientation and boreholes.

		Fracture Count					
Unit	**Orientation**	**st2**	**cb1**	**cb2**	**cb3**	**st1**	**mb4**
unit_1	**N-S**	53	20	9	14	27	10
	NE-SW	38	16	3	2	4	4
	E-W	3	12			1	
	SE-NW	10	2		3	10	1
unit_2	**N-S**	1	17	16		16	7
	NE-SW	29	47	42	7	42	32
	E-W	8	18	5		6	2
	SE-NW	0	15	4	2	2	
unit_3	**N-S**	12	16	11	4	9	10
	NE-SW	135	161	92	23	74	43
	E-W	56	125	38	12	23	14
	SE-NW	6	23	8	4	5	1
unit_4	**N-S**	27	10			22	10
	NE-SW	82	37			174	47
	E-W	46	39			71	6
	SE-NW	64	32			36	5

Table 7. Fracture counts per unit and orientations for all boreholes.

	Fracture count							
	N	S	NE	SW	E	W	SE	NW
unit_1	39	94	4	63	2	14	20	6
unit_2	17	40	4	195		39	14	9
unit_3	21	41	16	512	18	250	28	19
unit_4	36	33	14	326	27	135	34	103

Table 8. Fracture counts per unit and simplified orientations.

	Fracture count			
	N-S	NE-SW	E-W	SE-NW
unit_1	133	67	16	26
unit_2	57	199	39	23
unit_3	62	528	268	47
unit_4	69	340	162	137

7. Conclusions

The main conclusions reached though the analysis presented here are:

- The frequency of structures is, in general, low near the tunnel and it increases after below fault zones FZ-01 and FZ-02. Maximum frequencies are usually found in the mid-section of the boreholes while they decrease gradually towards the bottom.
- The main structure sets in terms of orientations are (from higher to lower occurrence):
    - NE-SW to E-W dipping to the North.
    - North-South dipping to the West.
    - NW-SE dipping both to the NE and SW.
- 90% of identified fault zones (i.e 69 out of 74) belong to the NE-SW oriented set.
- Fault zones were correlated across boreholes. A total of 15 connected fault zones were identified.
- In contrast with the constant orientation of fault zones, the dominant orientation of fractures changes across the BULGG. Based on these changes, the BULGG can be divided into 4 units according to the dominant orientation of fractures. These units are bounded by some of the fault zones correlated across the boreholes:
    - Unit I: This unit includes the BULGG section of the tunnel and the shallowest section of the boreholes. The dominant fracture orientation is N-S. The lower limit of this unit is a fault zone (FZ_1).
    - Unit II: Includes the volume between FZ_1 and the fault known as the "Bad Boy" (FZ_2 and FZ_3). It is a transitional unit where the orientation N-S becomes less frequent while fractures oriented NE-SW become more frequent.
    - Unit III: Unit below the "Bad Boy". Most fractures are oriented NE-SW.
    - Unit IV: Located towards the bottom of the boreholes. The NE-SW orientation is still dominant, but the NW-SE orientation becomes relatively more important.
- A conceptual structural model of the BULGG is proposed in which fault surfaces of around 30-200m length constitute the boundaries of structural units. Each one of these structural units presents a dominant fracture orientation. The structural units are around 100-200m thick. The orientation of fractures in units II and III are greatly influenced by the orientation of the main fault surfaces while the orientations in units I and IV are somewhat different.
- Some implications of this conceptual model are:
    - The orientation of main fault zones is unimodal. This is important to consider if fault zones constitute boundaries or pathways to fluid flow.
    - If the background fractures are in some way influencing fluid flow then it is expected that the interactions fluid flow-structure are different in distinct structural units.

- Fault zones and generic fractures are expected to behave differently because they have inherently different properties. In addition, the differing distribution of orientations is expected to accentuate these differences and influence of the interactions between structure and other reservoir parameters.

8. References

Chester, F. M., Evans, J. P., & Biegel, R. L. (1993). Internal structure and weakening mechanisms of the San Andreas Fault. Journal of Geophysical Research: Solid Earth, 98(B1), 771–786.

Debon F., M. Lemmet, 1999, Evolution of Mg/Fe Ratios in Late Variscan Plutonic Rocks from the External Crystalline Massifs of the Alps (France, Italy, Switzerland), Journal of Petrology, Volume 40, Issue 7, Pages 1151–1185, https://doi.org/10.1093/petroj/40.7.1151

Faulkner, D., Lewis, A., & Rutter, E. (2003). On the internal structure and mechanics of large strike-slip fault zones: field observations of the Carboneras fault in southeastern Spain. Tectonophysics, 367(3-4), 235–251.

Jordan, D., (2018), Geological Characterization of the Bedretto Underground Laboratory for Geoenergies, Master thesis, ETH Zurich.

Pfiffner, O. A. (2010): Geologie der Alpen, 2nd ed., Bern-Stuttgart-Wien: Haupt Verlag.

Sergeev, S. A., & Steiger, R. H. (1995). Caledonian and Variscan granitoids of the Gotthard massif: new geochronological and geochemical results. Schweizerische Mineralogische und Petrographische Mitteilungen, 75, 315–316.

Woodcock, N.H. & Mort, K. (2008). Classification of fault breccias and related fault rocks. Geological Magazine, 145(3), 435-440.

Lützenkirchen, V. and Loew, S., 2011, Late Alpine brittle faulting in the Rotondo granite (Switzerland): Deformation mechanisms and fault evolution. Swiss Journal of Geosciences, 104(1):31–54.

Lützenkirchen, V. H., 2002, Structural Geology and Hydrogeology of Brittle Fault Zones in the Central and Eastern Gotthard Massif, Switzerland (PhD Thesis). ETH Zürich.

Rast, M., 2020, Geology, Geochronology and Rock Magnetics Along Bedretto Tunnel (Gotthard Massif, Central Alps) and Numerical Modelling of Quartz-Biotite Aggregates. MSc thesis, ETH.

9. Appendix

			non-foliated	foliated
>30% large clasts >2 mm	75-100% large clasts (>2 mm)	fault breccia	crackle breccia	
	60-75% large clasts (>2 mm)		mosaic breccia	
	30-60% large clasts (>2 mm)		chaotic breccia	
<30% large clasts >2 mm	incohesive[1]		**fault gouge**	
	cohesive	glass or devitrified glass	**pseudotachylyte**	
		0-50% matrix (<0.1 mm)	**protocataclasite**	**protomylonite**
		50-90% matrix (<0.1 mm)	**(meso)cataclasite**	**(meso)mylonite**
		90-100% matrix (<0.1 mm)	**ultracataclasite**	**ultramylonite**
		pronounced grain growth		**blastomylonite**[2]

[1]incohesive at present outcrop

[2]some blastomylonites have >30% large porphyroclasts

Appendix 1. Classification of fault rocks by Woodcock and Mort (2008).

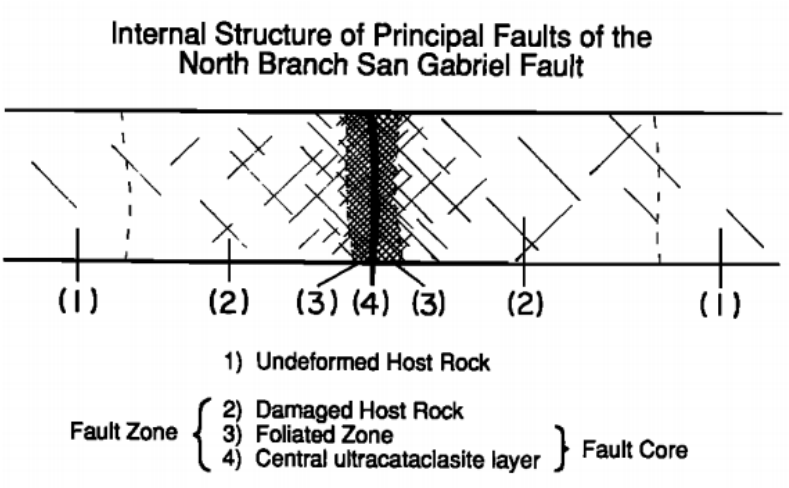

Appendix 2. Single Fault Core-Damage Zone model as proposed by Chester et al. (1993).

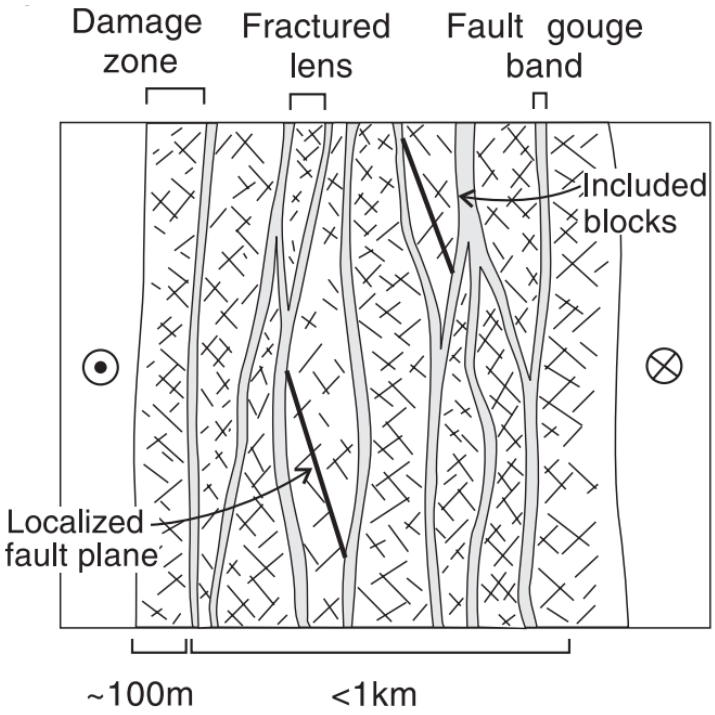

Appendix 3. Multi-branch fault zone model proposed by Faulkner et al. (2003).

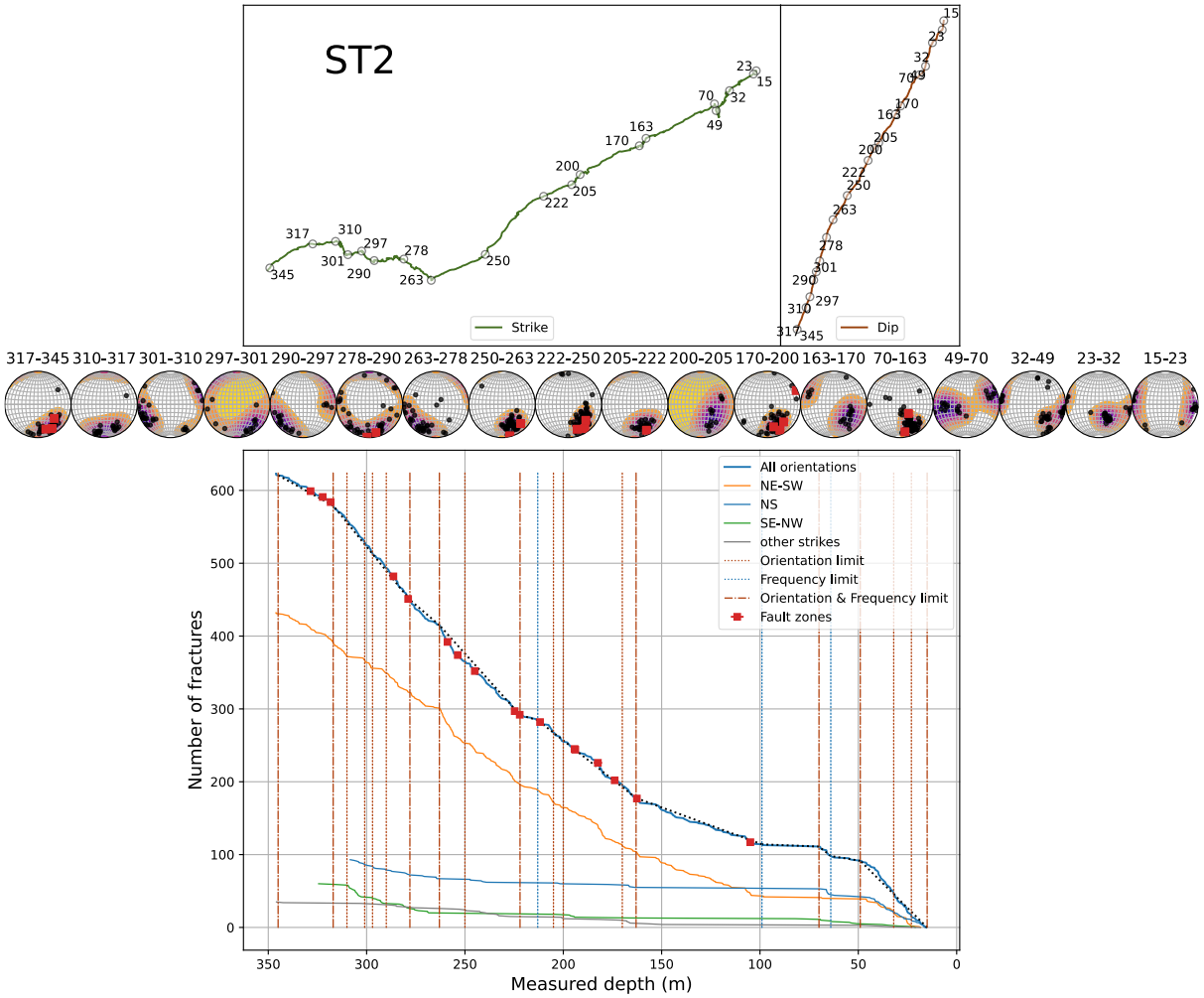

Appendix 4. Walkout, stereonets and frequency plots for fractures in ST2.

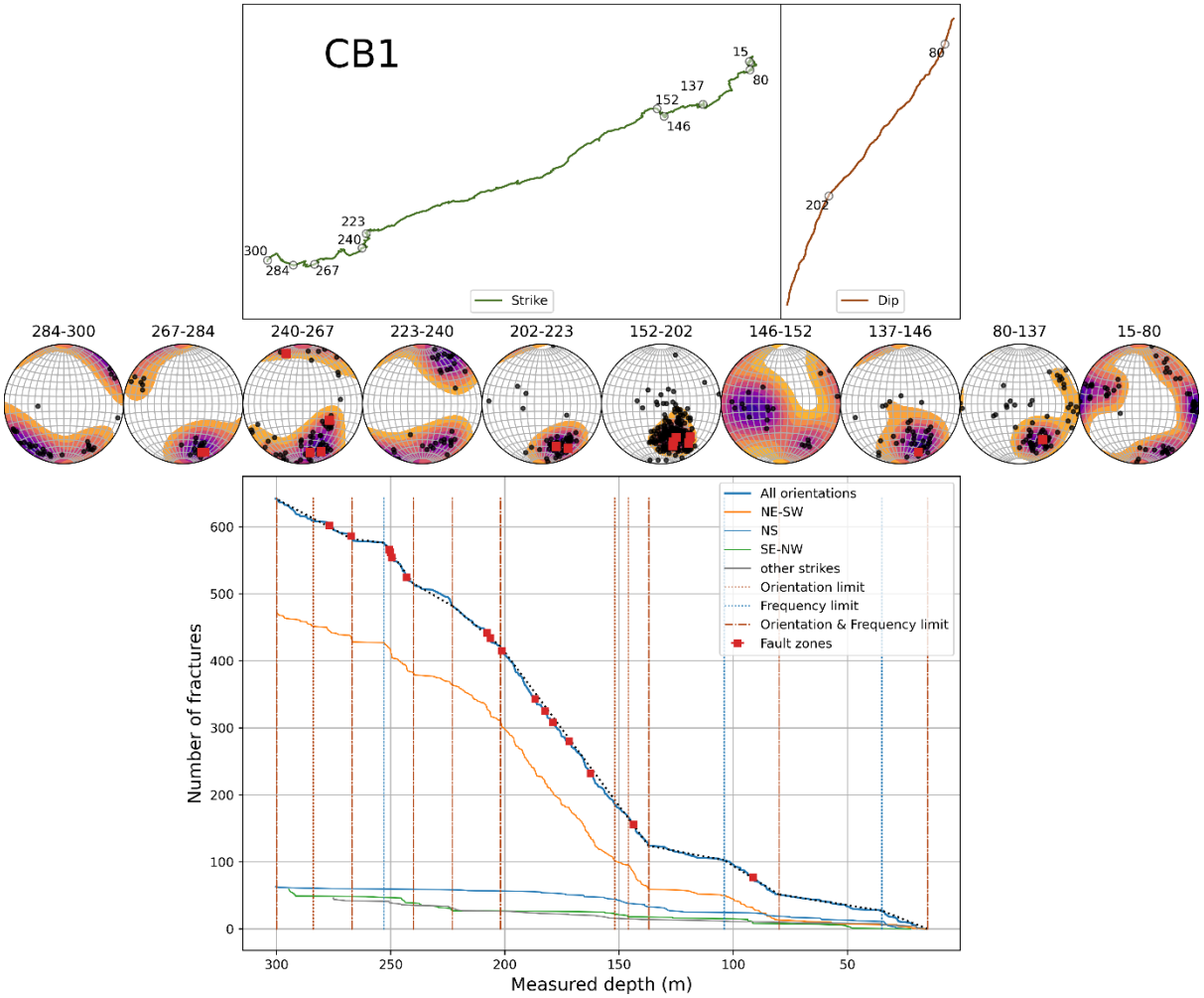

Appendix 5. Walkout, stereonets and frequency plots for fractures in CB1.

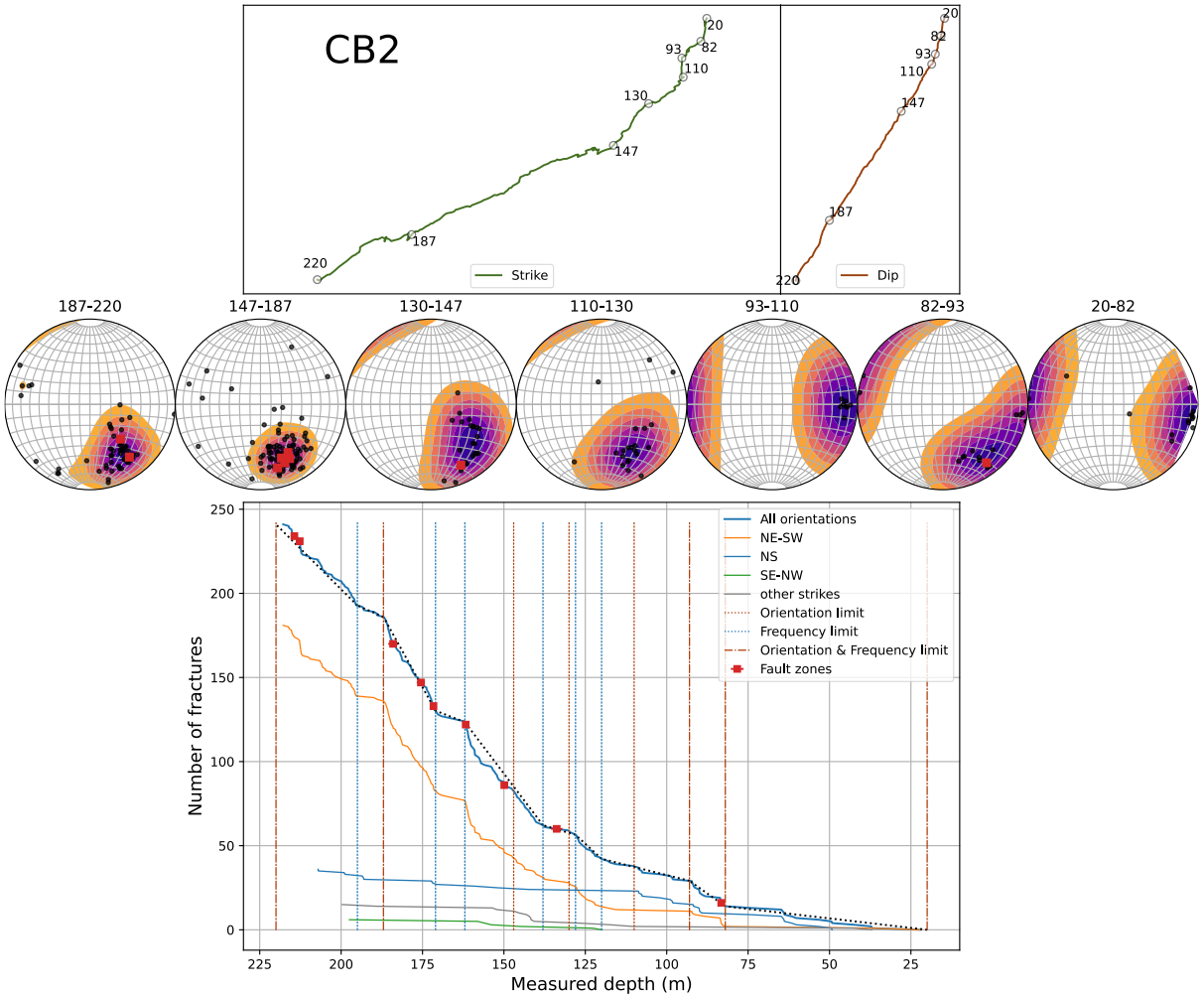

Appendix 6.Walkout, stereonets and frequency plots for fractures in CB2.

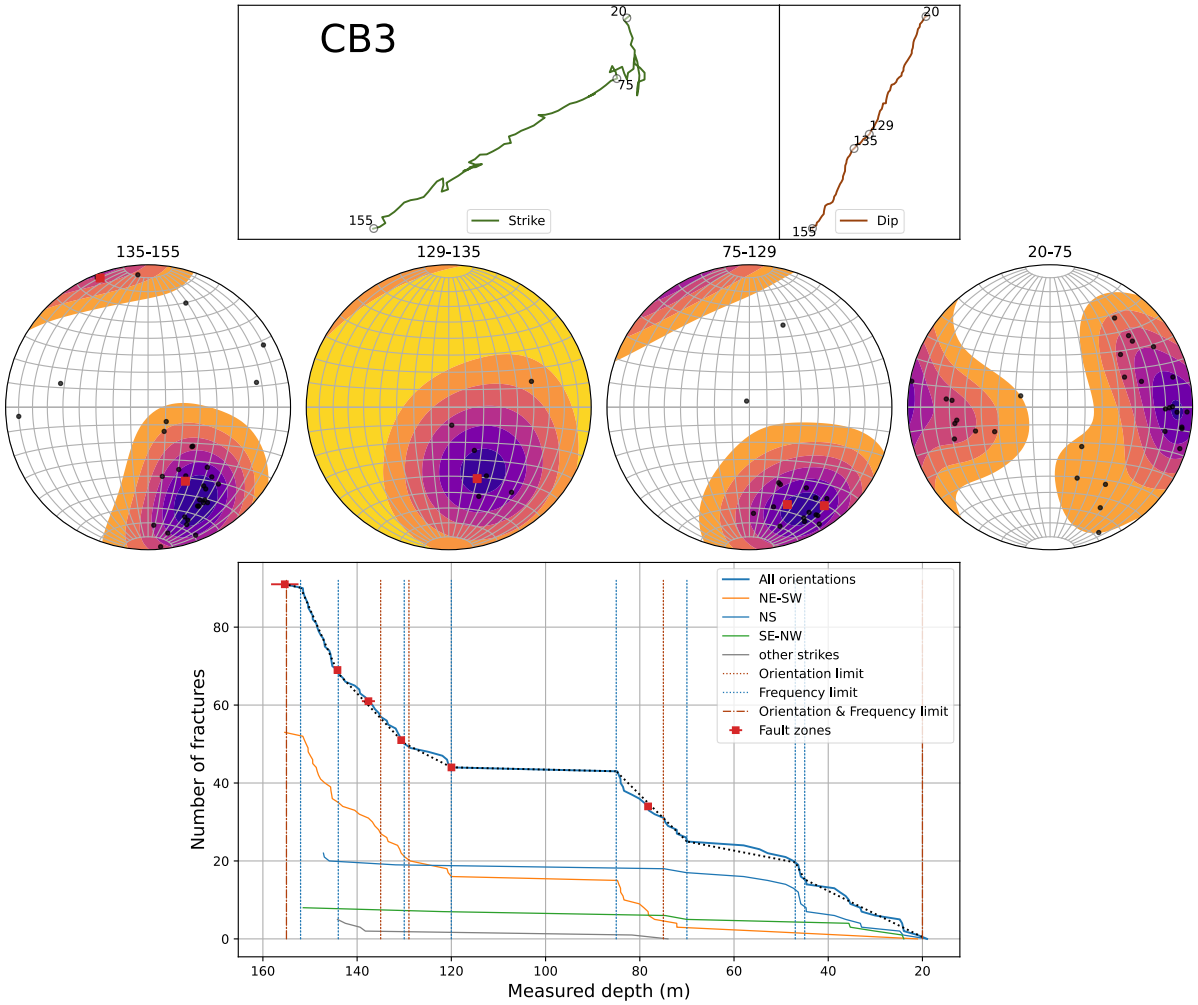

Appendix 7. Walkout, stereonets and frequency plots for fractures in CB3.

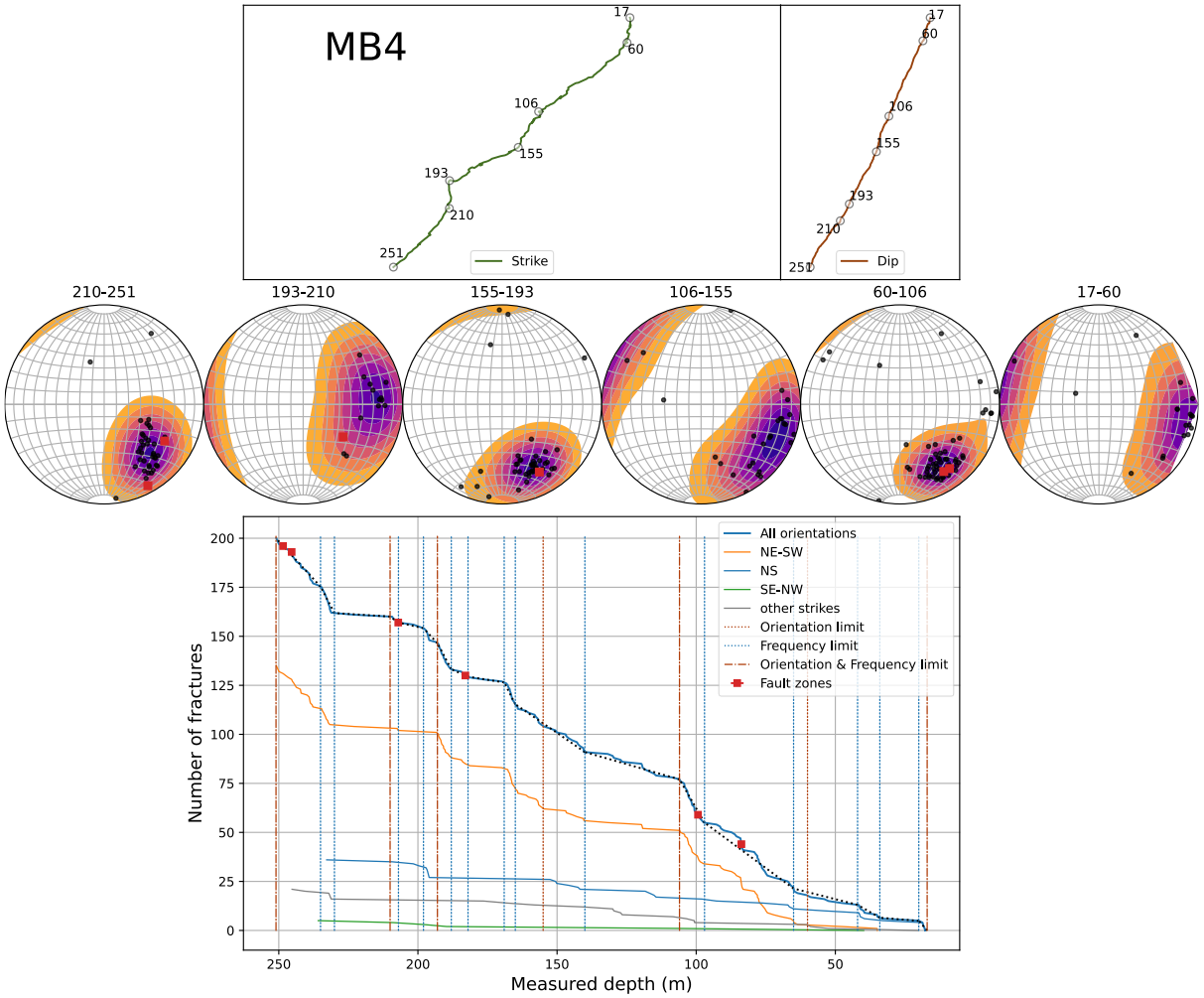

Appendix 8. Walkout, stereonets and frequency plots for fractures in MB4.

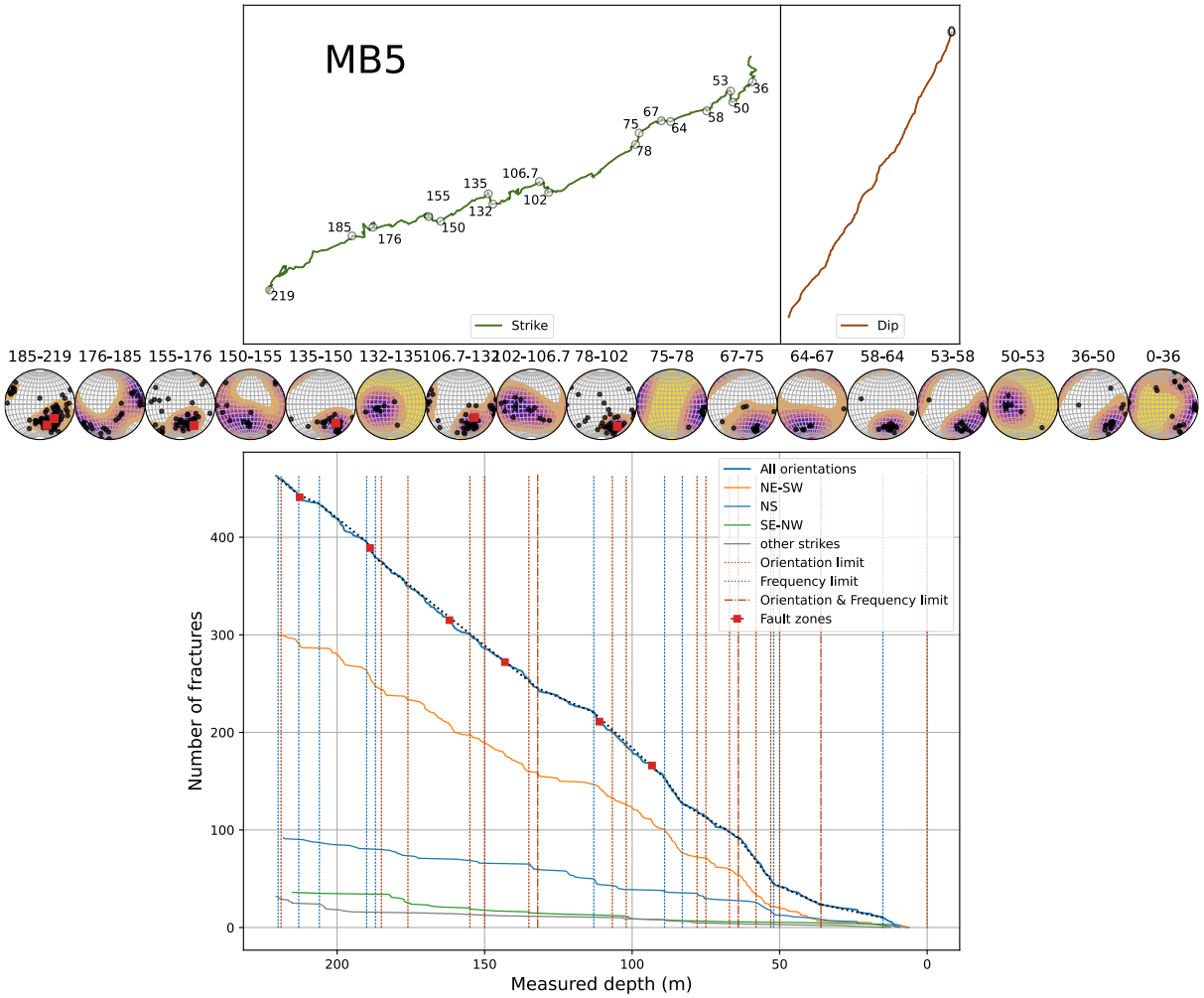

Appendix 9. Walkout, stereonets and frequency plots for fractures in MB5.

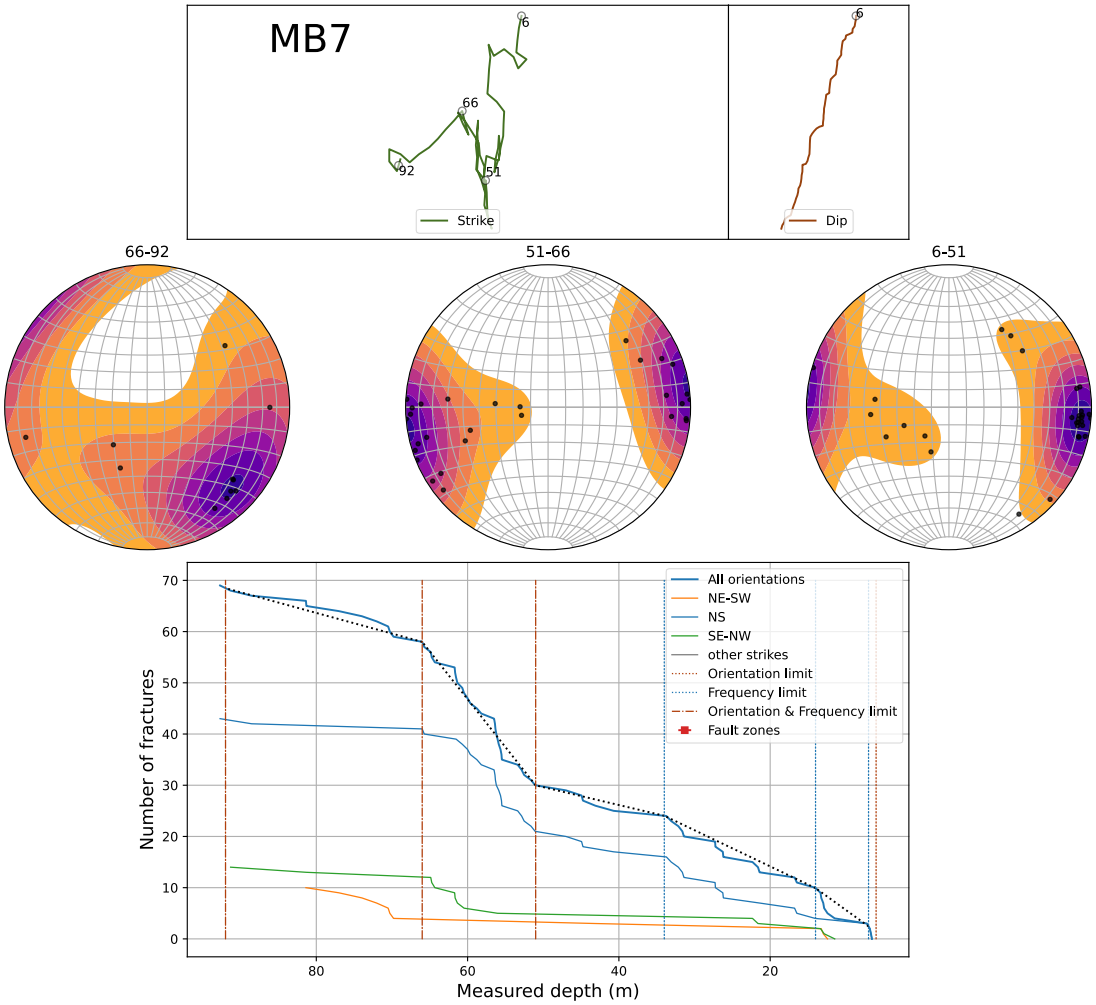

Appendix 10. Walkout, stereonets and frequency plots for fractures in MB7.

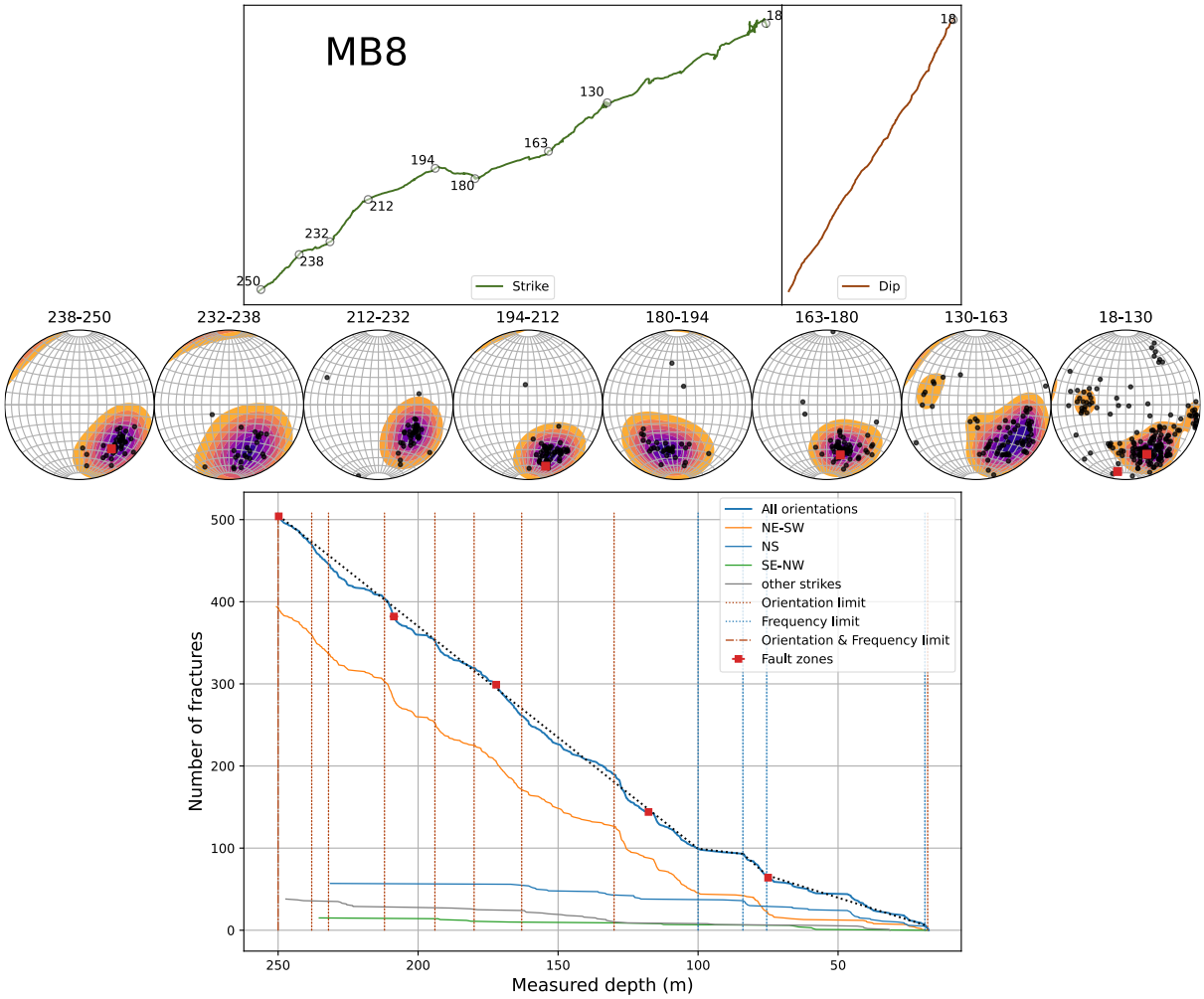

Appendix 11. Walkout, stereonets and frequency plots for fractures in MB8.

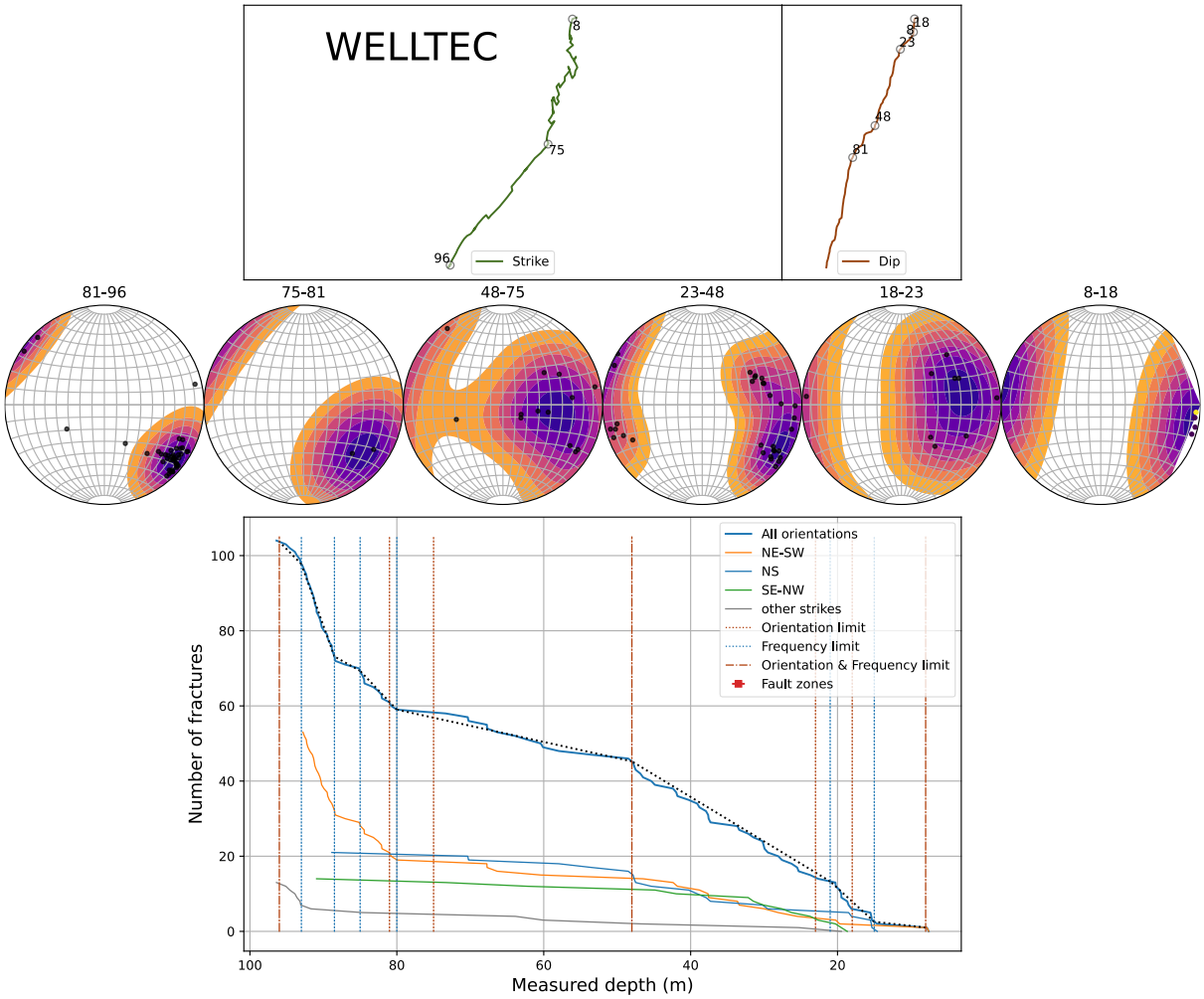

Appendix 12. Walkout, stereonets and frequency plots for fractures in WELLTEC.

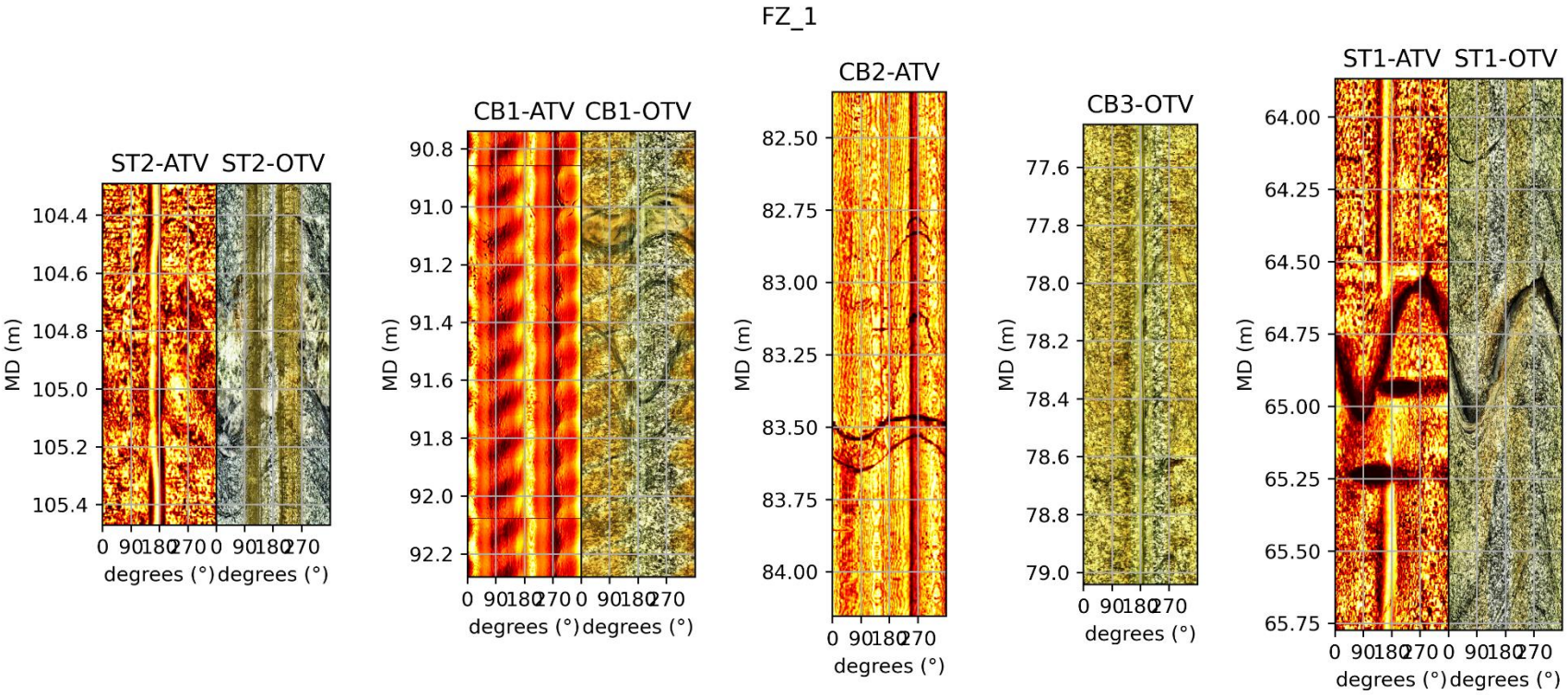

Appendix 13

FZ_4

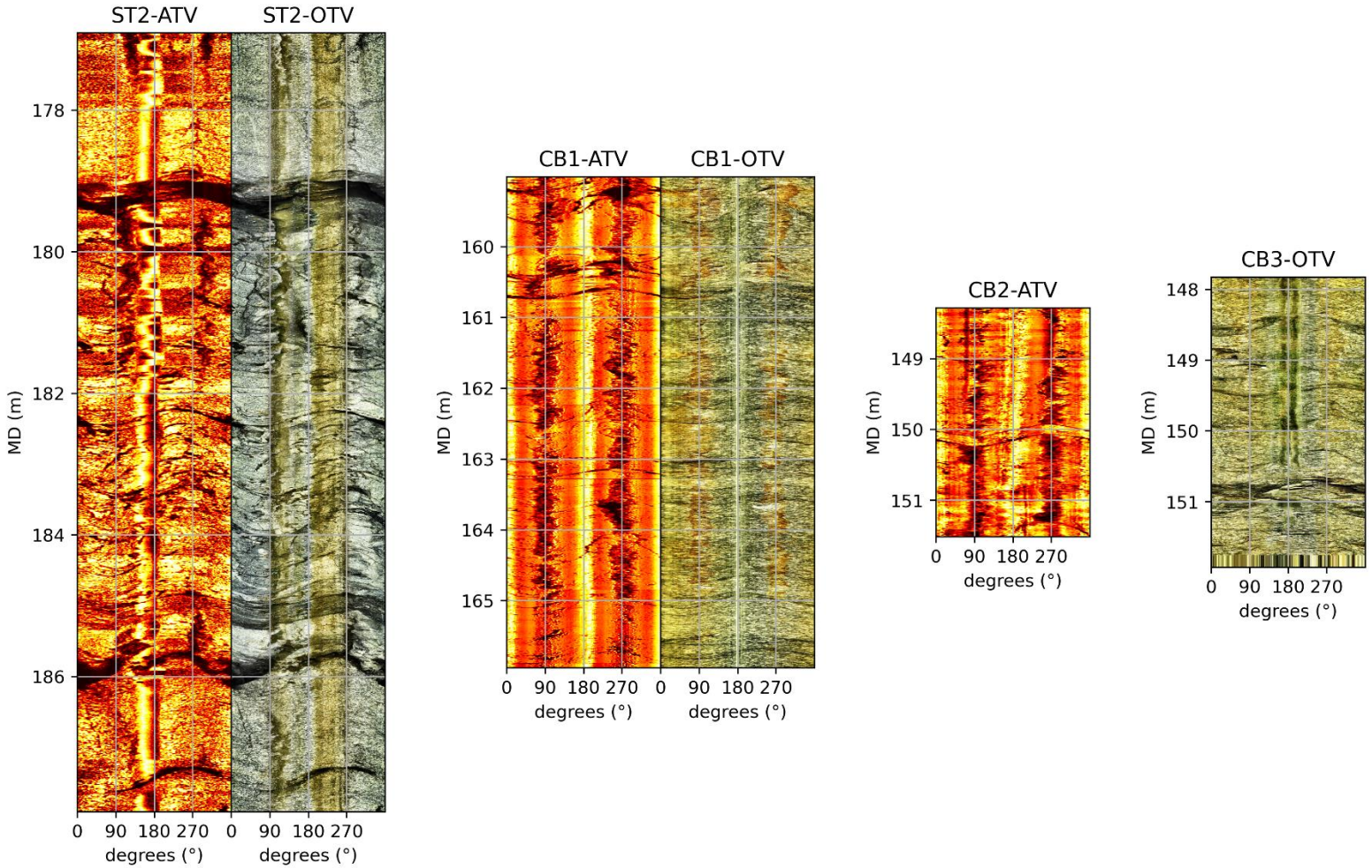

Appendix 14

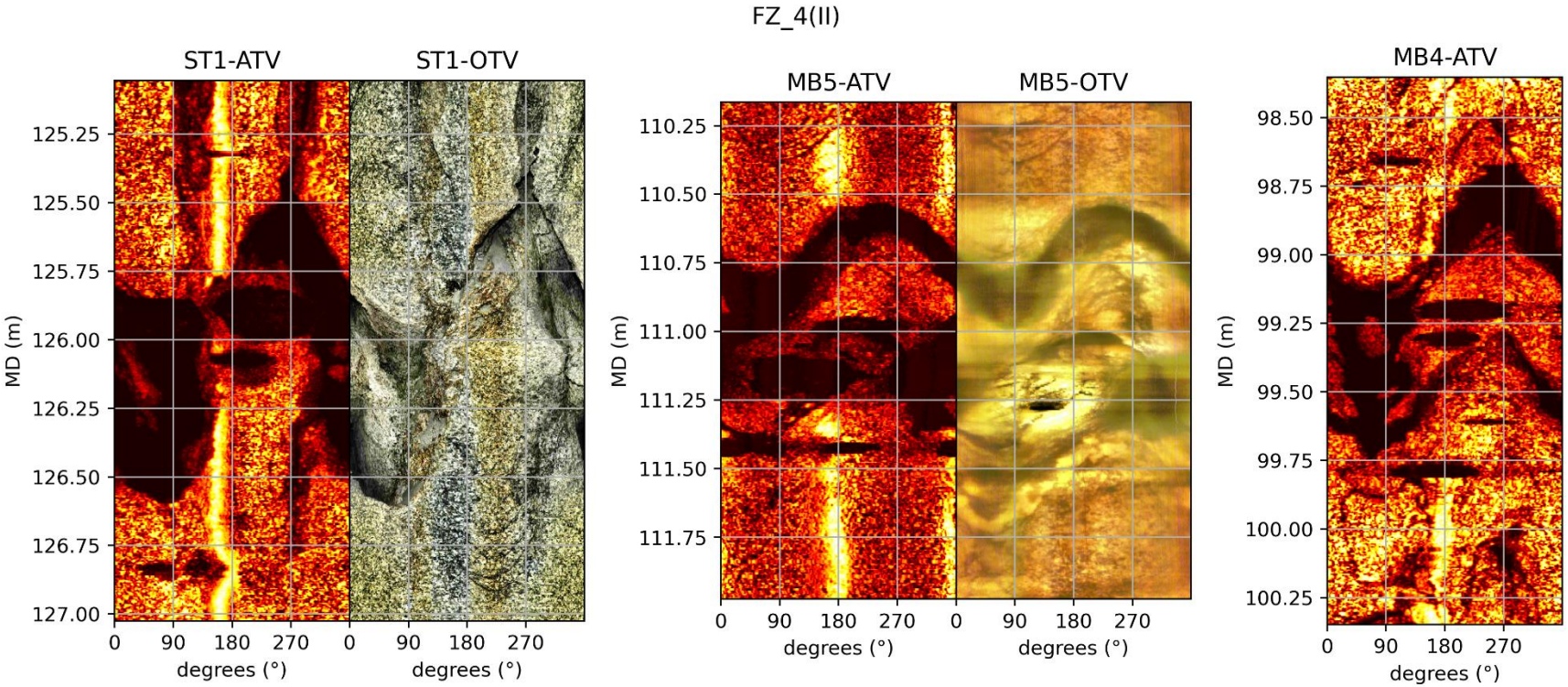

Appendix 15

FZ_6

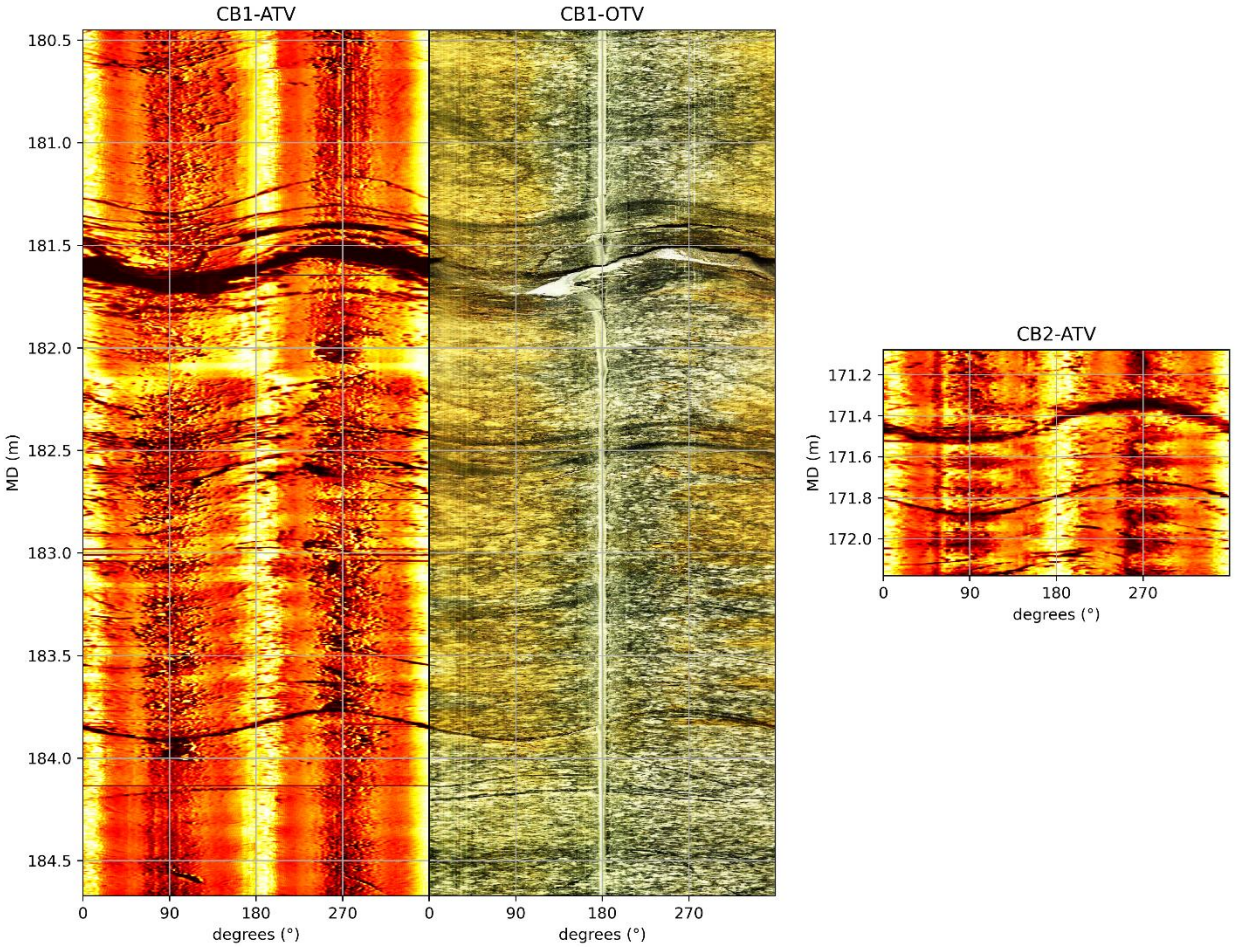

Appendix 16

FZ_7

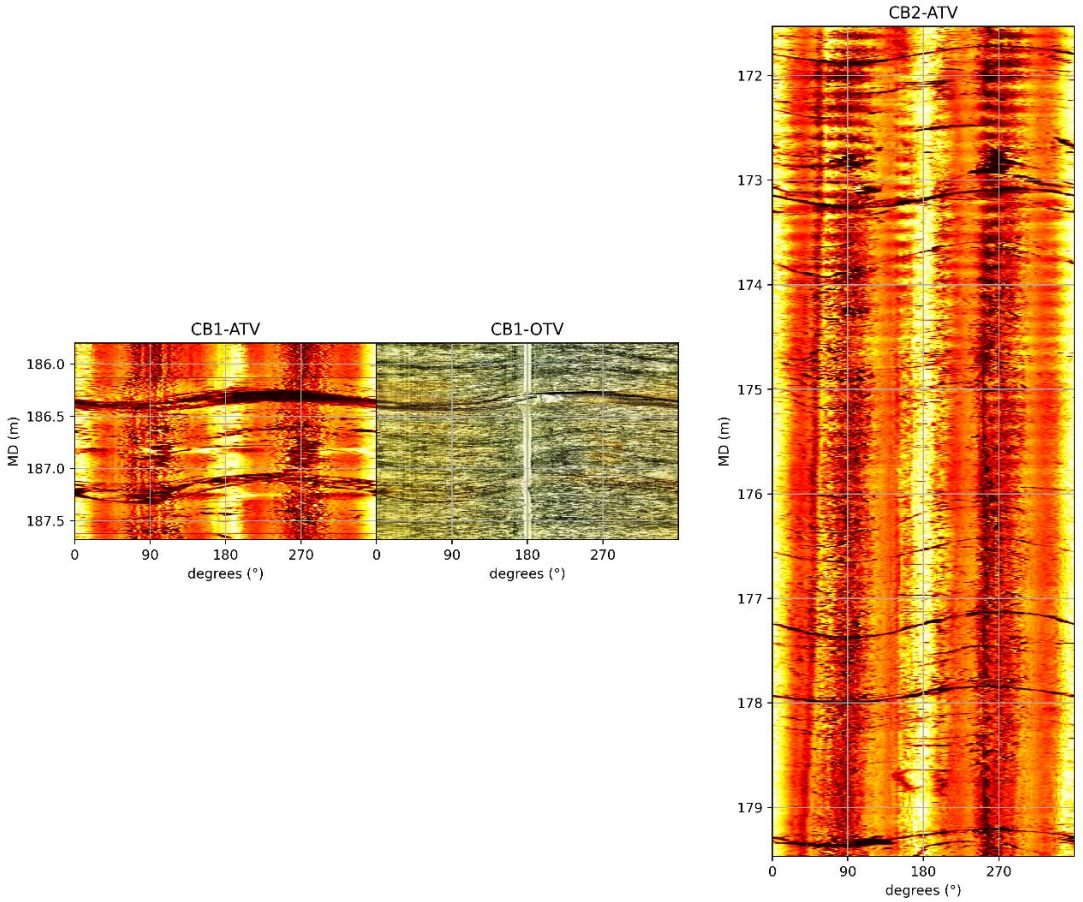

Appendix 17

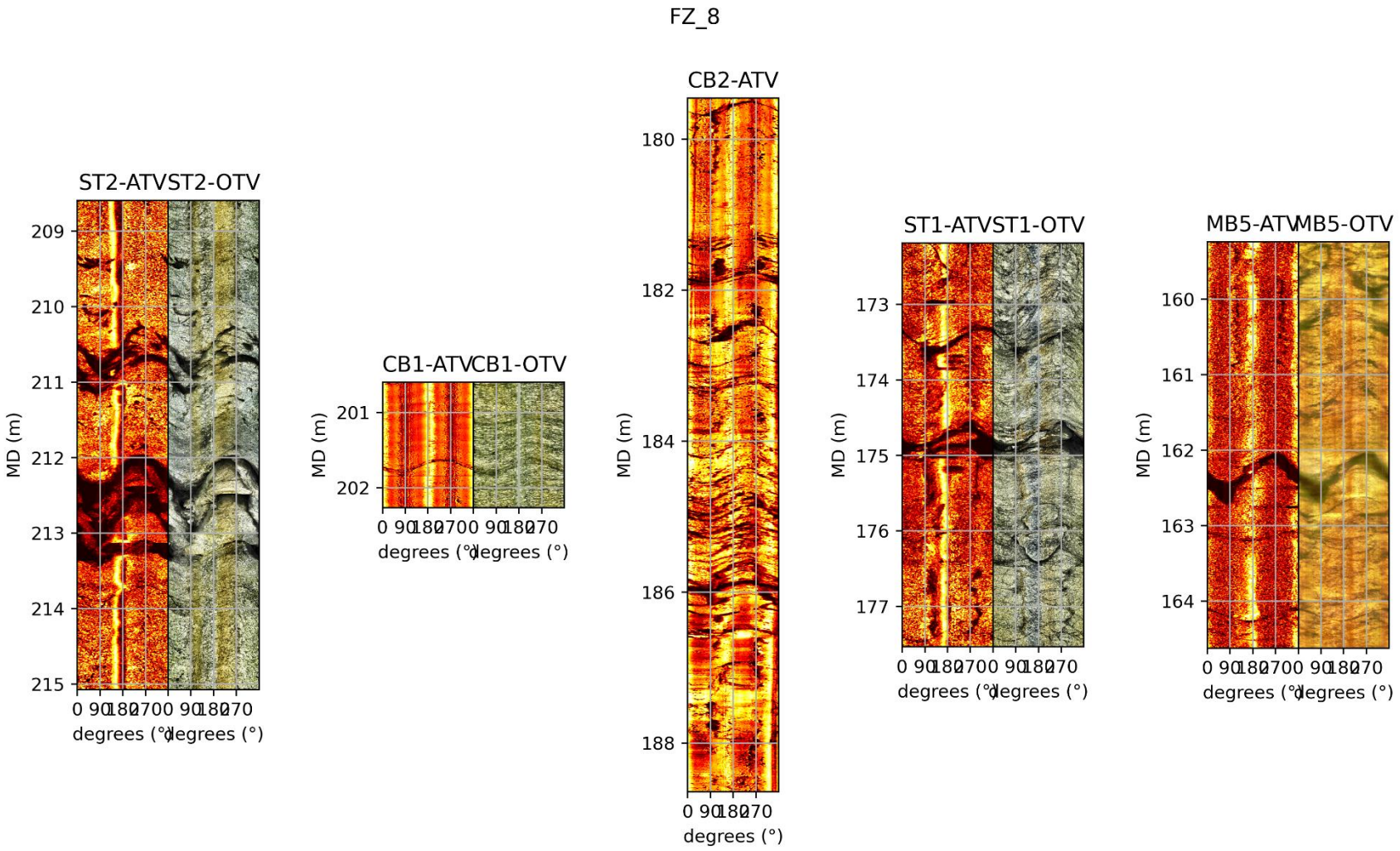

Appendix 18

FZ_9

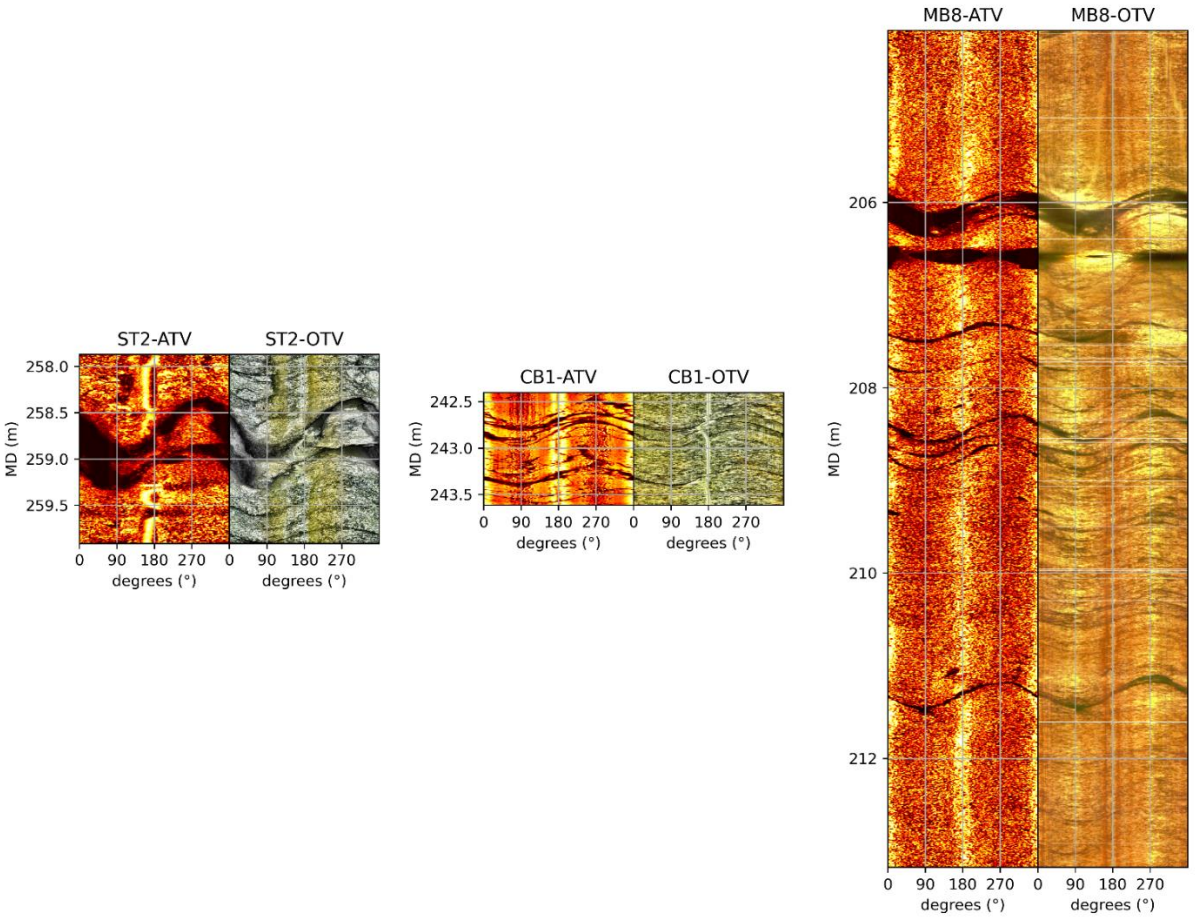

Appendix 19

FZ_10

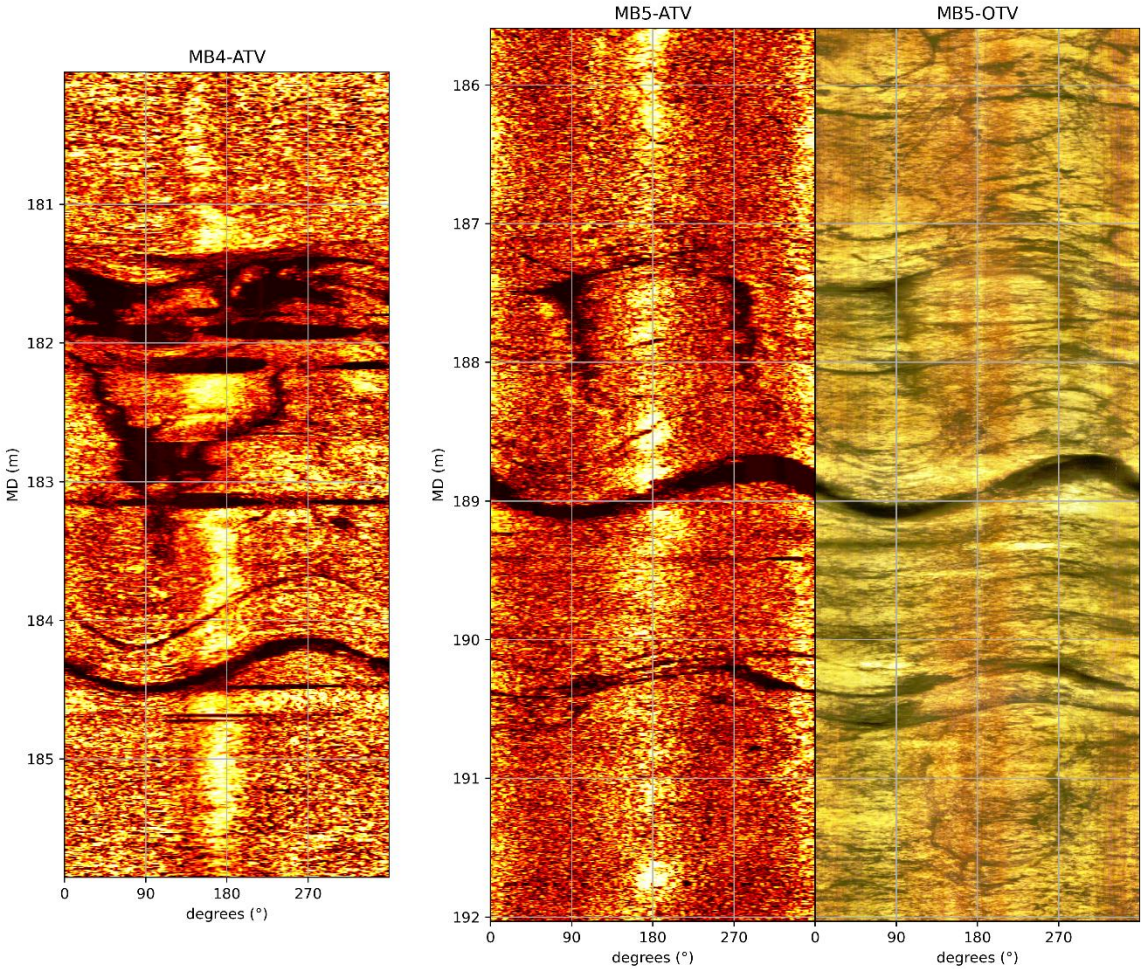

Appendix 20

FZ_11

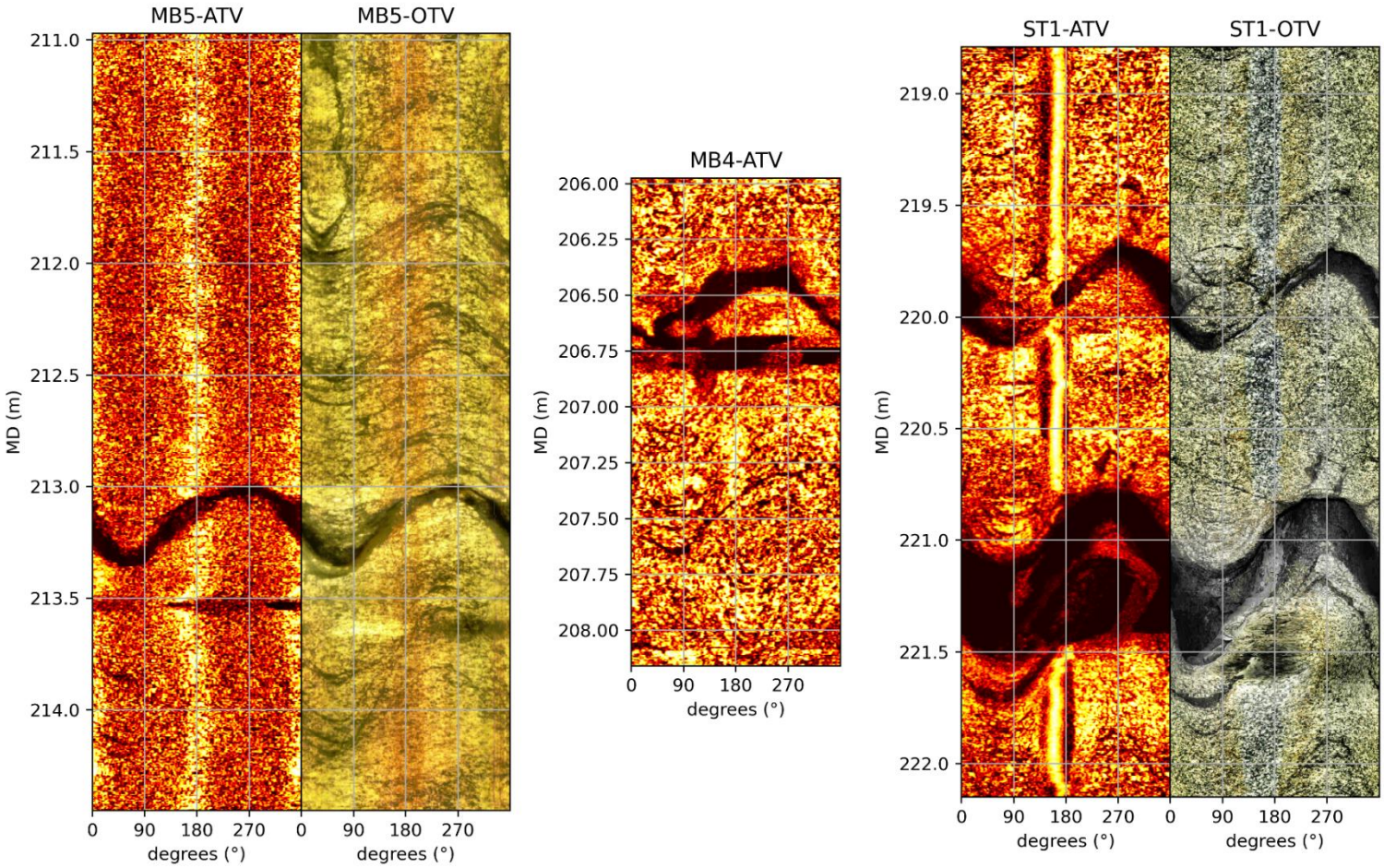

Appendix 21

FZ_12

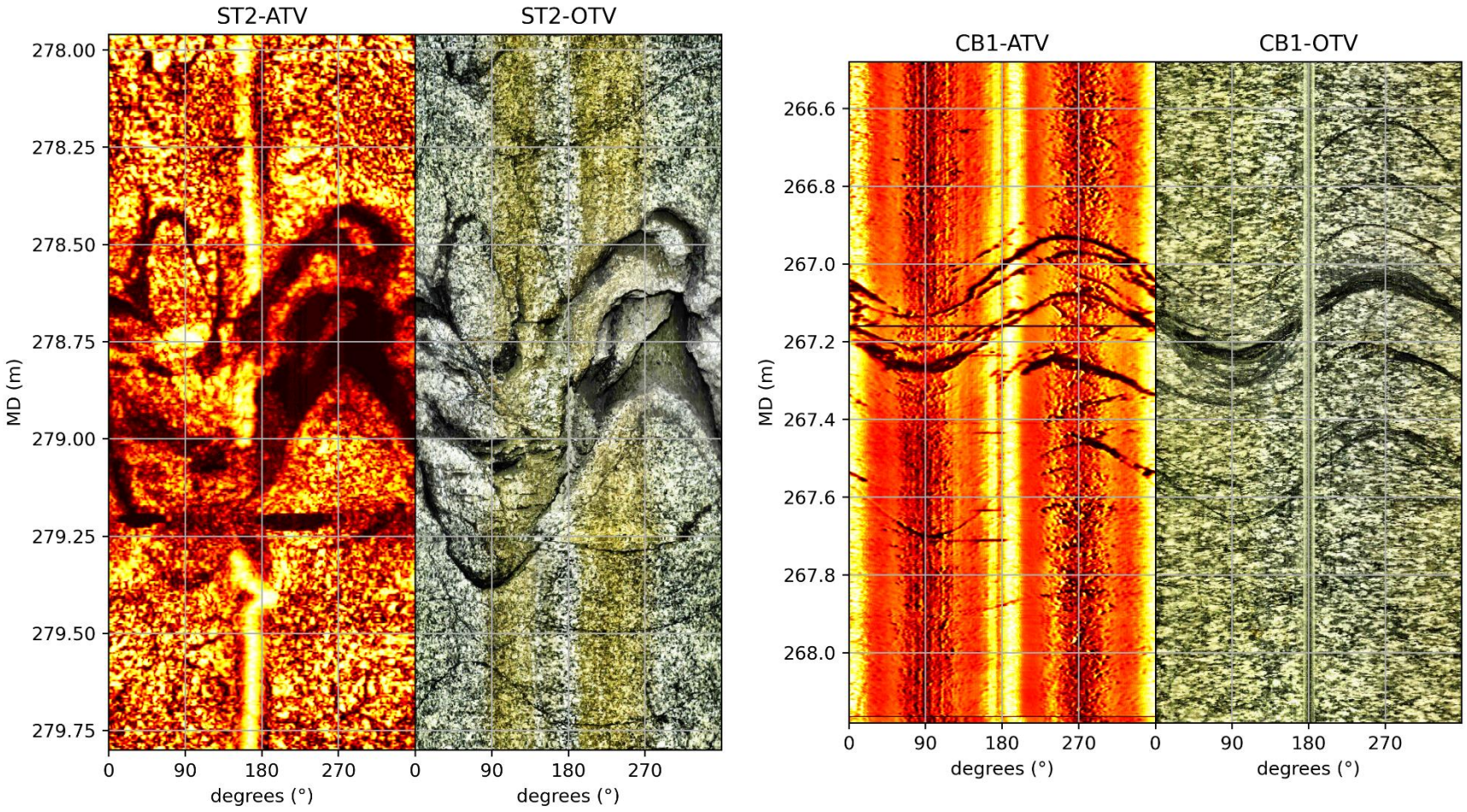

Appendix 22

FZ_13

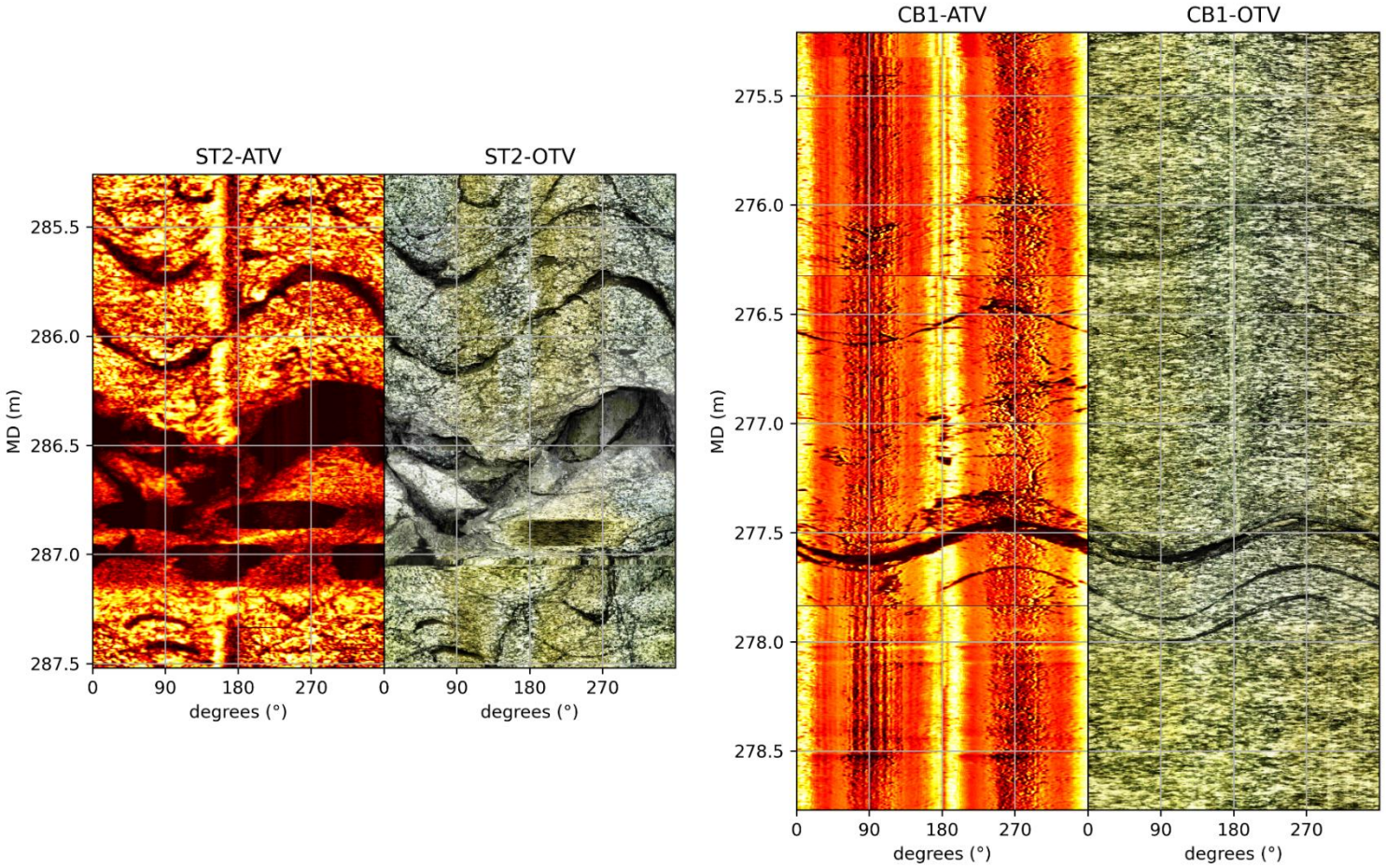

Appendix 23

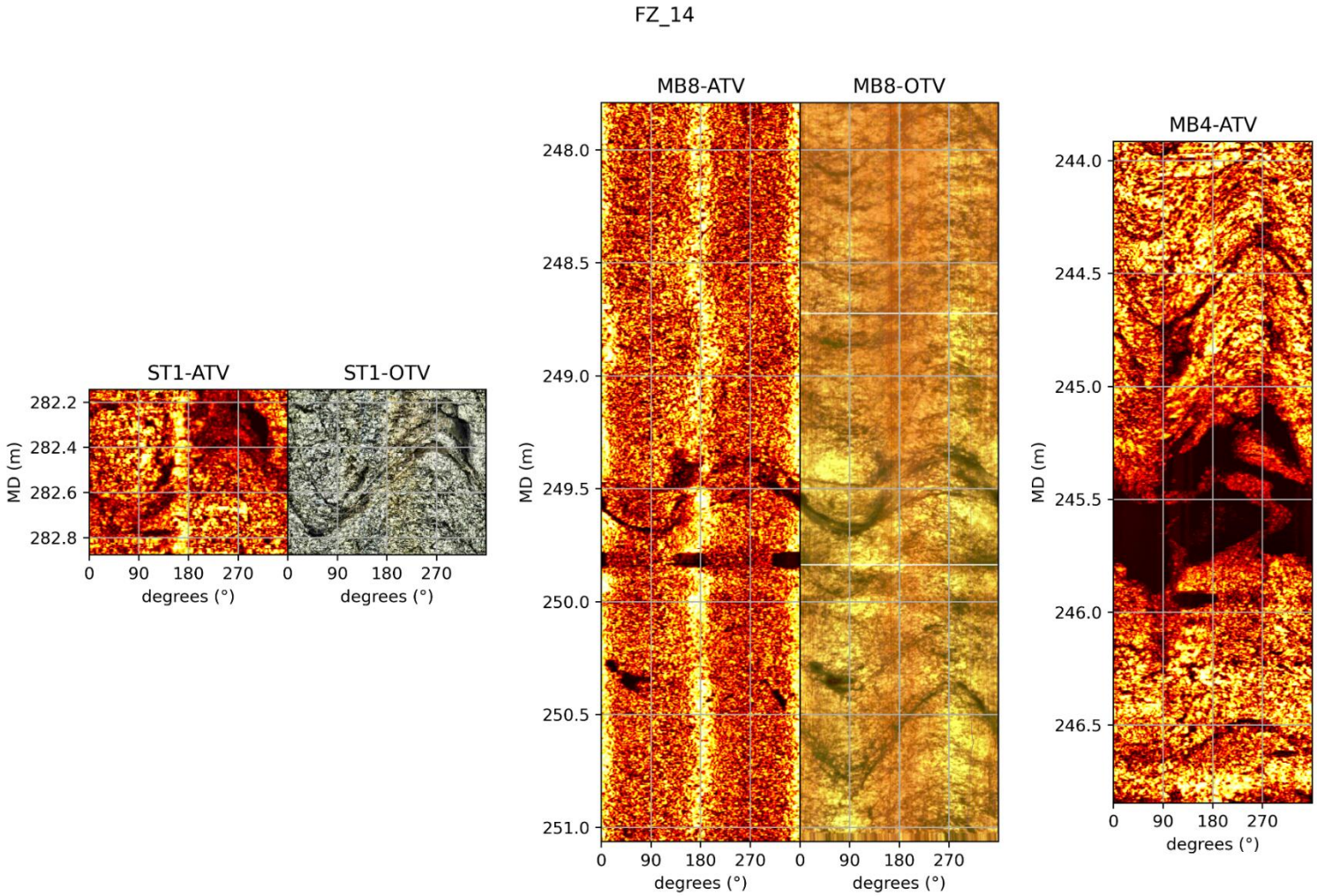

Appendix 24

FZ_15

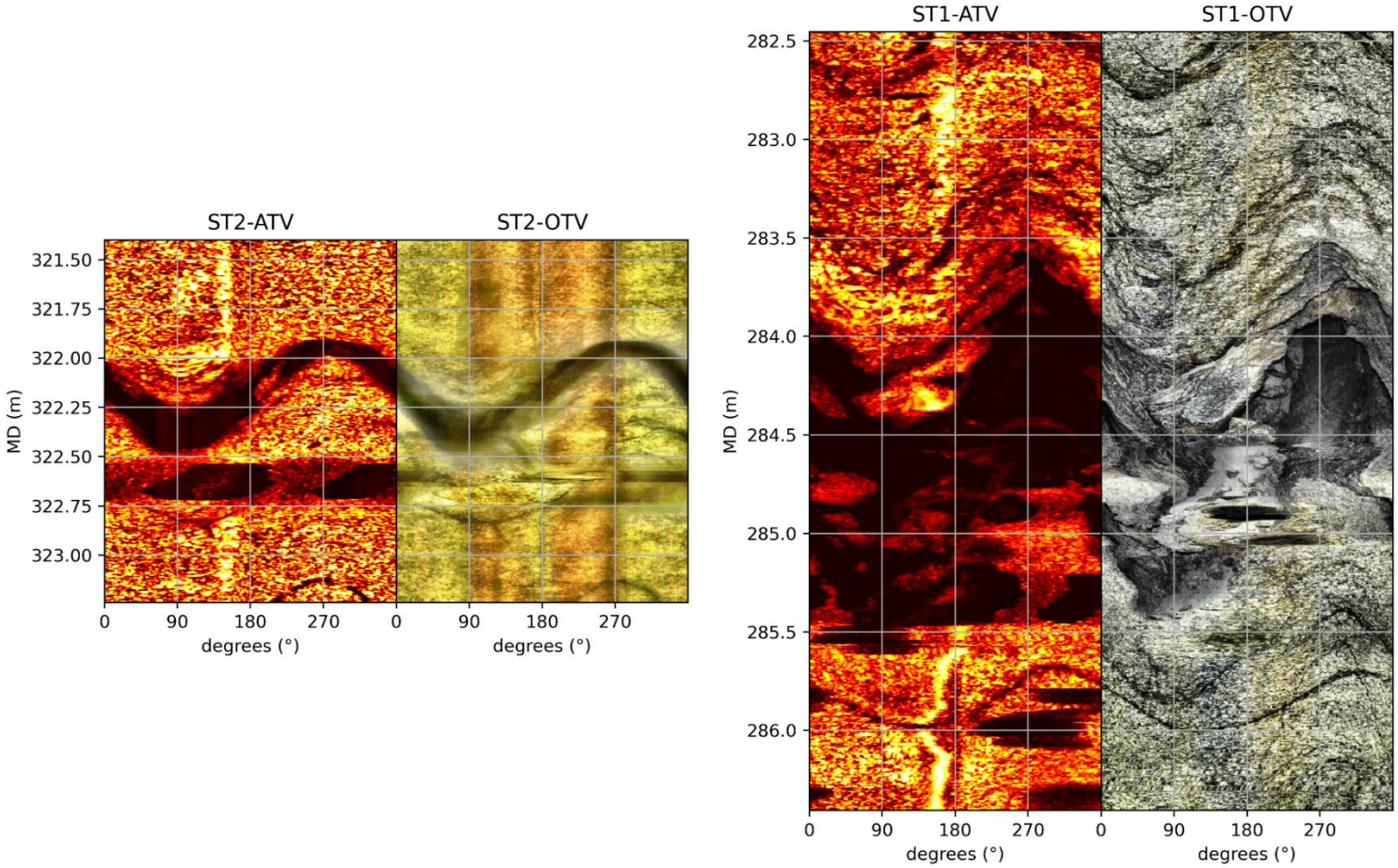

Appendix 25

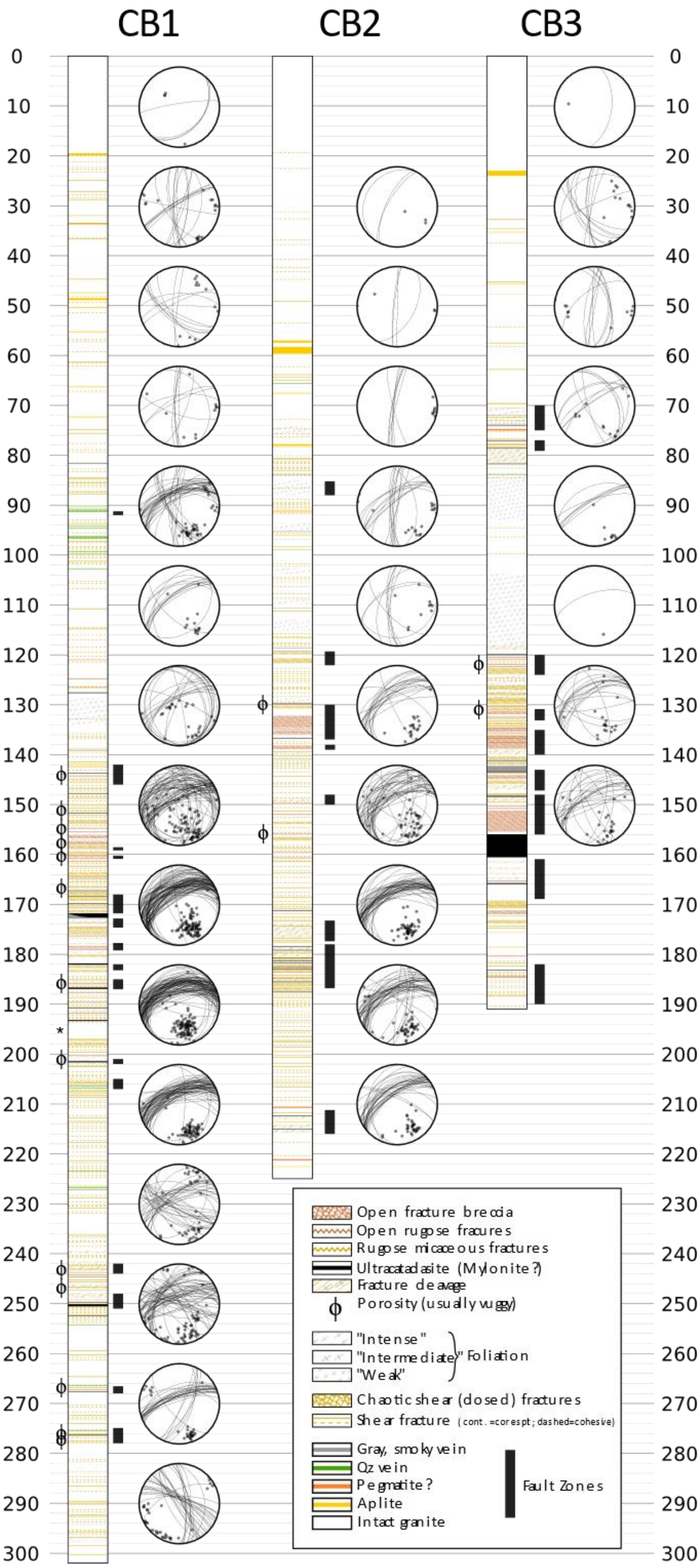

Appendix 26. Core log.